

## INFORMATION TO USERS

This manuscript has been reproduced from the microfilm master. UMI films the text directly from the original or copy submitted. Thus, some thesis and dissertation copies are in typewriter face, while others may be from any type of computer printer.

The quality of this reproduction is dependent upon the quality of the copy submitted. Broken or indistinct print, colored or poor quality illustrations and photographs, print bleedthrough, substandard margins, and improper alignment can adversely affect reproduction.

In the unlikely event that the author did not send UMI a complete manuscript and there are missing pages, these will be noted. Also, if unauthorized copyright material had to be removed, a note will indicate the deletion.

Oversize materials (e.g., maps, drawings, charts) are reproduced by sectioning the original, beginning at the upper left-hand corner and continuing from left to right in equal sections with small overlaps. Each original is also photographed in one exposure and is included in reduced form at the back of the book.

Photographs included in the original manuscript have been reproduced xerographically in this copy. Higher quality 6" x 9" black and white photographic prints are available for any photographs or illustrations appearing in this copy for an additional charge. Contact UMI directly to order.

# UMI

A Bell & Howell Information Company  
300 North Zeeb Road, Ann Arbor, MI 48106-1346 USA  
313:761-4700 800:521-0600



**EFFECT OF BACKFILL ON THE PERFORMANCE OF  
A VERTICAL U-TUBE GROUND-COUPLED HEAT PUMP**

A Dissertation

by

YIAN GU

Submitted to the Office of Graduate Studies of  
Texas A&M University  
in partial fulfillment of the requirements for the degree of

**DOCTOR OF PHILOSOPHY**

August 1995

**Major Subject: Mechanical Engineering**

**UMI Number: 9539211**

---

**UMI Microform 9539211**

**Copyright 1995, by UMI Company. All rights reserved.**

**This microform edition is protected against unauthorized  
copying under Title 17, United States Code.**

---

**UMI**

**300 North Zeeb Road  
Ann Arbor, MI 48103**

**EFFECT OF BACKFILL ON THE PERFORMANCE OF  
A VERTICAL U-TUBE GROUND-COUPLED HEAT PUMP**

A Dissertation

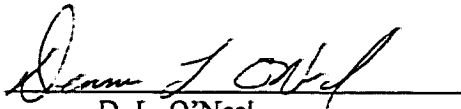
by

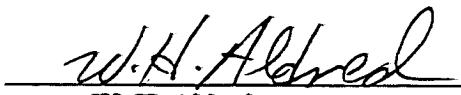
YIAN GU

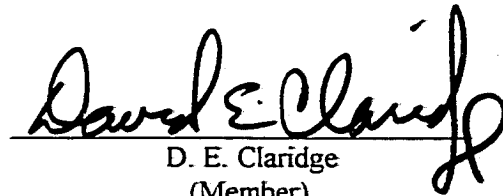
Submitted to Texas A&M University  
in partial fulfillment of the requirements  
for the degree of

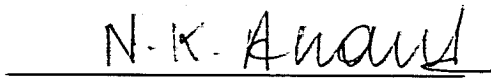
DOCTOR OF PHILOSOPHY


Approved as to style and content by:

  
D. L. O'Neal  
(Chair of Committee)

  
W. H. Aldred  
(Member)

  
D. E. Claridge  
(Member)

  
N. K. Anand  
(Member)

  
for G. P. Peterson  
(Head of Department)

August 1995

Major Subject: Mechanical Engineering

**ABSTRACT**

Effect of Backfill on the Performance of a Vertical U-Tube

Ground-Coupled Heat Pump. (August 1995)

Yian Gu, B.S., Jiaotong University, Xian, China;

M.S., Jiaotong University, Xian, China

Chair of Advisory Committee: Dr. Dennis L. O'Neal

The present work is concerned with developing a discretized analytical model to investigate the effect of a backfill on the performance of a vertical U-tube ground-coupled heat pump. This work involves the development of an analytical solution and an expression for the equivalent diameter, and the experimental verification of their applications in the system model.

The approximate analytical solution was developed to the transient heat-conduction problem in an infinite composite medium composed of a backfill and the soil with an internal cylindrical heat source. This was intended to improve the prediction of the performance of a U-tube ground heat exchanger. The generalized orthogonal expansion technique was utilized in deriving this solution. Solutions are presented in a wide range of the Fourier number for the non-dimensional temperature as a function of the ratios of the thermal conductivities and diffusivities of the backfill and soil. Sensitivities of the results to assumptions about the sizes of the backfilling region and the far-field boundary were also examined. To verify the correctness of the solution, comparisons were made between this solution and the classical homogeneous cylindrical solution and a finite difference solution.

To improve the equivalent diameter approach to the thermal interference problem between the legs of the U-tube, a general expression for the equivalent diameter was derived under steady state. The transient analytical solution developed earlier combined with the superposition method and the conformal mapping technique were used to justify this expression.

A small-scale U-tube test facility was constructed for the experimental validation of the system model of the U-tube heat exchanger using the analytical solution and the equivalent diameter expression. Two types of backfill materials: bentonite/masonry sand and bentonite/copper powder, were chosen for the tests.

Finally, the parametric studies were conducted to characterize the effects of the thermal properties of the backfill, the leg spacing as well as the size of the backfill region. A backfill effectiveness was proposed and discussed. These studies provide a number of insights into the heat transfer behavior of the U-tube heat exchanger buried in a non-homogeneous medium.

## ACKNOWLEDGMENTS

I would like to express my heartfelt thanks to Dr. Dennis L. O'Neal for his patient guidance, keen observation and invaluable educational experience during the course of this research. I am also grateful to Professor W. H. Aldred, Dr. D. E. Claridge, Dr. N. K. Anand, and Dr. R. M. Crooks for their helpful comments and for serving on my committee.

Thanks are also owed to Professor W. H. Aldred for his direction and assistance in constructing the experimental equipment. Special thanks go to Bert McJimsey for his help in designing and making the test facility. My sincere gratitude is extended to Chuck Bohmer, John Bryant, Kelly Milligan and Frank Scott from the Energy Systems Laboratory and Richard Epting from the Agricultural Engineering Shop who were of great help in the fabrication of the test equipment.

My deep appreciation goes to my parents, Yasheng Gu and Puying Zhang, and my wife, Ying Zhou. I am greatly indebted to Ying Zhou and my twin sons, Shi Gu and Xin Gu.



## TABLE OF CONTENTS

	Page
ABSTRACT .....	iii
ACKNOWLEDGMENTS .....	v
TABLE OF CONTENTS .....	vi
LIST OF TABLES .....	viii
LIST OF FIGURES .....	ix
NOMENCLATURE .....	xiv
 CHAPTER	
I INTRODUCTION .....	I
II LITERATURE SURVEY .....	8
Heat Conduction Models and Thermal Interference .....	8
Moisture Migration and Thermal Instability .....	15
Backfills .....	18
Conformal Mapping .....	21
III DEVELOPMENT AND VERIFICATION OF AN ANALYTICAL SOLUTION .....	25
Generalized Orthogonal Expansion Technique .....	25
Mathematical Model .....	29
Behaviors of the Solution .....	35
Example Calculations .....	38
Validation of the Solution .....	43
IV DETERMINATION OF THE EQUIVALENT DIAMETER .....	49
Establishment of the Expression .....	51
Errors During Transient Processes .....	55
Justification Using Conformal Mapping Technique .....	56
Summary .....	72

CHAPTER	Page
V SYSTEM MODEL FORMATION .....	74
Ground-Coil Model Development .....	74
Time Intervals and Number of Elements .....	86
VI EXPERIMENTAL SET-UP AND PROCEDURES .....	88
Experimental Set-Up .....	88
Soil Preparation .....	97
Backfill Preparation .....	98
Experimental Procedures .....	102
VII COMPARISON OF MODEL AND EXPERIMENTAL RESULTS .....	111
VIII PARAMETRIC STUDIES .....	134
Parameter Selection .....	134
Results and Discussion .....	137
Backfill Effectiveness .....	141
Summary .....	151
IX CONCLUSIONS AND RECOMMENDATIONS .....	152
REFERENCES .....	156
APPENDIX A INPUT DATA USED IN PARAMETRIC STUDIES .....	160
APPENDIX B EXPERIMENTAL UNCERTAINTY .....	162
VITA .....	165

## LIST OF TABLES

Table		Page
3.1	Values of the first ten eigenvalues for the case where $H = G = 1$ .....	36
4.1	Relative error for $ETR (S_b = 20, S_c = 128)$ .....	70
4.2	Relative error for $ETR (L_s = 2D, S_c = 128)$ .....	70
4.3	Relative error for $ETR (L_s = 2D, S_b = 8.8)$ .....	71
6.1	Variation of IWT with time and on/off modes in Test A and Test B .....	110
7.1	Variation of soil temperature distribution with time in Test A .....	130
7.2	Variation of soil temperature distribution with time in Test B .....	130
7.3	Typical wall temperature distribution along the U-tube in Test A .....	133
8.1	List of cases in the three groups used for parametric studies .....	136
8.2	Backfill effectiveness for all the twenty cases divided into three groups .....	150

## LIST OF FIGURES

Figure	Page
1.1 Typical ground loop configurations .....	2
1.2 Schematic diagram of a U-tube type GCHP .....	3
2.1 Comparison of simulated and experimental EWT values on September 4, 1990 .....	10
2.2 Comparison of simulated and experimental EWT values during a 22-minute on-time .....	11
2.3 Two heat transfer parts defined by Lei, 1993 .....	13
2.4 Thermal stability limits for a sandy silt soil .....	17
2.5 Transformation of the profile of a wing to a circle using the conformal mapping method .....	22
2.6 Procedure of conformal mapping used by Winders .....	24
3.1 Schematic of the pipe, backfill and surrounding soil .....	26
3.2 Values of $T^*$ as a function of $Fo$ , $G$ and $H$ .....	39
3.3 Sensitivity of the results to assumptions about $S_c$ .....	41
3.4 Sensitivity of the results to assumptions about $S_b$ .....	42
3.5 Values of the characteristic Fourier number as a function of $G$ and $H$ .....	44
3.6 Comparison of the heterogeneous analytical solution (with homogeneous assumptions) and the homogeneous solution presented in equation (3.26) .....	46
3.7 Comparison between the heterogeneous analytical solution and a finite difference solution for $H = G = 0.33$ .....	47

Figure	Page
3.8 Comparison between the heterogeneous analytical solution and a finite difference solution for $H = G = 3.0$ .....	48
4.1 Procedure for derivation of the equivalent diameter .....	50
4.2 Comparison of the temperature rises calculated for the U-tube and a single pipe with the equivalent diameter $D_{eq} = 2D$ when $H = G = 1$ .....	57
4.3 Comparison of the temperature rises calculated for the U-tube and a single pipe with the equivalent diameter $D_{eq} = 2D$ when $H = G = 3$ .....	58
4.4 Comparison of the temperature rises calculated for the U-tube and a single pipe with the equivalent diameter $D_{eq} = 2\sqrt{2}D$ when $H = G = 1$ .....	59
4.5 Eccentric assumption of the backfill region for use in the justification applying the conformal mapping technique .....	60
4.6 An example of mapped soil and backfill regions using equation (4.12) .....	61
4.7 Varied shapes of backfill boundary after mapping with increased eccentricity .....	64
4.8 Varied shapes of backfill boundary after mapping with increased radius of backfill region .....	65
4.9 Schematic of the thermal resistive network for <i>ETR</i> analysis under the eccentric assumption .....	67
5.1 Superposition of heat pulses for the analytical solution .....	76
5.2 Schematic of computational domain and unknown temperatures .....	78
6.1 Schematic diagram of the U-tube test facility .....	89

Figure	Page
6.2 U-tube heat exchanger and thermocouple locations used in the small-scale simulator .....	91
6.3 Cross-section of the tank and the contents used in the simulator .....	92
6.4 Variation of IWT from start-up to steady state (0 - 48 min) in Test A .....	104
6.5 Variation of IWT during the two on/off cycles (48 - 65 min) in Test A .....	105
6.6 Oscillation of IWT during the last phase (65 - 350 min) in Test A .....	106
6.7 Variation of IWT during the first phase (0 - 50 min) in Test B .....	107
6.8 Variation of IWT during the two on/off cycles (50 - 69 min) in Test B .....	108
6.9 Oscillation of IWT during the last phase (69 - 420 min) in Test B .....	109
7.1 Comparison of OWT during the first phase in Test A .....	114
7.2 Comparison of OWT during the second phase in Test A .....	115
7.3 Comparison of OWT during the third phase in Test A .....	116
7.4 Comparison of temperature drop across the U-tube heat exchanger during the first phase in Test A .....	118
7.5 Comparison of temperature drop across the U-tube heat exchanger during the second phase in Test A .....	119
7.6 Comparison of temperature drop across the U-tube heat exchanger during the third phase in Test A .....	120
7.7 Comparison of OWT during the first phase in Test B .....	121
7.8 Comparison of OWT during the second phase in Test B .....	122
7.9 Comparison of OWT during the third phase in Test B .....	123

Figure	Page
7.10 Comparison of temperature drop across the U-tube heat exchanger during the first phase in Test B .....	124
7.11 Comparison of temperature drop across the U-tube heat exchanger during the second phase in Test B .....	125
7.12 Comparison of temperature drop across the U-tube heat exchanger during the third phase in Test B .....	126
7.13 Variations of ambient air and tank wall temperatures during Test A .....	128
7.14 Variations of ambient air and tank wall temperatures during Test B .....	129
8.1 Comparison of $\Delta T$ during 30-day simulation for Group I .....	138
8.2 Comparison of daily energy exchange between the soil and coil during 30-day simulation for Group I .....	139
8.3 Comparison of cumulative energy exchange between the soil and coil over 30-day operation for Group I .....	140
8.4 Comparison of $\Delta T$ during 30-day simulation for Group II .....	142
8.5 Comparison of daily energy exchange between the soil and coil during 30-day simulation for Group II .....	143
8.6 Comparison of cumulative energy exchange between the soil and coil over 30-day operation for Group II .....	144
8.7 Comparison of $\Delta T$ during 30-day simulation for Group III .....	145
8.8 Comparison of daily energy exchange between the soil and coil during 30-day simulation for Group III .....	146

Figure	Page
8.9 Comparison of cumulative energy exchange between the soil and coil over 30-day operation for Group III .....	147



### NOMENCLATURE

- $A_c$  = cross-sectional flow area,  $m^2$
- $AG, AT$  = surface area in Fig. 2.3,  $m^2$
- $BE$  = backfill effectiveness
- $c$  = specific heat,  $J / kg-K$
- $c_p$  = specific heat at constant pressure,  $J / kg-K$
- $C$  = coefficient or correction factor
- $C_n$  = coefficients in equation (3.25)
- $d_{in}$  = inner pipe diameter,  $m$
- $D$  = outer pipe diameter,  $m$
- $D \times H$  = outer diameter (cm)  $\times$  height (cm)
- $E$  = eccentricity,  $m$
- $ETR$  = external thermal resistance per unit length,  $m-K / W$
- $(ETR)_{tot}$  = defined in equation (4.4),  $m-K / W$
- $\Delta ETR$  = defined in equation (4.21)
- $Fo$  = Fourier number =  $\alpha_2 t / r_c^2$
- $Fo_c$  = characteristic Fourier number
- $g$  = gravitational acceleration,  $m / s^2$
- $G$  = ratio of thermal diffusivity =  $G_1 = \alpha_1 / \alpha_2$
- $G_r$  = ratio of thermal diffusivity =  $\alpha_1 / \alpha_2$
- $Gr_r$  = Grashof number =  $g\beta r_m^3 \Delta T / \nu^2$
- $h$  = convection coefficient,  $W / m^2-K$
- $H$  = ratio of thermal conductivity =  $k_1 / k_2$
- IWT = inlet water temperature of the U-tube,  $^{\circ}C$

- $j$  = unit vector in a complex variable  
 $J$  = defined in equation (7.2)  
 $J_0, J_1$  = Bessel functions of the first kind  
 $k$  = thermal conductivity, W/ m-K  
 $k_1, k_2$  = thermal conductivity of backfill and soil, W/ m-K  
 $L$  = length or depth of a ground coil, m  
 $L_S$  = leg spacing, m  
 $\Delta L$  = length of element, m  
 $\dot{m}$  = mass flow rate, kg / s  
 $M, N$  = number of intervals into which a resistive network is divided  
 $MC$  = moisture content, %  
 $Nu$  = Nusselt number =  $h d_{in}/k$   
 $OWT$  = outlet water temperature of the U-tube, °C  
 $P_i(r^*, t)$  = functions in equation (5.1)  
 $Pr$  = Prandtl number =  $c_p \mu / k$   
 $Q$  = total energy exchange between soil and coil, kWh  
 $Q_{acc}$  = accumulative energy exchange between soil and coil, kWh  
 $Q_d$  = daily energy exchange between soil and coil, kWh  
 $Q'$  = heat transfer rate per unit length, W/m  
 $r$  = radius or module of a vector, m  
 $r_{in}$  = inner pipe radius, m  
 $r^*$  = dimensionless radius =  $r / r_a$   
 $R$  = thermal resistance of pipe wall, m-K / W  
 $Re_d$  = Reynolds number =  $u d_{in} / \nu$

$R_c$  = internal thermal resistance of a pipe in equation (5.12), m-K / W

$R_u, R_v$  = horizontal and vertical resistance, m-K / W

$S_b$  = ratio of radius =  $r_b / r_a$

$S_c$  = ratio of radius =  $r_c / r_a$

$t$  = time, s

$\Delta t$  = time interval, s

$T$  = temperature, °C or K

$T_c$  = temperature at heat source, °C or K

$T_{sm}$  = mean ground surface temperature, °C or K

$T^*$  = dimensionless temperature =  $k_2 \theta / Q'$

$\bar{T}_f$  = mean fluid temperature, °C

$\Delta T$  = temperature increase or temperature drop across the U-tube, °C

$\Delta T_1, \Delta T_{11}, \Delta T_{12}$  = temperature rise in equations (4.1) - (4.3), °C

$u$  = coordinates after mapping, or flow velocity, m / s

$v$  = coordinates after mapping

$\Delta u, \Delta v$  = distance in equation (4.17)

$U$  = inner pipe perimeter, m

$\Delta U$  = width of the resulting rectangle after mapping

$\bar{V}$  = volumetric flow rate, m<sup>3</sup> / s

$w, z$  = complex variables

$W_i(r^*)$  = functions in equation (3.25)

$x, y$  = original coordinates

$Y_0, Y_1$  = Bessel functions of the second kind

$\alpha$  = thermal diffusivity =  $k / \rho c$ , m<sup>2</sup> / s

- $\alpha_1, \alpha_2$  = thermal diffusivity of backfill and soil,  $\text{m}^2/\text{s}$   
 $\beta$  = thermal expansion coefficient,  $\text{K}^{-1}$   
 $\beta_n$  = the  $n$ th eigenvalue  
 $\chi, \delta$  = dimensionless variables in equation (5.5)  
 $\varepsilon, \phi$  = dimensionless variables in equations (5.9) and (5.11)  
 $\gamma$  = angle in Fig. 2.3, deg  
 $\varphi_{in}$  = the  $n$ th eigenfunction for region  $i$   
 $\mu$  = dynamic viscosity,  $\text{kg}/\text{m}\cdot\text{s}$   
 $\nu$  = kinematic viscosity,  $\text{m}^2/\text{s}$   
 $\theta$  = excess temperature =  $T - T_{ff}$ ,  $^{\circ}\text{C}$ ,  
 or angle of a vector, radian  
 $\rho$  = density,  $\text{kg}/\text{m}^3$   
 $\omega$  = angle in Fig. 4.5, radian

### Subscripts

- $0$  = state of calibration  
 $a$  = outer pipe surface  
 $b$  = soil-backfill interface  
*Base* = base case  
 $c$  = far-field boundary  
*ecc* = eccentric  
*eq* = equivalent properties  
 $f$  = fluid  
 $ff$  = far-field

$i = 1, 2$  for backfill and soil region, respectively

$pipe$  = pipe wall

$s$  = outer pipe surface

$w$  = inner pipe surface

### Superscripts

$'$  = equivalent pipe

## CHAPTER I

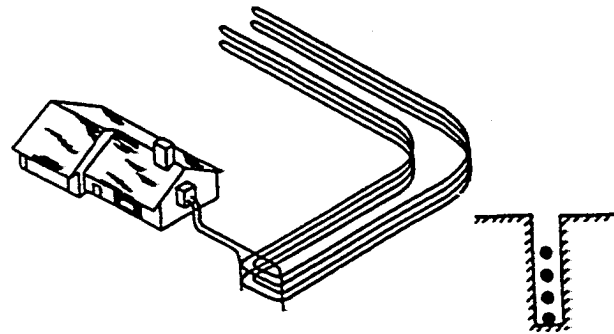
### INTRODUCTION

A ground-coupled heat pump (GCHP) utilizes the ground as a heat source in heating and a heat sink in cooling mode operation. In the heating mode, a GCHP absorbs heat from the ground and uses it to heat the house or building. In the cooling mode, heat is absorbed from the conditioned space and transferred to the earth through its ground heat exchanger. A GCHP has the potential to operate at a higher efficiency than a conventional air source heat pump (ASHP) which uses the outdoor air as the heat source or sink. For example, the working fluid (water or ethylene glycol-water solution) circulated through the heat exchanger of a GCHP is a much better heat transfer medium than air. Also, the earth is normally at a much more stable and favorable temperature than the ambient air when demand for heating or cooling is greatest. Summer daytime temperatures of over 35 °C are very common in the southern U.S., but the ground temperature at depths greater than 10 m remains close to 22 °C throughout the year in central Texas (Dobson, 1991).

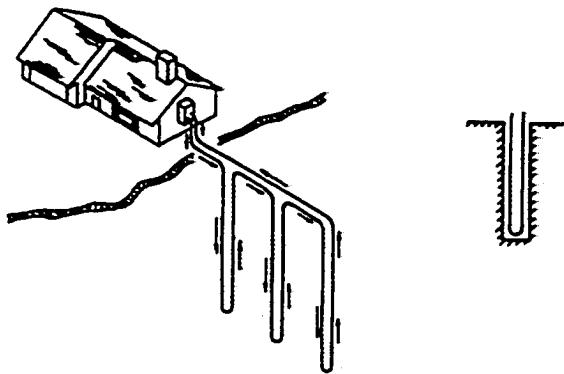
A ground heat exchanger can be buried either horizontally in trenches or vertically in bore holes. Figure I.1 shows typical horizontal and vertical installations. The vertical U-tube ground heat exchanger (as shown in Fig I.1(b)) is one of the most popular configurations used in GCHPs. Its connection with other system components is shown in Fig. I.2. The working fluid circulates through the ground loop and the refrigerant-to-water heat exchanger (outdoor coil) to exchange heat alternately with the earth and the

---

Style and format follow *ASME Journal of Heat Transfer*.



(a)



(b)

**Fig. 1.1 Typical ground loop configurations. (a) horizontal installation; (b) vertical U-tube installation**

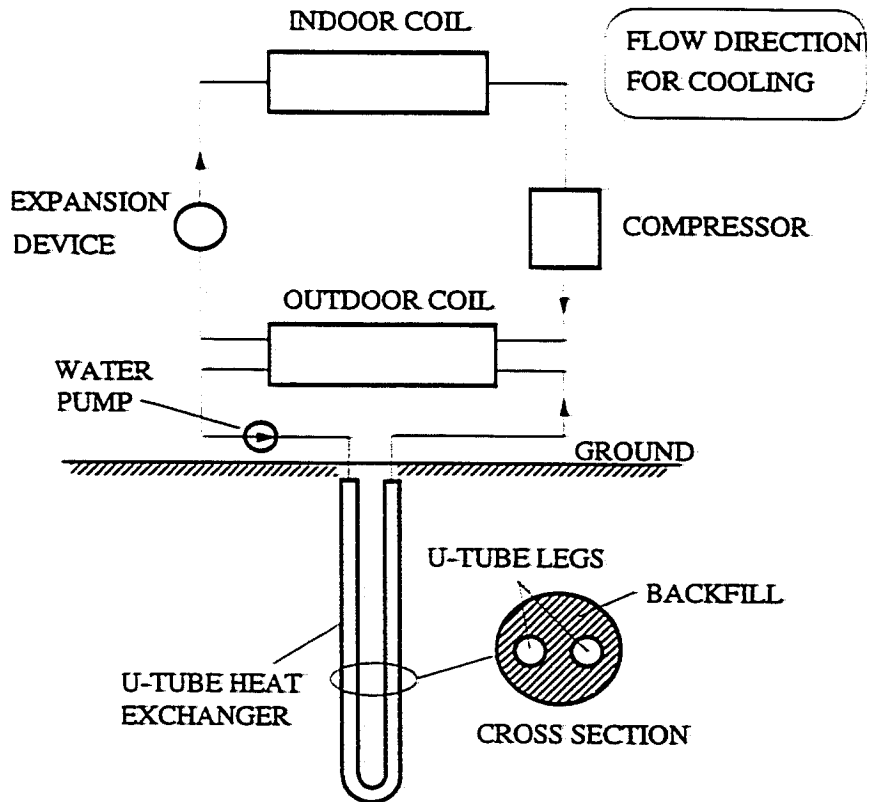


Figure 1.2 Schematic diagram of a U-tube type GCHP



refrigerant. In the cooling mode, the water carries away heat from the condenser and dissipates it to the ground through the U-tube. One or more bore holes, usually 10 cm wide and 15 to 183 m deep (Bose, Parker and McQuiston, 1985) are drilled to accommodate one or several parallelly buried vertical coils. The U-tube is typically made of 1.9 to 5.1 cm polyvinylchloride (PVC), polybutylene or high-grade polyethylene pipe. After the installation, a different material is commonly used to fill the gap between the tube and the native soil to provide good thermal contact between them and prevent soil dry-out during summer operations. This material is called the backfill.

Heat rejection by the ground heat exchanger may cause moisture migration away from the pipe surface during cooling-mode operation. If the moisture content decreases significantly which can happen during prolonged periods of heat rejection to the soil, the conductivity of the soil can be sharply reduced (Bose, Parker and McQuiston, 1985). If moisture migration continues, dry regions can develop in the soil. In soils with a high clay content, this drying can cause shrinkage of the soil away from the U-tube. The shrinkage can create air gaps, which increase the overall resistance between the soil and the circulating fluid, and can render a GCHP less effective than an ASHP. High-conductivity backfills that are insensitive to moisture migration can improve the performance of a GCHP by preventing these phenomena. ~~The improvement of the thermal response near the pipe surface plays an important role in designing GCHPs.~~

The existence of a backfill, however, results in a non-homogeneous medium around the heat exchanger. Even without significant moisture migration, the backfill complicates the analysis of the heat transfer process. Previous models for GCHPs treated this problem in two ways. They either ignored the presence of the backfill and assumed a

homogeneous medium around the coil (Dobson, 1991) or implemented numerical techniques to solve it (Couvillion and Cotton, 1990 and Muraya, 1994). The former obviously would lose accuracy if thermal properties of the backfill materials differ significantly from those of the native soil. Numerical models can be time consuming for long term predictions and may not be easy to adapt to design purposes of sizing the heat exchangers. Therefore, a more effective way to predict the transient heat transfer in such an infinite composite medium composed of the soil and the backfill is desired. An analytical solution will allow one to obtain simultaneous solutions for different times and could easily be incorporated into a GCHP simulation program. However, it is extremely difficult to find an exact analytical solution. In this study, an approximate analytical solution has been developed and validated by comparing it with both numerical models and experimental data. This solution is given in non-dimensional form for easy analysis and application.

Another problem that arises in analyzing GCHPs is the thermal interference (or thermal short circuiting) between the two pipe legs of the U-tube. The thermal interference leads to an unsymmetric boundary condition. Fluid temperatures inside the two legs are different and the heat transfer from each is influenced by the other. Considering a backfill region around the U-tube presents another complication in the treatment of this problem. Basically, there are three different approaches to simplifying this problem: (1) superposition of individual thermal fields based on the assumption that the heat conduction equations are linear (Claesson and Dunand, 1983), (2) assumption of an equivalent diameter method to collapse the two legs into a single source (Mei and Baxter, 1986), and (3) thermal short-circuiting model in which heat transfer between the

two legs are accounted for simply by Fourier's law (Hopkins, 1983 and Lei, 1993) as explained later in Chapter II. The first two can be used for models in which the basic mathematical solutions are derived for a single heat source while the last one can only be useful in numerical calculations. The first approach is straightforward and has been successfully used by Dobson (1991). Some authors (Mei and Baxter, 1986) have stated that the technique must be applied with caution when the two legs with finite diameters are very close to each other. Previous application of the equivalent diameter technique did not show satisfactory results. The equivalent diameter was determined either mathematically or experimentally by researchers. The only mathematically derived relation was originally for the situation of two horizontally buried pipes in direct contact (Claesson and Dunand, 1983). The experimental results were scattered. They have been inevitably affected by factors such as operation modes, ambient air conditions and even geography of installations.

The present work deals with GCHPs which operate in cooling-dominated areas. The objective is to develop a model that can be used to estimate the effect of a backfill on the heat transfer of a vertical U-tube heat exchanger. An analytical solution is derived for a single cylindrical source with radial heat flow, while the actual heat flow from a U-tube is two-dimensional. Therefore, if one can find a proper equivalent diameter expression for the two-leg configuration surrounded by an annular backfill region, this solution could be easily applied to the analysis of a U-tube heat exchanger. This work has been done using conformal mapping. The principle of superposition was also used for comparison.

A test facility was set up to demonstrate the applicability of the analytical solution for transient/cyclic performance prediction of a vertical U-tube GCHP where no dry-out of the soil occurred.

Some parametric studies were conducted to investigate the behavior of important GCHP design parameters such as leg spacing of the U-tube and dimension of the backfill region. A backfill effectiveness measure was proposed and analyzed.

Chapter II presents a literature survey about heat conduction models, approaches to thermal interference, moisture migration and backfills. Chapter III describes the development of the analytical solution, its behavior and theoretical verification. Chapter IV provides the procedure of the equivalent diameter determination. Chapter V shows the U-tube heat exchanger modeling and the application of the analytical solution to realistic cyclic operations. Chapters VI and VII describe the laboratory test facility build-up and discuss the experimental results and comparisons with model predictions. The parametric studies, conclusions and recommendations for future research are provided in the last two chapters.

In general, this study represents a step in the development of a more complete understanding of the heat transfer behavior of a U-tube ground coupling under various backfilling conditions. Based on the analytical and experimental investigations presented herein, an improved approach to sizing a GCHP system can be achieved.

## CHAPTER II

### LITERATURE SURVEY

The literature survey is divided into four categories: (1) heat conduction models and thermal interference, (2) moisture migration and thermal instability, (3) backfills, and (4) conformal mapping. These topics are discussed below.

#### Heat Conduction Models and Thermal Interference

**Homogeneous-Media Solutions.** In the simulation of a GCHP, how to treat the heat conduction problem in the soil/backfill surrounding the ground heat exchanger is important. Most of the previous heat conduction models have focused on heat flow in a homogeneous medium. The presence of the backfill was often neglected. The buried heat exchanger was considered as a line or a cylindrical heat source. Carslaw and Jaeger (1959) and Ingersoll et al. (1954) discussed the analytical solutions for these two types of sources with constant strength in an infinite homogeneous medium. They are the Kelvin line source solution and Carslaw and Jaeger's cylindrical source solution. The line source solution is an approximation of the more complex cylindrical source solution when the Fourier number is greater than twenty ( $Fo > 20$ ) (Ingersoll et al., 1954). Numerical methods were also used for cylindrical sources. Such models, however, may achieve satisfactory results, if the thermal conductivities and diffusivities of the soil and backfill are close to each other.

Dobson (1991) applied the cylindrical source solution in the ground-loop portion of a model to simulate a 3-ton vertical U-tube GCHP system installed in Abilene, Texas.

The ground coil was discretized into elements so that each element could be considered as a constant cylindrical or line source acting within a time interval. The principle of superposition suggested by Claesson and Dunand (1983) was used to account for the time-dependent heat dissipation rates for each element. Dobson also applied superposition to deal with the thermal interference between the two adjacent legs. Figure 2.1 shows the comparison of daily simulated and experimental ground heat exchanger outlet water temperature (OWT)\*. Figure 2.2 shows the simulated and experimental values of OWT over a 22-minute start-up process. The model tracked experimental data well, with the daily averaged OWT being within 1.1 °C in the worst case, and within 0.3 °C on the average. It overestimated the OWT at start-up of a cycle by up to 1.1 °C. This later discrepancy might have been caused by the fact that there was an end effect at the bottom of the U-tubes which caused the adjacent soil temperatures to be somewhat lower than calculated. The lower temperatures would have had much more influence on the model during the off-cycle.

Mei and Baxter (1986) performed experiments on a GCHP system with multiple dissimilar U-tube coils in series for one cooling and one heating season. They also conducted two weeks of continuous and five days of cyclic controlled tests. They stated when two legs of the U-tube with finite diameters were within a very short distance of each other, the ordinary method of superimposing two solutions would not work. Thus, they proposed an equivalent diameter,  $D_{eq}$  which was defined as  $D_{eq} = C \cdot D$  where  $C$

---

\* Because Dobson's study focused on the performance of the heat pump, he labeled the water temperature leaving the ground heat exchanger as the entering water temperature (EWT) to the heat pump. Dobson's EWT is the same as OWT used here.

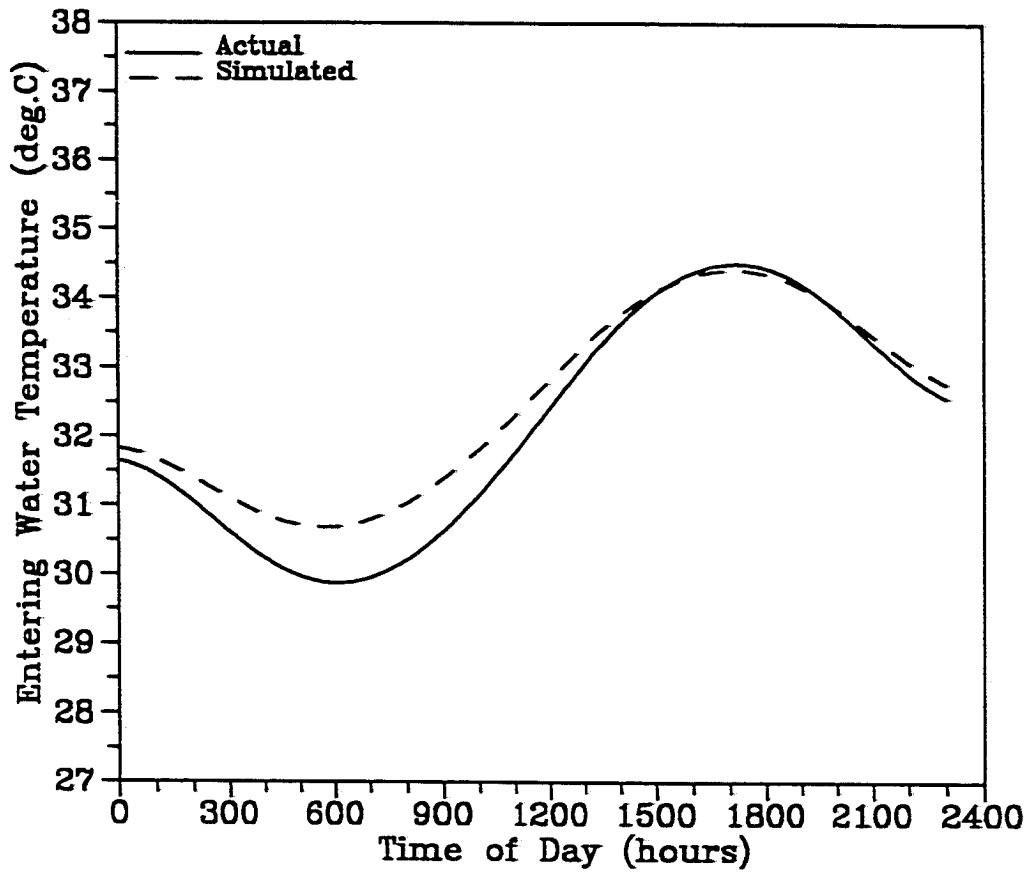


**Fig. 2.1** Comparison of simulated and experimental EWT values on September 4, 1990 (after Dobson, 1991). Note: EWT (entering water temperature to the heat pump) is equivalent to OWT in this study

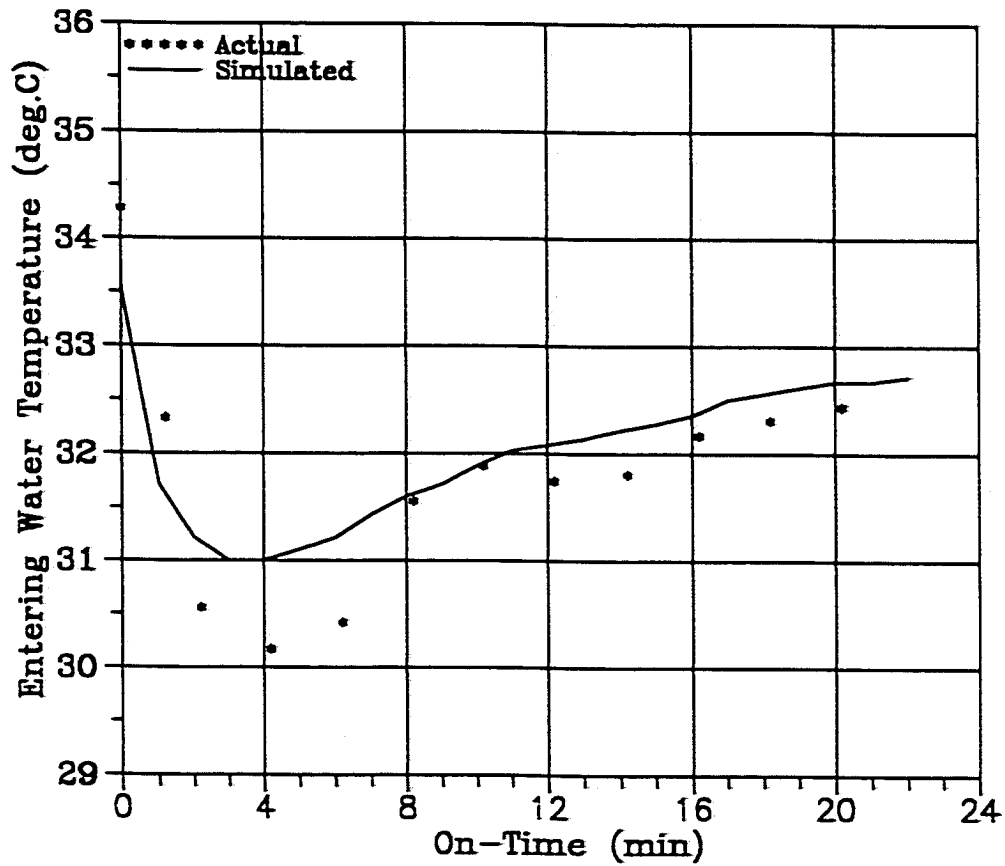


**Fig. 2.2 Comparison of simulated and experimental EWT values during a 22-minute on-time (after Dobson, 1991). Note: EWT (entering water temperature to the heat pump) is equivalent to OWT in this study**



was a correction factor. Mei and Baxter used a detailed finite difference model established by Mei and Emerson (1985) to analyze the U-tube systems mathematically. They found that each of the six wells of the same bore had a different  $C$ -value and that the differences from well to well were in some cases quite large ( $C = 1.0$  to  $1.662$ ). The average  $C$ -value ( $1.279$ ) was smaller than the previously proposed values of  $\sqrt{2}$  by Claesson and Dunand (1983) and  $1.84$  by Fischer and Stickford (1983). It should be noted that the value of  $\sqrt{2}$  was for the situation of two pipes in direct contact. Their results also showed that the equivalent diameter method was only good for continuous operation. When the heat pump was in cyclic operation, the model was inadequate. Five of the six U-tubes were insulated between the two legs with a piece of expanded rubber insulation. It was hoped that the insulation would reduce thermal interference. They found that the insulation did more harm than good. Even though it prevented some thermal short circuiting, it insulated part of the coil so that the total heat transfer was reduced.

Lei (1993) used a finite difference technique to simulate a vertical U-tube ground-coupled heat exchanger for 160 minutes. He adopted the thermal short-circuiting model suggested by Hopkins (1983) for the section between the adjacent legs. His model divided the interval surface area of the tube into two parts. As shown in Fig. 2.3, one surface area ( $AC$ ) exchanges heat with the earth, which maintains a fixed temperature at a large radial distance and the other ( $AT$ ) with the adjacent tube section whose temperature varies with time. The rate of heat transfer between the two facing areas ( $AT$ ) was calculated simply by applying Fourier's law  $Q' = (k AT \Delta T) / \Delta X$  where  $\Delta T$  was the

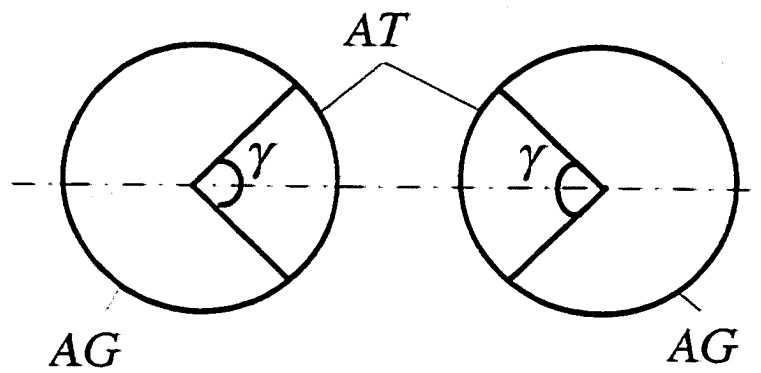


Figure 2.3 Two heat transfer parts defined by Lei, 1993

temperature difference between the pipe surfaces and  $\Delta X$  the equivalent separating distance. The predicted outlet water temperature agreed reasonably well with the experimental data for the on-time periods but did not agree with the measured data for the off-time periods. Lei computed the angle  $\gamma$  that determined the portion of tube whose heat transfer was primarily short-circuited between the two legs. He achieved a  $\gamma$  value of 90 deg to best fit the data and concluded that the value of  $\gamma$  depended on the geometric relationship between the two pipes.

**Heterogeneous-Media Solutions.** Recent experiments and simulations have shown that backfills have a significant effect on the ground heat exchanger performance. The effects can vary with different types of backfill materials (Mei, 1987). Unfortunately, few models (Mei, 1987; Couvillion and Cotton, 1990; Muraya, 1994) have taken into account the existence of backfills in their mathematical models. Most of these models were for horizontal ground coils instead of vertical U-tubes. Mei (1987) adopted a finite difference technique to simulate a GCHP system having a backfill of square cross-section while Couvillion and Cotton (1990) selected a finite element method to simulate an experimental apparatus with an imaginary rectangular backfilling region subject to the controlled heating and cooling cycles. Muraya (1994) used his finite element model to investigate the transient thermal interference between legs of a vertical U-tube heat exchanger. He considered coexistence of the two legs instead of using the superposition method. The simulation results from Muraya's model showed that the equivalent diameter varied with both the leg spacing and the thermal conductivity of the backfill material. He

concluded that the equivalent diameter approach was not suitable for application because it was hard to find a general way to obtain an equivalent diameter value and the value would be time-dependent. Further discussions concerning backfills that Mei (1987) and Couvillion and Cotton (1990) used are given in the section on Backfills.

No exact analytical solution was available either to the U-tube configuration (double heat sources) in a homogeneous medium or to a single source in a non-homogeneous medium. The complex heat transfer process at the pipe surface of an actual heat exchanger has been accounted for in the literature by the superposition of a series of positive and negative step changes (rectangular pulses). This method was discussed thoroughly by Claesson and Dunand (1983).

### **Moisture Migration and Thermal Instability**

Although this study did not consider moisture migration in the simulation model, the knowledge of this physical phenomenon is helpful to the design of the experiments and the preparation of soil and backfill materials.

Thermal gradients in a moist soil can induce moisture movement that, in turn, can result in a decrease in the thermal conductivity of the soil in contact with the heat source. If this process is significant, the development of a dry zone adjacent to the heat source creates an insulating layer that further inhibits dissipation of heat from the source. This condition, in an underground electrical cable installation, can result in so-called "thermal instability." In GCHP systems, a similar phenomenon could occur if the native soil is dry without a proper backfill and the heat source transfers a large enough heat flux.

Experimental and analytical studies have been conducted in the electric power industry for many years in an effort to characterize moisture movement under thermal gradients. Hartley (1987) summarized the previous work done by many researchers (e.g., Couvillion, 1981; Boo, 1984; Hartley and Black, 1981) and stated that the value of the Fourier number when a thermally unstable condition is reached depends on the initial moisture content for a given soil and the heat transfer rate per unit length of the heat source,  $Q'$ . Note that this conclusion is drawn based on coupled non-dimensional heat and mass transfer equations for a uniform medium around a cylindrical heat source. This is illustrated in Fig. 2.4, where  $q'$  has the same definition as  $Q'$  in this study, and  $m$ ,  $t$  and  $d$  denote the moisture content, the time and the diameter of a heat source, respectively. In this plot, the thermal stability limit can be interpreted as the Fourier number when  $\alpha = 1$  with  $d$  as the characteristic length. Hartley explained that thermally stable behavior persists longer for higher initial moisture contents and lower values of  $Q'$  and that low heat transfer rates and relatively high initial moisture contents lead to drying rates that are sufficiently low so that accelerated drying at the surface of the heat source can be delayed almost indefinitely. Because the average heat transfer rate over an entire GCHP ground loop spans the lower limit of the range (20 - 180 W/m) found in buried electrical cables, soil dry-out near the pipe surface may not occur or moisture content should not change significantly until near the end of cooling season (Mei, 1991) unless the soil is relatively dry or sensitive to moisture migration. If the thermal response of the native soil proved unacceptable, the response of the soil at higher densities could be investigated. One could then determine whether proper compaction of the backfill material would sufficiently

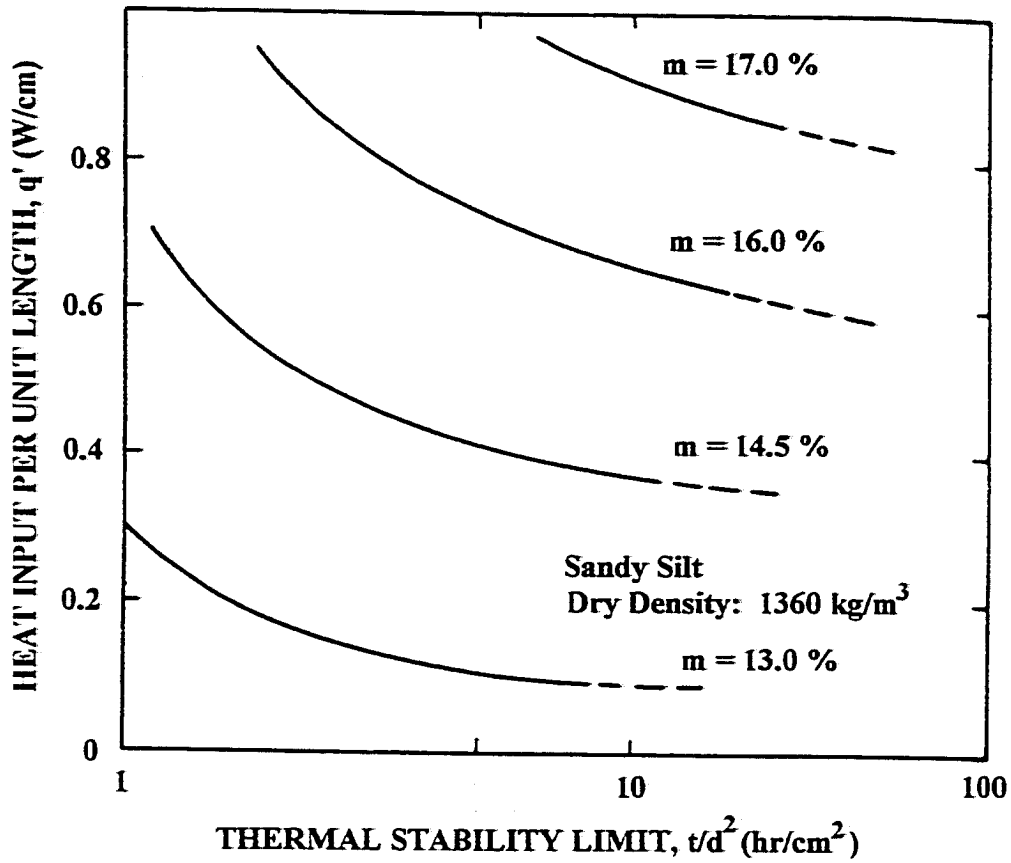


Fig. 2.4 Thermal stability limits for a sandy silt soil (after Hartley, 1987).

enhance the thermal response. Otherwise, special backfills or soil additives should be considered. In this manner, thermal stability problems could be avoided.

### **Backfills**

As stated in Chapter I, backfills have two purposes: (1) they provide good thermal contact between the soil and the heat exchanger, (2) they help prevent soil dry-out. Because the heat flux at the backfill/soil boundary is much smaller than at the pipe surface, the addition of a backfill can substantially help reduce drying in the soil. A backfill material should have a strong resistance to moisture migration and can maintain good contact with the pipe and the soil. Backfills typically have thermal conductivities near those of the native soil and have good flowability during installation (Boggs, et al., 1981; Couvillion and Cotton, 1990; Mei, 1987). Commonly used backfill materials reported in the literature include (Boggs, et al., 1981; Couvillion and Cotton, 1990; Mei, 1987; Mei and Baxter, 1986; Remund and Lund, 1993):

- native soils,
- cement,
- masonry sand,
- sands with various kinds of binders (such as epoxy, acrylic resin and paraffin, etc., often mixed with fillers such as graphite, silicon or quartz), and
- fluidized mixtures, composed of a fine aggregate, a coarse aggregate, a cement or cement-based material, a fluidizing component (e.g., fly ash or

bentonite) and steel cuttings as the additive.

In field installations of vertical U-tubes, fluidized backfill can be easily pumped into the holes.

Mei (1987) analyzed three different backfills: clay (native soil), sand, and a fluidized mixture usually used for underground cable backfilling (Boggs et al., 1981). He indirectly included the effects of moisture migration and contact resistance in the energy equations by introducing the time-averaged thermal conductivity data for both the native soil and the backfills measured from field tests. Only 32 days were simulated for a horizontal GCHP. The information obtained was not adequate because the thermal properties kept on changing due to continuous moisture migration during the whole cooling season. His parametric study indicated that the fluidized mixture backfill dissipated 47% and 23% more heat than the clay and the sand, respectively. Contact resistance for sand should not exist and, therefore, sand has often been used as the backfill material to reduce the contact resistance (Svec et al., 1983). However, sand cannot stop the moisture migration that could lead to a dried-out region, even though this region should usually be very small. Mei concluded:

A good thermal backfill, however, will reduce the effect of moisture migration due to the increase of soil heat transfer area. It should also eliminate, or minimize, the contact resistance, as well as maintain a high thermal conductivity even at very dry ground conditions. The effect of the thermal backfilling material is very difficult to analyze for GCHP application because the heat pump is not always running and the ground coil fluid temperature is quite low, usually not over 48.9 °C (120 °F).

Couvillion and Cotton (1990) made laboratory and computer comparisons of several backfills. They chose the finite element technique to solve the coupled



dimensionless heat and mass transfer equations directly and compared the results to the measured data on the horizontal coil. The four backfills used in this investigation consisted of the native soil, masonry sand, sand mixed with an acrylic resin binder (Jackson, 1980), and sand mixed with paraffin. A binder can partially fill the voids in the sand, creating thermal bridges between the sand grains. The thermal bridges formed by the binder do not evaporate or move like the water bridges in native soil. They used a scale model to simulate one-year cyclic heating and cooling operations with only 60 hours of running based on the same Fourier number. The inlet water temperature for all runs ranged from 10 °C to 50 °C and the outlet water temperature varied from 13 °C to 43 °C. They defined and calculated the backfill effectiveness. The higher values indicate better heat exchanger performance. Their comparison showed that the native soil at an initial moisture content of 14% (dry basis) provided the best effectiveness of all four backfills. However, this effectiveness could decrease if the heat pump were operated at values of heat rejection rates high enough to cause significant drying in the summer. The effectiveness for acrylic/sand backfill was approximately 90% of that for the native soil and would retain that value for a long time since it is not susceptible to moisture migration. The moist sand backfill's effectiveness was lower than those of above two due to extensive moisture migration and the associated drop in conductivity. Johnson et al. (1987) made the similar observation for moist sand backfill. The paraffin/sand backfill had the lowest effectiveness, due to the low conductivity of paraffin although it was impervious to water. However, it should be noted that the acrylic/sand backfill would not

be practical for a vertical ground loop, because it is difficult to pump the mixture into a hole.

Mei and Baxter (1986) operated a GCHP with six dissimilar U-tube coils in series. All wells were backfilled with cement except one well, which was backfilled with sand. The sand backfill seemed to provide better performance, but the test site was in the relatively wet southern United States and the insulation for the U-tubes backfilled with cement could have affected the comparison.

Dobson (1991) and Margo (1992) used bentonite as a soil fluidizer to build up the backfills, but no detailed information and analyses of their performances were available.

### **Conformal Mapping**

Conformal mapping is a mathematical method used to map a geometry from one coordinate plane onto another. The term *conformal* means that the intersecting angle of any pair of curves in the original plane remains unchanged after mapping. This method has been a powerful tool of science and engineering. The most important applications of conformal mapping are connected with the problems of physics and mechanics. One famous example is the study about fluid flow around an airfoil. As shown in Fig. 2.5, the complex profile of the wing of an airplane is transformed to a circle so as to solve the problem easily. At the same time, the flow regime around the airfoil is mapped onto the one around the circular cylinder. Conformal mapping has also been used to obtain the effective external thermal resistance (*ETR*) of single or multi-cable installations in steady state heat flow. It can deal with backfill regions of any shape. Contributions have been

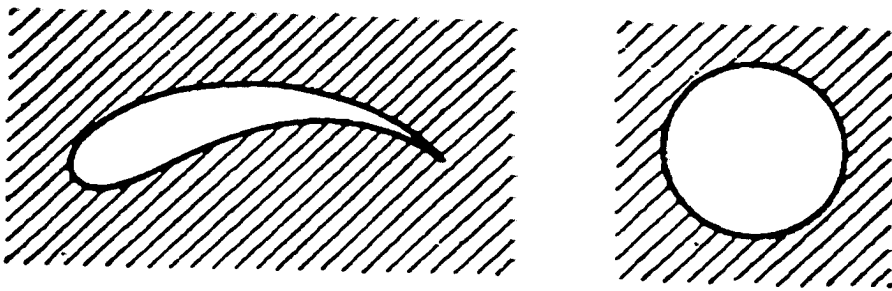


**Fig. 2.5 Transformation of the profile of a wing to a circle using the conformal mapping method**

—

made by Fink and Smerke (1958), Goldenberg (1969), and Winders (1973), etc. Figure 2.6 presents the procedure used by Winders to transform the cable system to a thermal resistive network. The reference cable and the ground surface were mapped onto the edges of the rectangle. The geometry of the backfill boundary was also distorted after the mapping.

The transformed network was then solved by the iterative method on the computer. Fink and Smerke obtained essentially the same transformation as Winders' to map the semi-infinite planes to the corresponding rectangular shape. However, the thermal field was represented by an electrical resistive network and was solved on a d-c network analyzer. The answer obtained in Fink and Smerke's electrical network was an electrical resistance in ohms between the cable and the earth surface. This value was then transferred to thermal resistance by a simple relation. The thermal field generated by the multi-cable installation was described by the superposition of the fields of the individual sources.

The method required that the surface of the heat source be isothermal and the temperature distribution in the surrounding medium do not vary with time. Although not applicable to the estimation of GCHPs' dynamic behavior, it can be used as an auxiliary approach to compare and appraise the effectiveness of different backfills. Moreover, this technique can also be utilized to find the equivalent diameter of the U-tube under steady state based on the equivalent *ETR*. This later application is described in Chapter IV.

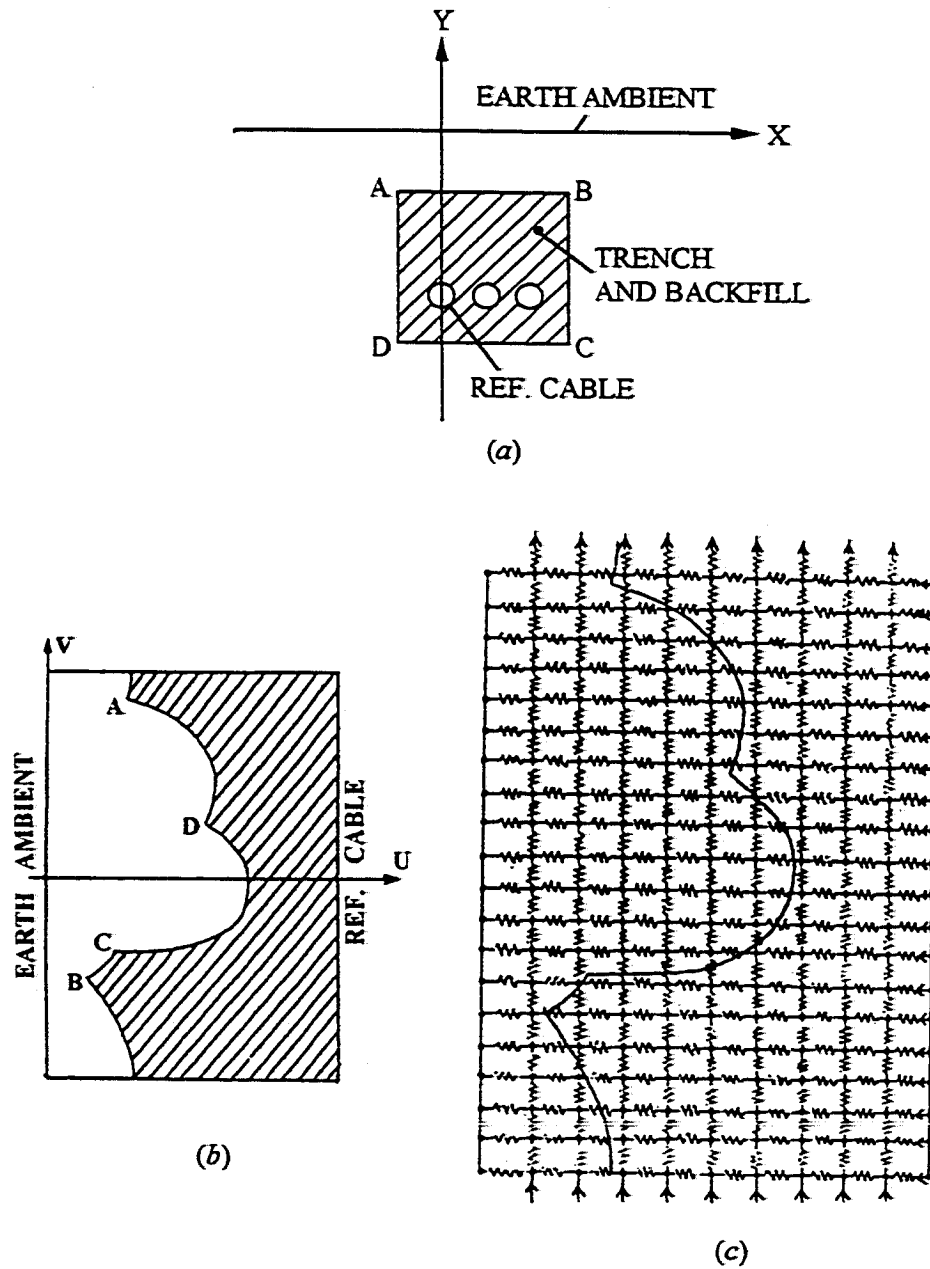


**Fig. 2.6 Procedure of conformal mapping used by Winders (after Winders, 1977). (a) cable system; (b) mapped rectangular region; (c) thermal resistive network**

### CHAPTER III

#### DEVELOPMENT AND VERIFICATION OF AN ANALYTICAL SOLUTION

The existing analytical solutions — the Kelvin line source solution and Carslaw and Jaeger's cylindrical source solution, are all for homogeneous media. However, a non-homogeneous region, consisting of the backfill and the soil, typically surrounds the ground heat exchanger in a GCHP system. Because this region is layered with the backfill nearest the heat exchanger and the soil further out, it is an infinite composite region. Investigations of the effect of the backfill on the U-tube performance were desired and an analytical solution was derived in this chapter.

#### Generalized Orthogonal Expansion Technique

An analytical solution was developed for the transient temperature distribution in a finite composite medium internally bounded by a permanent cylindrical heat source. The medium is composed of the soil and the backfill regions that are concentric with the heat source. This is illustrated in Fig. 3.1. The primary assumptions and discussion of them are provided below.

1. The soil and the backfill regions are homogeneous, respectively. Soils can be extremely non-homogeneous, with different layers of soils, different moisture content, etc. However, the distribution of the non-homogenous properties are often not known in GCHP applications.
2. Thermal contact resistance is neglected at any interface. If the backfill material makes good contact with both the pipe surface and soil interface, this assumption would not be violated.

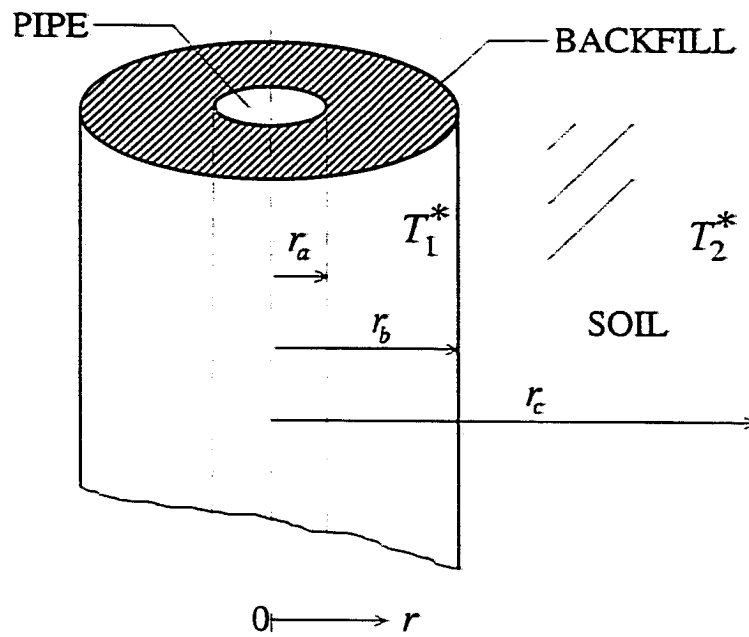


Fig. 3.1 Schematic of the pipe, backfill and surrounding soil

3. A constant and uniform heat emission,  $Q'$ , is applied to the ground at the pipe surface. In a real system, the heat transfer from the system varies with the load on the building as well as the temperature of the backfill adjacent to the pipe. The system cycles on and off with load. Cycling can be approximated by a series of "on-off" pulses utilizing superposition with the solution derived here.
4. The initial temperature is uniform throughout the whole domain at an arbitrary value. These provide initial conditions for the solution. With a system that has been operating for a period of time, the surrounding temperatures are not uniform.
5. The buried pipe is assumed infinitely long. Most GCHP loops have length to diameter ratios over 1000. Thus, end effects should be negligible.
6. An imaginary far-field boundary is set at  $r = r_c$  (See Fig. 3.1) where the temperature may be taken as a constant (far-field temperature) equal to the initial value. If this point is far enough away from the pipe surface, then its temperature will not change unless exceptionally long periods of time are considered. This assumption has been justified experimentally (Coogan, 1949; Dobson, 1991).

The geometric symmetry shown in Fig. 3.1, plus assumptions 1 and 5, makes the heat flow one dimensional in the radial direction. Several analytical methods are available in principle for solving transient boundary-value problems. They include the Laplace transformation, the integral transform technique, the adjoint-solution technique, and the generalized orthogonal expansion technique. Although the Laplace transformation of the differential equations established for the current problem is a



straightforward matter, the inversion of the transform will be quite involved. The integral transform and the generalized orthogonal techniques both derive their basis from the classical method of separation of variables. However, the application of the integral transform technique to this heat-conduction problem will entail more complicated calculations. The primary disadvantage of the adjoint-solution method is that only the solutions on the boundaries/interfaces can be determined. Thus, it was not used here.

The orthogonal expansion technique is essentially an extension of the Sturm-Liouville problem (see Guenther and Lee, 1988) to the case of a one-dimensional multilayer region. It has the advantage over other analytical methods in that its application to transient heat-conduction problems is relatively simple, straightforward and similar to the ordinary expansion process in one-layer problems. As was explained by Tittle (1965): "The theorem allows a solution of multiregion problems by a direct expansion without resort to integral transformation or Green's functions. It is an extension of the method of separation of variables heretofore beyond its scope." This technique is based on the contributions by Vodicka (1950 and 1955) and Tittle (1965) and was discussed rigorously in the late 1960s and early 1970s. Among these are Bulavin and Kascheev (1965), Tittle and Robinson (1965), Beach (1967), Özisik (1968 and 1980) and Mulholland and Cobble (1972), with Özisik (1968) providing a comprehensive review of the literature. Mulholland and Cobble (1972) considered the case of a three-layered composite of lead, aluminum and tin with the temperatures at both ends prescribed. They provided the time dependent temperature distributions from 0.0008 hours to nearly one hour. Many other examples were given by Özisik (1968 and 1980).

The generalized orthogonal expansion technique was chosen in this study. The technique can only be used for a finite medium. However, under a proper assumption of a fictitious far-field boundary far enough from the pipe surface as stated in assumption 6, the method can be applied to the infinite medium in the real case. In this sense, the obtained solution is an approximate analytical solution. The solution is derived below in dimensionless form.

### Mathematical Model

In the cylindrical coordinates and in terms of the temperature in excess of the initial value  $\theta(r, t)$ , the basic heat conduction equation becomes (Fig. 3.1)

$$\frac{\partial^2 \theta_i}{\partial r^2} + \frac{1}{r} \frac{\partial \theta_i}{\partial r} = \frac{1}{\alpha_i} \frac{\partial \theta_i}{\partial t} \quad (i=1,2) \quad r_a \leq r \leq r_c, t \geq 0 \quad (3.1)$$

The subscript 1 stands for the backfill material, and subscript 2 refers to the soil. Subject to the following boundary and initial conditions:

$$-k_1 \frac{\partial \theta_1}{\partial r} = \frac{Q'}{2\pi r_a} \quad r=r_a, t>0 \quad (3.2a)$$

$$\theta_1 = \theta_2, \quad k_1 \frac{\partial \theta_1}{\partial r} = k_2 \frac{\partial \theta_2}{\partial r} \quad r=r_b, t>0 \quad (3.2b)$$

$$\theta_2 = 0 \quad r=r_c, t>0 \quad (3.2c)$$

$$\theta_{1,2} = 0 \quad t=0, r_a \leq r \leq r_c \quad (3.2d)$$

If a group of non-dimensional numbers are chosen as

$$Fo = \alpha_2 t / r_a^2, \quad T^* = k_2 \theta / Q', \quad r^* = r / r_a$$

with the following definitions:

$$G_1 = \alpha_1 / \alpha_2, G_2 = \alpha_2 / \alpha_2 = 1, H = k_1 / k_2, S_b = r_b / r_a, S_c = r_c / r_a$$

the above equation can be put into non-dimensional form

$$\frac{\partial^2 T_i^*}{\partial r^{*2}} + \frac{1}{r^*} \frac{\partial T_i^*}{\partial r^*} = \frac{1}{G_i} \frac{\partial T_i^*}{\partial Fo} \quad (i = 1, 2) \quad 1 \leq r^* \leq S_c, \quad Fo \geq 0 \quad (3.3)$$

Subject to the following boundary (non-homogeneous) and initial conditions:

$$\frac{\partial T_1^*}{\partial r^*} = -\frac{1}{2\pi H} \quad r^* = 1, \quad Fo > 0 \quad (3.4a)$$

$$T_1^* = T_2^*, \quad \frac{\partial T_1^*}{\partial r^*} = \frac{1}{H} \frac{\partial T_2^*}{\partial r^*} \quad r^* = S_b, \quad Fo > 0 \quad (3.4b)$$

$$T_2^* = 0 \quad r^* = S_c, \quad Fo > 0 \quad (3.4c)$$

$$T_{1,2}^* = 0 \quad Fo = 0, \quad 1 < r^* < S_c \quad (3.4d)$$

Let

$$T_i^*(r^*, Fo) = U_i(r^*, Fo) + V_i(r^*) \quad (i = 1, 2) \quad (3.5)$$

The functions  $U_i(r^*, Fo)$  and  $V_i(r^*)$  are solved in the following two subproblems:

I. The functions  $V_i(r^*), i = 1, 2$  satisfy the steady-state heat-conduction problem given

as

$$\frac{d^2 V_1}{dr^{*2}} + \frac{1}{r^*} \frac{dV_1}{dr^*} = 0 \quad 1 \leq r^* \leq S_b \quad (3.6a)$$

$$\frac{d^2 V_2}{dr^{*2}} + \frac{1}{r^*} \frac{dV_2}{dr^*} = 0 \quad S_b \leq r^* \leq S_c \quad (3.6b)$$

Subject to the boundary conditions

$$\frac{dV_1}{dr^*} = -\frac{1}{2\pi H} \quad r^* = 1 \quad (3.7a)$$

$$V_1 = V_2, \quad \frac{dV_1}{dr^*} = \frac{1}{H} \frac{dV_2}{dr^*} \quad r^* = S_b \quad (3.7b)$$

$$V_2 = 0 \quad r^* = S_c \quad (3.7c)$$

The solutions are obtained as

$$V_1(r^*) = -\frac{1}{2\pi H} \ln\left(\frac{S_b^{H-1} r^*}{S_c^H}\right), \quad V_2(r^*) = -\frac{1}{2\pi} \ln\left(\frac{r^*}{S_c}\right) \quad (3.8)$$

2. The functions  $U_i(r^*, Fo)$ ,  $i = 1, 2$  are the solutions of the following transient heat conduction problem:

$$\frac{\partial^2 U_i}{\partial r^{*2}} + \frac{1}{r^*} \frac{\partial U_i}{\partial r^*} = \frac{1}{G_i} \frac{\partial U_i}{\partial Fo} \quad (i = 1, 2) \quad 1 \leq r^* \leq S_c, \quad Fo \geq 0 \quad (3.9)$$

Subject to the following homogeneous boundary conditions:

$$\frac{\partial U_1}{\partial r^*} = 0 \quad r^* = 1, \quad Fo > 0 \quad (3.10a)$$

$$U_1 = U_2, \quad \frac{\partial U_1}{\partial r^*} = \frac{1}{H} \frac{\partial U_2}{\partial r^*} \quad r^* = S_b, \quad Fo > 0 \quad (3.10b)$$

$$U_2 = 0 \quad r^* = S_c, \quad Fo > 0 \quad (3.10c)$$

and to the initial conditions (Note: different from the original):

$$U_{1,2} = -V_{1,2} \quad (i = 1, 2) \quad Fo = 0, \quad 1 < r^* < S_c \quad (3.11)$$

To solve this problem, assume separation of variables in the form

$$U_i(r^*, Fo) = \varphi_i(r^*) \Gamma(Fo) \quad (i = 1, 2) \quad (3.12)$$

Substituting equation (3.12) into equation (3.9) results in the following separated equations for the functions  $\Gamma(Fo)$  and  $\varphi_i(\beta, r^*)$ :

$$\frac{d\Gamma(Fo)}{dFo} + \beta_n^2 \Gamma(Fo) = 0 \quad Fo > 0 \quad (3.13)$$

and

$$\frac{d^2 \varphi_{in}}{dr^{*2}} + \frac{1}{r^*} \frac{d \varphi_{in}}{dr^*} + \frac{\beta_n^2}{G_i} \varphi_{in} = 0 \quad (i = 1, 2) \quad 1 \leq r^* \leq S_c \quad (3.14)$$

where  $\beta_n$  are the eigenvalues and  $\varphi_{in} \equiv \varphi_i(\beta_n, r^*)$  the eigenfunctions. There are an infinite number of discrete values of  $\beta_n$

$$\beta_1 < \beta_2 < \beta_3 < \dots < \beta_n < \dots$$

and the corresponding eigenfunctions  $\varphi_{in}$ .

The solution for the transient function  $\Gamma(\text{Fo})$  is immediately obtained from equation (3.13) as

$$\Gamma(\text{Fo}) = \exp(-\beta_n^2 \text{Fo}) \quad (3.15)$$

The boundary conditions for equations (3.14) are obtained by introducing equation (3.12) into the boundary conditions (3.10) as

$$\frac{d \varphi_{1n}}{dr^*} = 0 \quad r^* = 1 \quad (3.16a)$$

$$\varphi_{1n} = \varphi_{2n}, \quad \frac{d \varphi_{1n}}{dr^*} = \frac{1}{H} \frac{d \varphi_{2n}}{dr^*} \quad r^* = S_b \quad (3.16b)$$

$$\varphi_{2n} = 0 \quad r^* = S_c \quad (3.16c)$$

Equations (3.14) subject to the boundary conditions (3.16) constitute an eigenvalue problem for the determination of the eigenvalues  $\beta_n$  and the corresponding eigenfunctions  $\varphi_{in}$ . The solutions for the eigenfunctions  $\varphi_{in}$  take the following form:

$$\varphi_{in}(r^*) = A_{in} J_0 \left( \frac{\beta_n r^*}{\sqrt{G_i}} \right) + B_{in} Y_0 \left( \frac{\beta_n r^*}{\sqrt{G_i}} \right) \quad (i = 1, 2) \quad (3.17)$$

where  $A_{1n}$  and  $B_{1n}$ ,  $i = 1, 2$  are coefficients. By introducing boundary conditions (3.16) into the above equations and taking  $A_{1n}$  as unity,  $B_{1n}$ ,  $A_{2n}$  and  $B_{2n}$  become

$$A_{1n} = 1 \quad (3.18a)$$

$$B_{1n} = -J_1(\beta_n / \sqrt{G_1}) / Y_1(\beta_n / \sqrt{G_1}) \quad (3.18b)$$

$$A_{2n} = \frac{J_0(\beta_n S_b / \sqrt{G_1}) / B_{1n} Y_0(\beta_n S_b / \sqrt{G_1})}{J_0(\beta_n S_b) - [J_0(\beta_n S_c) / Y_0(\beta_n S_c)] Y_0(\beta_n S_b)} \quad (3.18c)$$

$$B_{2n} = -A_{2n} J_0(\beta_n S_c) / Y_0(\beta_n S_c) \quad (3.18d)$$

The eigenvalues  $\beta_n$  are found by solving the following transcendental equation:

$$\begin{vmatrix} J_1(\beta_n / \sqrt{G_1}) & Y_1(\beta_n / \sqrt{G_1}) & 0 & 0 \\ J_0(\beta_n S_b / \sqrt{G_1}) & Y_0(\beta_n S_b / \sqrt{G_1}) & -J_0(\beta_n S_b) & -Y_0(\beta_n S_b) \\ FJ_1(\beta_n S_b / \sqrt{G_1}) & FY_1(\beta_n S_b / \sqrt{G_1}) & -J_1(\beta_n S_b) & -Y_1(\beta_n S_b) \\ 0 & 0 & J_0(\beta_n S_c) & Y_0(\beta_n S_c) \end{vmatrix} = 0 \quad (3.19)$$

where  $F = H / \sqrt{G_1}$ . The general solution for  $U_i(r^*, Fo)$ ,  $i = 1, 2$  is constructed as

$$U_i(r^*, Fo) = \sum_{n=1}^{\infty} C_n \varphi_{in}(r^*) \exp(-\beta_n^2 Fo) \quad (i = 1, 2) \quad (3.20)$$

where the summation is over all eigenvalues  $\beta_n$ . This solution satisfies the differential equations (3.9) and the boundary conditions (3.10). We now constrain this solution to satisfy the initial condition (3.11), and obtain

$$-V_i(r^*) = \sum_{n=1}^{\infty} C_n \varphi_{in}(r^*) \quad (i = 1, 2) \quad 1 < r^* < S_c \quad (3.21)$$

The coefficients  $C_n$  can be determined by utilizing the following orthogonality relation:

$$\frac{H}{G_1} \int_1^{S_b} r^* \varphi_{1m}(r^*) \varphi_{1n}(r^*) dr^* + \int_{S_b}^{S_c} r^* \varphi_{2m}(r^*) \varphi_{2n}(r^*) dr^* = \begin{cases} 0 & \text{for } m \neq n \\ N_n & \text{for } m = n \end{cases} \quad (3.22)$$

where  $N_n$  is called norm and defined as

$$N_n = \frac{H}{G_1} \int_1^{S_b} r^* \varphi_{1n}^2(r^*) dr^* + \int_{S_c}^{S_e} r^* \varphi_{2n}^2(r^*) dr^* \quad (3.23)$$

and  $C_n$  is then

$$C_n = \left[ \frac{H}{G_1} \int_1^{S_b} r^* \varphi_{1n}(r^*) V_1(r^*) dr^* + \int_{S_c}^{S_e} r^* \varphi_{2n}(r^*) V_2(r^*) dr^* \right] / N_n \quad (3.24)$$

Finally, the solution for the dimensionless temperature  $T_i^*(r^*, Fo)$  is given as

$$T_i^*(r^*, Fo) = \frac{1}{2\pi H} \left( \sum_{n=1}^{\infty} C_n \varphi_{in}(r^*) \exp(-\beta_n^2 Fo) - W_i(r^*) \right) \quad (i = 1, 2) \quad (3.25)$$

where

$$W_1(r^*) = \ln \left( \frac{S_b^{H-1} r^*}{S_c^H} \right), \quad W_2(r^*) = H \ln \left( \frac{r^*}{S_c} \right)$$

In the following discussion and all the subsequent chapters,  $G$  refers to  $G_1$ . The generality of the normalized solution above is highly conditional on the relationship between the soil and the backfill properties accounted for by ratios  $H$ ,  $G$ ,  $S_b$  and  $S_c$  which include the thermal properties of soil  $k_2$  and  $\alpha_2$  in the non-dimensional numbers. But as far as the investigation on effects of backfills is concerned, one may fix all the parameters except  $H$  and  $G$ . One of the concerns in the design or simulation to a GCHP system is how the temperature at the pipe surface varies. These surface temperatures reflect the temperature of the water circulating through the pipes.

To calculate a useful solution to the problem for ground coupled heat exchangers, it was first necessary to look at ranges in values of some of the variables that would be applicable to ground coupled heat pump applications. Equations (3.23) and (3.24) required fixed values for  $S_b$  and  $S_c$  for the limits of integration.  $S_b$ , which was the ratio of

the radius of the hole drilled for the backfill and pipe to the pipe radius, could be expected to vary from 3 to 10, depending on the installation. The value of  $S_c$  fixed the far-field boundary conditions and should be far enough away from the pipe to not show any change in temperature for long periods of time. Dobson (1991) used temperature probes at a distance of 6.1 m away from the ground heat exchanger and at a depth of 12 m to measure ambient ground temperatures for a vertical ground coupled heat pump. Changes of less than 0.5 °C were found at that location throughout the 155 days' cooling season. For a 12.7 mm radius pipe, this would correspond to an  $S_c$  value of 480. A more conservative value of 909 was used here. This would correspond to a radius of 11.5 m. The ratios  $H$  and  $G$  may vary from 0.5 to 2.0 for most GCHPs. However, a wide range of values of  $H$  (0.1 to 10) and  $G$  (0.33 to 3.0) were selected in the following sections to facilitate the understanding of the backfill's impact. The range in Fourier numbers selected was from 0.3 to 840,000. For a soil with a thermal diffusivity of  $0.97 \times 10^{-6} \text{ m}^2/\text{s}$  and a pipe radius of 12.7 mm, this range in Fourier numbers would correspond to times from one minute to five years.

### Behaviors of the Solution

Although the calculation of the determinant in equation (3.19) was not straightforward, it was found that the arrangement of the zeros was surprisingly regular. The interval between any two adjacent zeros was nearly a constant (the variation was less than 0.5%) for all the cases considered below. Note that such a situation may not be true for other cases (see, e.g., Mulholland and Cobble, 1972). Table 3.1 lists the first ten eigenvalues for the homogeneous case, where the thermal properties of the backfill were



**Table 3.1** Values of the first ten eigenvalues for the case where  $H=G=1$

$n$	$\beta_n$	$n$	$\beta_n$
1	0.0570	6	0.4286
2	0.1309	7	0.5031
3	0.2052	8	0.5776
4	0.2797	9	0.6521
5	0.3541	10	0.7266

the same as those of the surrounding soil ( $G = 1$  and  $H = 1$ ). The calculation of the coefficients,  $C_n$ , required an extremely fine grid for use in the numerical integration, otherwise the series would not converge. Up to one thousand terms in the series had to be used to achieve satisfactory results for a short-time simulation (say, Fourier numbers less than one). The exponential form of the series in equation (3.25), however, rapidly reduced the number of the terms required for longer term simulations.

Initially, a small temperature oscillation around zero occurred instead of the expected  $T^* \equiv 0$ . The oscillation started from the pipe surface and decayed quickly for increasing values of  $r^*$ . It is speculated that this oscillation was probably caused by the inconsistency between the initial and boundary conditions in the original equations. There was a specified heat flux instead of a temperature boundary condition at the pipe surface but the initial condition demanded the excess temperature be zero everywhere including the surface. While not specifically calculated, the value of the net area integration of the wave appeared to be close to zero. The amplitude of the oscillation depended on how many terms in the series were taken. For example, for the homogeneous case, the maximum deviation in  $T^*$  which appeared at the pipe surface decreased from a value of 0.08 to 0.02 as the number of the terms increased from 345 to 1680. The oscillations also disappeared very rapidly with increasing values of the Fourier number. For Fourier numbers above 0.35, which would correspond to approximately one minute with a thermal diffusivity of  $0.97 \times 10^{-6} \text{ m}^2/\text{s}$  and radius of 0.012 m, there were no oscillations in the solution. Accurate solutions for smaller time increments would require either using more terms or using a numerical solution.

### Example Calculations

Some example calculations were made to show how the properties  $H$ ,  $G$ ,  $S_b$  and  $S_c$  affect the temperature profiles. The solution for  $T^*$  is presented as a series of curves (Fig. 3.2) plotted against the Fourier number for fifteen cases of different  $G$  and  $H$  values. In this plot, a wide range of values of  $H$  (0.1 to 10) and  $G$  (0.33 to 3.0) were combined to obtain these cases. The curves show the impact of the thermal properties of the backfill material on the non-dimensional surface temperature ( $T^*$ ) of the cylindrical heat source. For Fourier numbers smaller than 10,000, both  $H$  and  $G$  had a strong influence on the value of  $T^*$ . For example, at a Fourier number equal to one, and  $H$  equal to one, the value of  $T^*$  was almost twice as large for  $G = 3.0$  compared to  $G = 0.33$ . However, for a Fourier number of 10,000, there was no difference in  $T^*$  for the two values of  $G$ . Because GCHPs are often only on for less than 15 minutes at a time ( $Fo < 100$ ), these differences in  $T^*$  for small values of  $Fo$  would be significant in determining the water temperature in the heat exchanger.

The combination that produced the smallest  $T^*$  was a high value of  $H$  and a small value of  $G$ . Thus, what is most desirable from a backfill material is one that has a low thermal diffusivity compared to the surrounding soil (low  $G$ ) as well as a much higher thermal conductivity than the surrounding soil (high  $H$ ). The impact of  $G$  gradually decreased as conditions began to approach steady state with increasing value of the Fourier number. As would be expected,  $H$  became the sole influence on the value of  $T^*$ . The curves with the same  $H$  and different  $G$  values all converged into a single curve at large Fourier numbers. Higher  $H$  values resulted in lower values of  $T^*$ . However, the

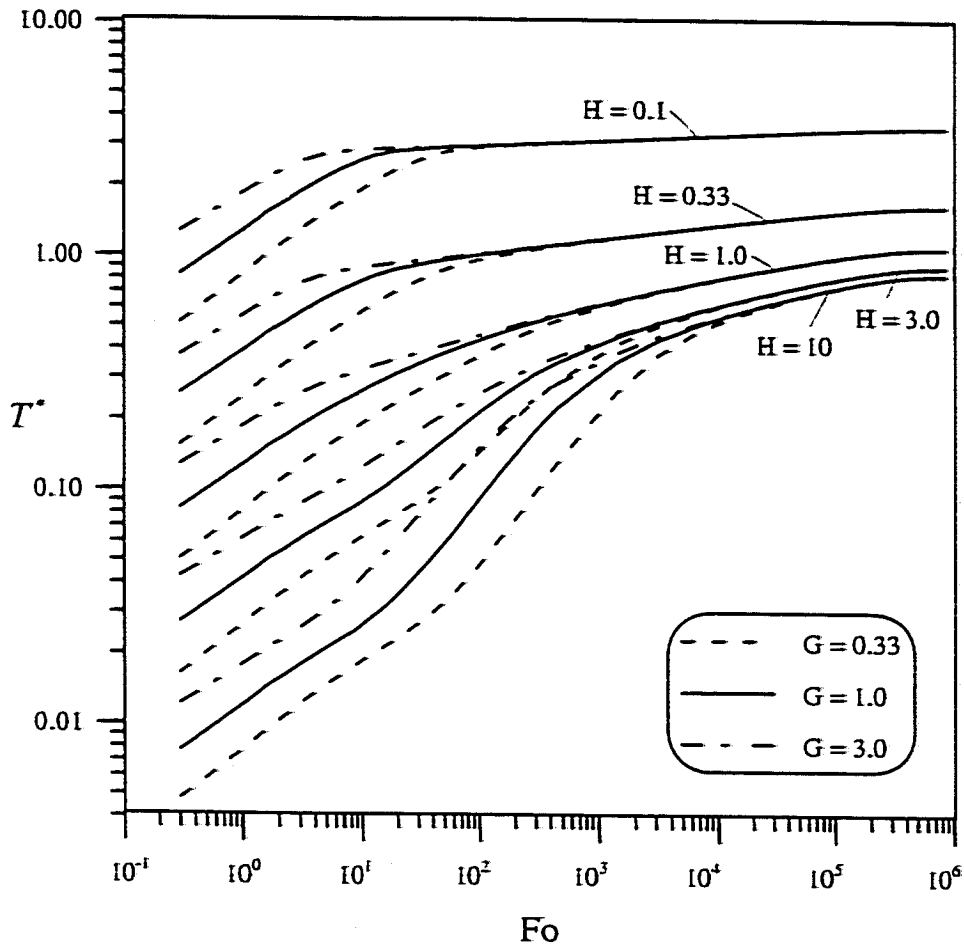


**Fig. 3.2** Values of  $T^*$  as a function of  $Fo$ ,  $G$  and  $H$

long term effect of a high  $H$  appears to be small. Increasing  $H$  from one to ten made approximately a 20% change in the value of  $T^*$  at a Fourier number equal to 10,000.

Figures 3.3 and 3.4 show the sensitivity of the results in Fig. 3.2 to assumptions regarding the values of  $S_c$  and  $S_b$ , respectively. In Fig. 3.3,  $S_b$  was fixed at 5.7 and the values of  $S_c$  were varied from 100 to 900. Fig. 3.3 shows that the value of  $T^*$  does not change for Fourier numbers less than approximately 2,000 by reducing the value of  $S_c$  down to 100 from 900. A Fourier number of 2,000 would be acceptable for evaluating the source surface temperature for small time intervals (about four days for many soils and heat exchanger configurations). If  $S_c$  was increased to 750, the deviation from the values calculated with  $S_c = 900$  begin to occur at Fo equal to approximately 100,000. Such a large Fourier number would allow accurate evaluations of the surface temperature for up to 9 months with many soils. It is noted that the time when those curves began to approach to their steady states was independent of  $H$  and  $G$ .

In Fig. 3.4, the value of  $S_c$  was fixed at 900 and the values of  $S_b$  were allowed to vary from 3 to 20. Two sets of curves are displayed from  $H = G = 3.0$  and  $H = G = 0.33$ . These curves started to separate from one another at very small Fourier numbers. The differences between values of  $T^*$  with different values of  $S_b$  were noticeably greater for the case of a poorly conducting backfill ( $H = 0.33$ ) than of a high thermal conductivity backfill ( $H = 3.0$ ).

In Fig. 3.2, one can also note that each of the lines with the same  $H$ , but different  $G$  values, eventually converged into a single curve at large enough Fourier numbers. The values of Fo at which these curves merged into one were examined. This value of the

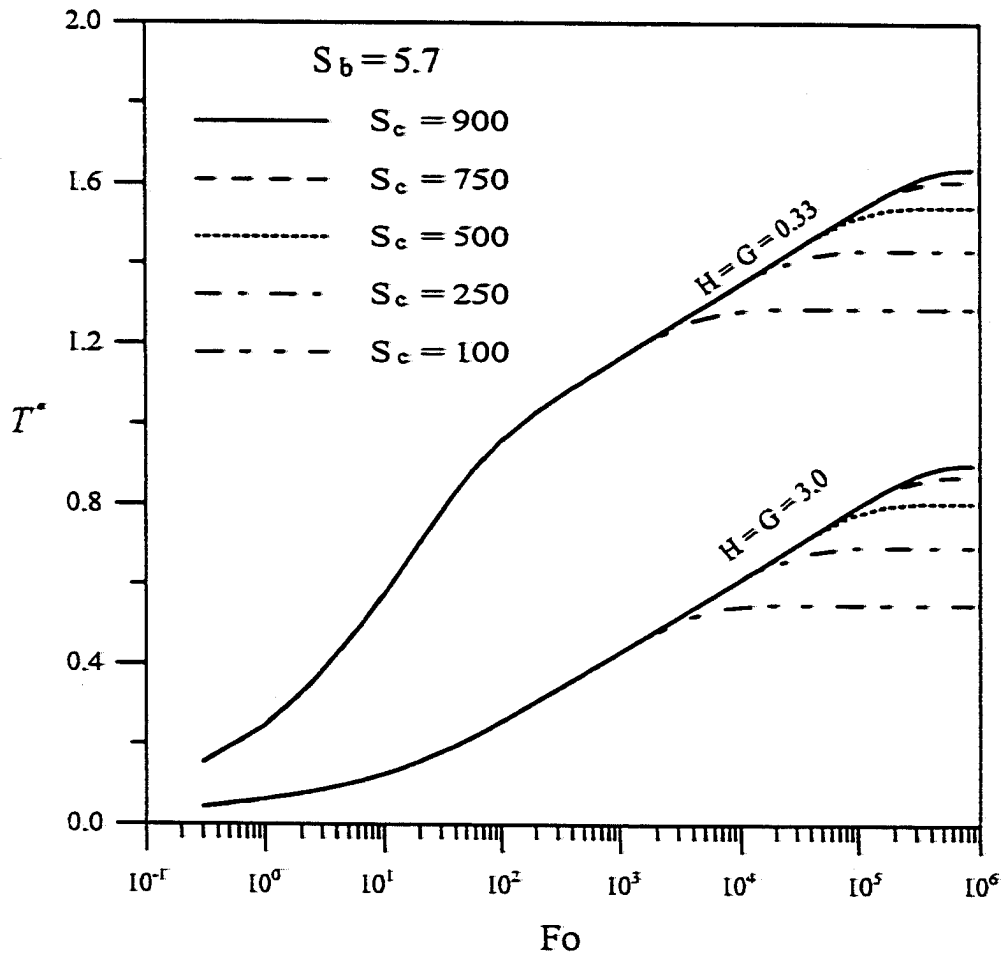


Fig. 3.3 Sensitivity of the results to assumptions about  $S_c$

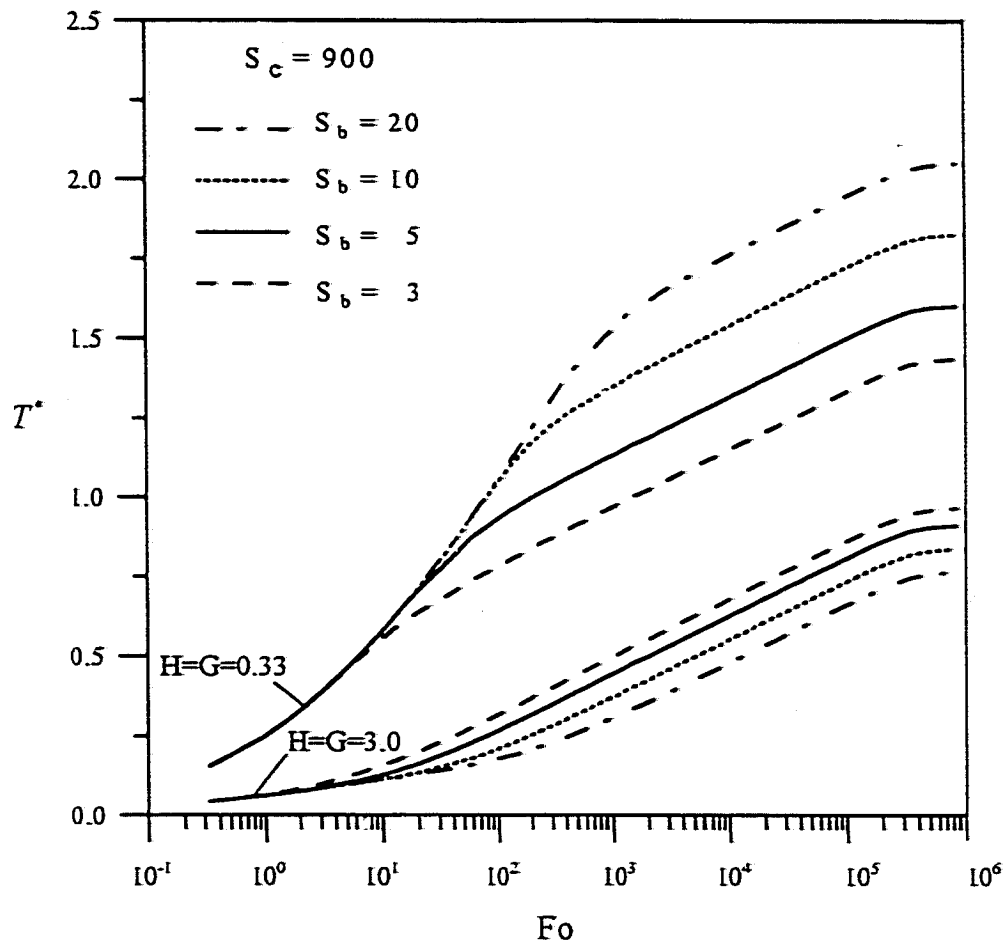


Fig. 3.4 Sensitivity of the results to assumptions about  $S_b$

Fourier number was designated as the characteristic Fourier number,  $Fo_c$  and is plotted in Fig. 3.5. For increasing values of  $H$ ,  $Fo_c$  increased as long as  $G$  was not equal to one. If  $p$  was any number greater than one, then lines with  $G = p$  had smaller  $Fo_c$  than ones with  $G = 1/p$ .

### Validation of the Solution

For the validation of this approach, two steps were taken. First, the entire region was made homogeneous by setting  $H = G = 1$  so that the results could be compared to those from the solution given by Jaeger (1942), which was also used by Ingersoll et al. (1954). This solution was commonly used for problems in an infinite homogeneous region with a long cylindrical source. It is reorganized in the non-dimensional form and shown below for reference

$$T^*(r^*, Fo) = \frac{1}{\pi^2} \int_0^{\infty} \frac{\exp(-\eta^2 Fo) - 1}{J_1^2(\eta) + Y_1^2(\eta)} [J_0(r^* \eta) Y_1(\eta) - J_1(\eta) Y_0(r^* \eta)] \frac{d\eta}{\eta^2} \quad (3.26)$$

Second, a conventional finite difference technique was applied with the same imaginary far-field boundary at  $r = r_c$  for the comparison in two heterogeneous cases.

The following parameters were chosen for the two steps

1. Homogeneous Medium

$$H = G = 1.0$$

2. Heterogeneous Medium

Case 1:  $H = G = 0.33$ ,

Case 2:  $H = G = 3.0$ .



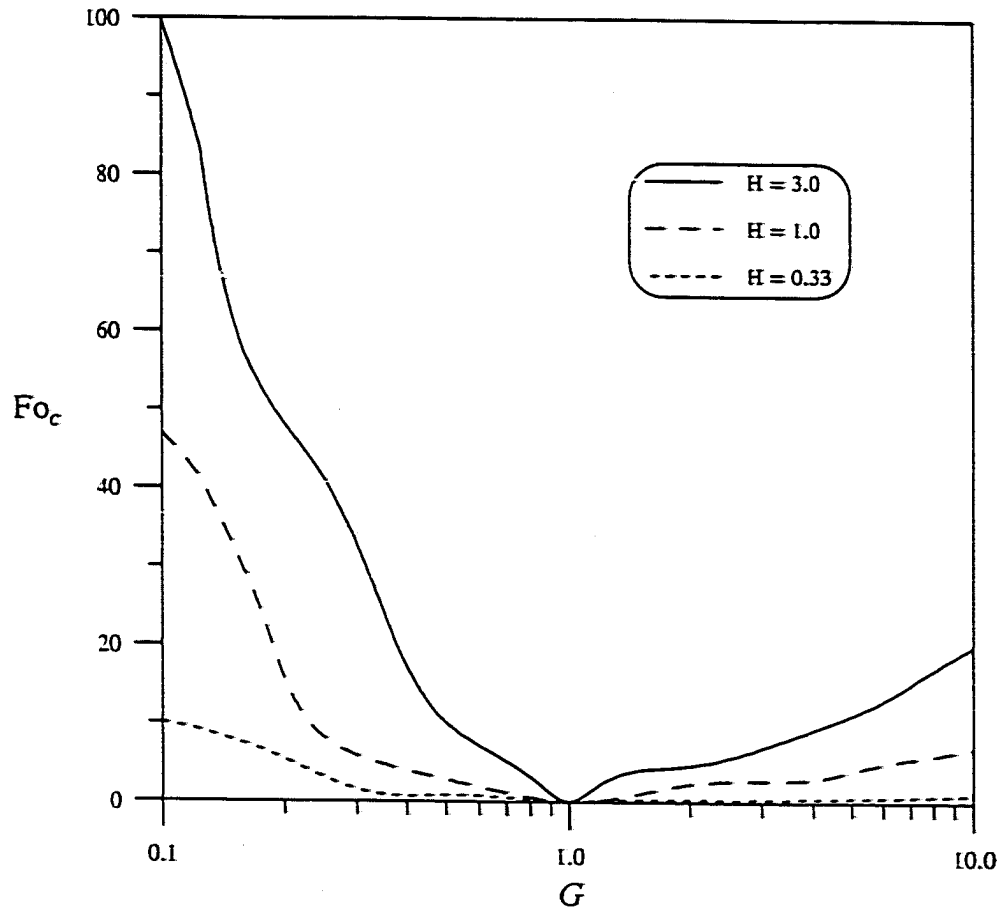


**Fig. 3.5 Values of the characteristic Fourier number as a function of  $G$  and  $H$**

For both steps,

$$k_2 = 1.73 \text{ W/m-K}, \alpha_2 = 0.97 \times 10^{-6} \text{ m}^2/\text{s}$$

$$r_a = 0.013 \text{ m}, S_b = 5.7, S_c = 909$$

$$Q' = +13.3 \text{ W/m (positive sign means heat rejection to the ground)}$$

The range of the Fourier number was from 0.3 to  $837 \times 10^3$ , which corresponded to times from one minute to five years.

The results are presented in Figs. 3.6 through 3.8. In these plots, the effectiveness of this method in predicting temperature change at any location within a wide range of time was verified. Figure 3.6 shows a comparison stated in step 1 at several representative times. They agreed very well except at the time of five years, which was because of the assumption of a finite boundary mentioned previously. Thus, the solution presented here for the composite medium would attain steady state while the infinite homogeneous solution would continue to rise because of the infinite boundary. The discrepancy between the pipe surface temperature rises calculated from these two methods varied from 0.04 to 2.2% for times from one minute to one year (not necessarily in that order) and is about 6% for year 5.

Comparisons between the analytical and the finite difference method for the two heterogeneous cases are shown in Figs. 3.7 and 3.8. The time intervals used in the numerical calculations were 1.0 and 0.3 minutes for cases 1 and 2, respectively. No comparisons were made available for year 5 due to a long time needed for the numerical calculations. The analytical and numerical solutions agreed reasonably well with the discrepancy at the pipe surface in the range of 0.73 to 4.5%.

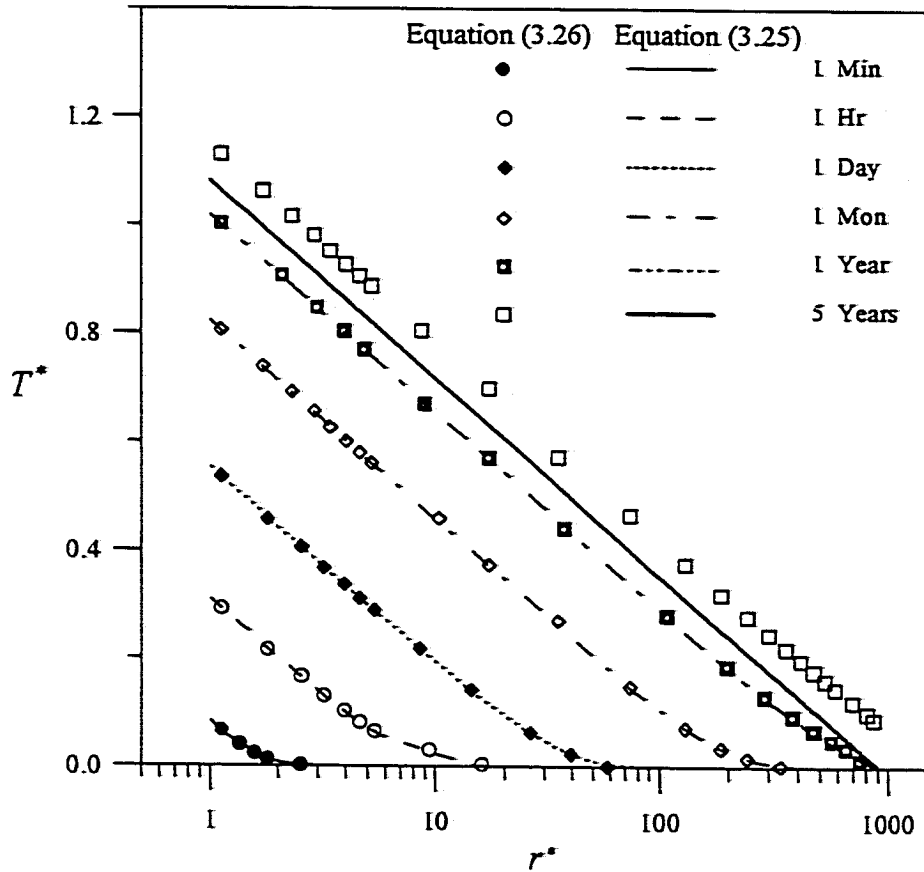


**Fig. 3.6 Comparison of the heterogeneous analytical solution (with homogeneous assumptions) and the homogeneous solution presented in equation 3.26**

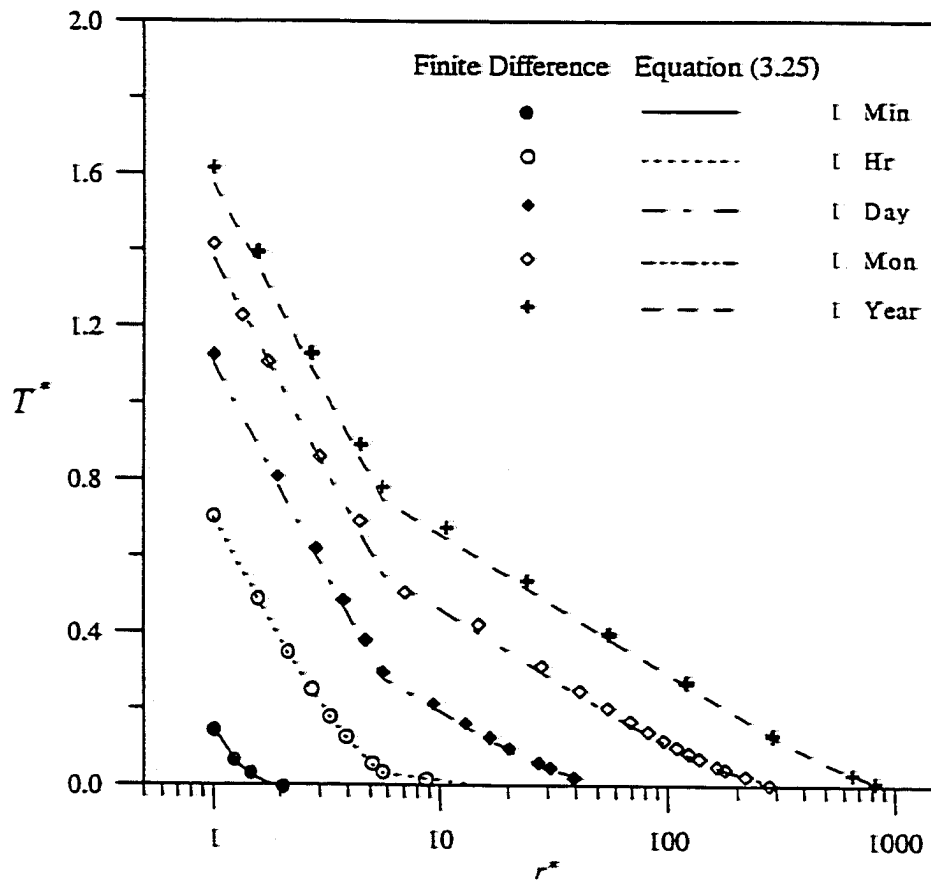
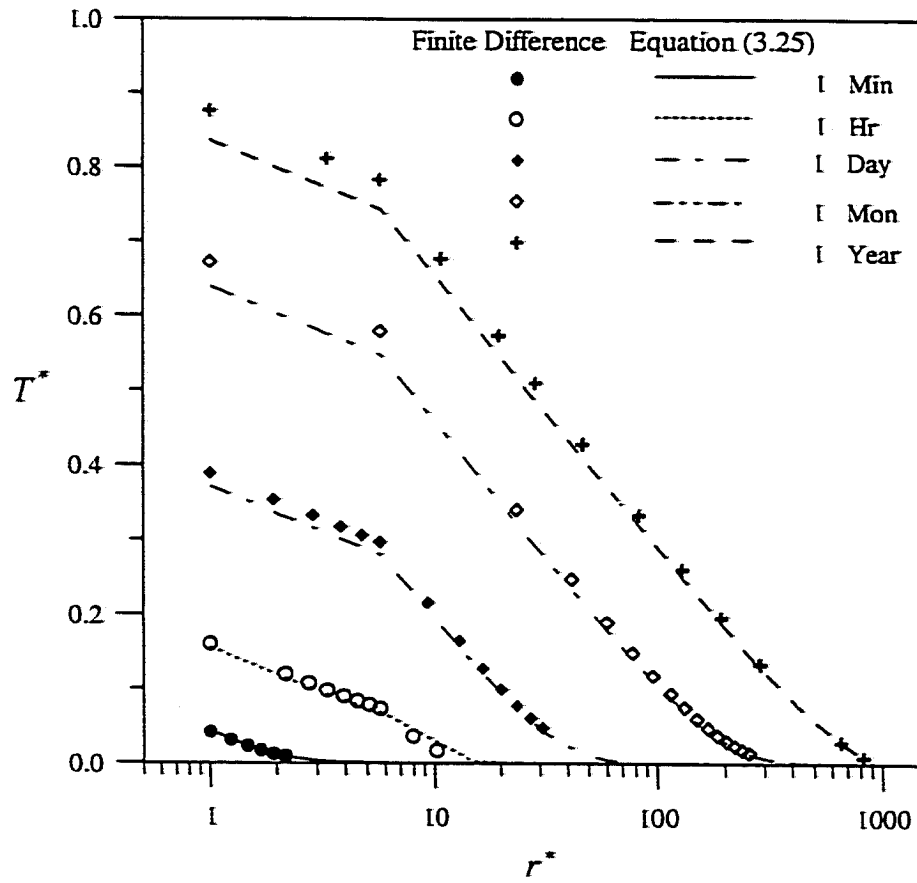


Fig. 3.7 Comparison between the heterogeneous analytical solution and a finite difference solution for  $H = G = 0.33$



**Fig. 3.8 Comparison between the heterogeneous analytical solution and a finite difference solution for  $H = G = 3.0$**

## CHAPTER IV

### DETERMINATION OF THE EQUIVALENT DIAMETER

Two questions arise about the application of the analytical solution obtained in the last chapter. First, this solution is given for a single heat source, while the U-tube heat exchanger has two parallel legs, or double sources. Because of this, there is thermal interference between the two legs. Can the analytical solution be extended to a U-tube heat exchanger geometry? Second, in deriving the solution, the pipe was assumed concentric with the backfill region as shown in Fig. 3.1. In a U-tube heat exchanger, neither of the legs is concentric with the backfill region (see Fig. 4.1(a)). Therefore, is it still possible to use a superposition technique in which the two legs are assumed concentric with the backfill region to develop a solution for a U-tube ground coil with the backfill around it?

If one imagines the existence of a single pipe instead of the two legs (Fig. 4.1(a)) and could find a general expression for the equivalent diameter ( $D_{eq}$ ) of this pipe for a variety of U-tube configurations with different pipe diameters ( $D$ ) and leg spacing ( $L_s$ ), it would then be possible to apply the analytical solution. The previously proposed values of  $D_{eq}$  were either for a specific case (legs touching) or the experimental data were too scattered to be useful as was discussed in Chapters I and II. Moreover, the researchers never directly related the equivalent diameter to the leg spacing in their analyses.

Simplifying assumptions must be made to obtain a general solution for the equivalent diameter. Therefore, the following procedure was used to obtain a general expression for the equivalent diameter:

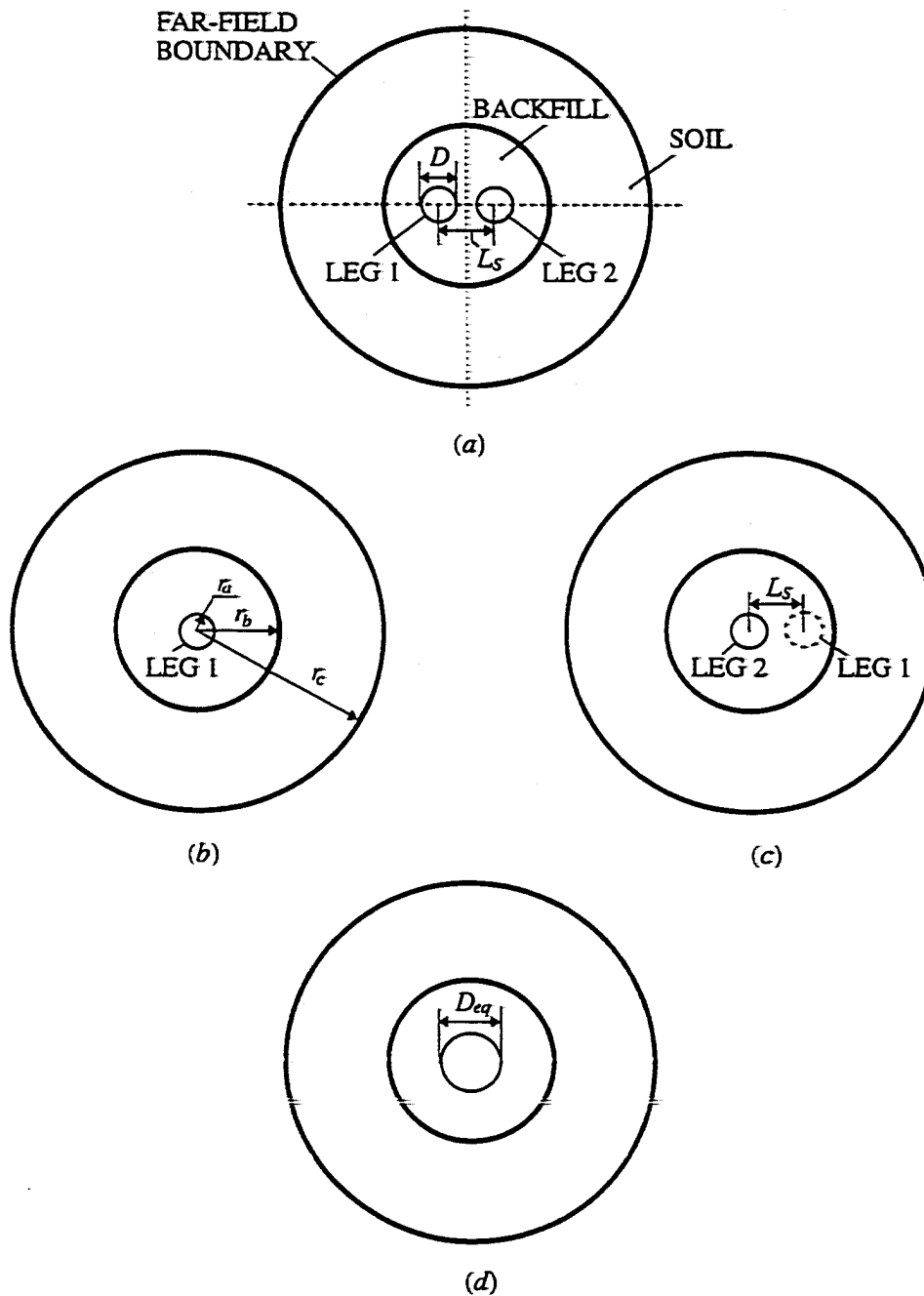


**Fig. 4.1 Procedure for derivation of the equivalent diameter**

1. An expression for  $D_{eq}$  was first developed under steady state. In the derivation, one of the legs was assumed concentric with the backfill region and the thermal influence of the other leg was estimated using the principle of superposition. The expression was obtained based on the equivalent external thermal resistance ( $ETR$ ) under steady state.
2. The analytical solution was used to calculate the transient temperature rise at the pipe surface for two cases: (1) a U-tube with equal constant heat flux at each leg, (2) the equivalent pipe with twice the heat flux as in case (1). The results were compared to examine the error caused by the application of the expression derived under steady state to a transient process.
3. Conformal mapping was used to evaluate the  $ETR$  of various U-tube configurations without the concentric assumption used in step 1. The results were compared with those obtained for the equivalent pipe as shown in Fig. 4.1(d) with corresponding values of  $D_{eq}$  determined using the expression. The assumption was justified in this way for a wide range of GCHP applications.

These steps are discussed in detail in the following sections.

### **Establishment of the Expression**

Figure 4.1 illustrates the derivation of the equivalent diameter. The following assumptions were used in the development of the expression for  $D_{eq}$ :

1. As shown in Fig. 4.1(b), one leg (leg 1) is first assumed concentric with both



the backfill and the far-field boundaries when calculating its surface temperature rise due to heat rejection of itself only. The same assumption is then made to the other leg (leg 2) for the estimation of its thermal effect on leg 1 (Fig. 4.1(c)). The leg spacing remains unchanged.

2. The leg spacing ( $L_S$ ) is defined as the distance between the two pipe centers. For the simplification of the derivation, let  $D \leq L_S \leq r_b$ , so that the center of leg 1 in Fig. 4.1(c) is never beyond the backfill boundary. This assumption is met by most GCHP applications.
3. Both sources of the U-tube dissipate heat at the same rates,  $Q'$ , while the source with the equivalent diameter emits heat at a rate of  $2Q'$ .
4. When considering the thermal field generated by one source, the existence of the other one is ignored.

According to Fourier's law, the temperature difference under steady state between the pipe surface of leg 1 and the far-field boundary (Fig. 4.1(b)) can be written as

$$\Delta T_{11} = \frac{Q'}{2\pi} \left[ \frac{\ln(r_b/r_a)}{k_1} + \frac{\ln(r_c/r_b)}{k_2} \right] \quad (4.1)$$

This is the temperature rise at leg 1 caused by its own heat flux. The average temperature rise at leg 1 created by leg 2 as shown in Fig. 4.1(c) (angular temperature variation around the pipe neglected) is determined as

$$\Delta T_{21} = \frac{Q'}{2\pi} \left[ \frac{\ln(r_b/L_S)}{k_1} + \frac{\ln(r_c/r_b)}{k_2} \right] \quad (4.2)$$

The total temperature rise at leg 1,  $\Delta T_1$ , is obtained by adding  $\Delta T_{21}$  to  $\Delta T_{11}$

$$\Delta T_1 = \frac{Q'}{2\pi} \left[ \frac{\ln(r_b^2/r_a L_S)}{k_1} + \frac{2\ln(r_c/r_b)}{k_2} \right] \quad (4.3)$$

Similarly, the total temperature rise at leg 2 can also be evaluated in this way and should achieve the same value, because the two legs are symmetric about the center line shown in Fig. 4.1(a). Thus, dividing equation (4.3) by  $2Q'$  yields the *ETR* between the two legs and the far-field boundary

$$(ETR)_{tot} = \frac{1}{2\pi} \left[ \frac{\ln(r_b/\sqrt{r_a L_S})}{k_1} + \frac{\ln(r_c/r_b)}{k_2} \right] \quad (4.4)$$

With the equivalent pipe shown in Fig 4.1(d), the resistance is immediately written as

$$(ETR)_{eq} = \frac{1}{2\pi} \left[ \frac{\ln(r_b/r_{eq})}{k_1} + \frac{\ln(r_c/r_b)}{k_2} \right] \quad (4.5)$$

where  $r_{eq} = D_{eq}/2$ . By comparing equations (4.4) and (4.5), one finds the expression for the equivalent diameter

$$D_{eq} = 2r_{eq} = 2\sqrt{r_a L_S} = \sqrt{2DL_S} \quad D \leq L_S \leq r_b \quad (4.6)$$

$D_{eq}$  derived here is proportional to the square root of  $D$  and  $L_S$  and is independent of other geometric parameters as well as the temperature boundary conditions.

With equation (4.6) and the definition of  $D_{eq} = CD$  stated in Chapter II, several specific cases are discussed below.

(1)  $L_S = D$ ,  $D_{eq} = \sqrt{2}D$ ,  $C = \sqrt{2}$ . This is the case of two pipes in contact and the

$C$  value is exactly the same as suggested by Claesson and Dunand (1983).

(2)  $L_S = 2D$ ,  $D_{eq} = 2D$ ,  $C = 2$ .

$$(3) L_S = 3D, D_{eq} = \sqrt{6}D, C = \sqrt{6}.$$

$$(4) L_S = 4D, D_{eq} = 2\sqrt{2}D, C = 2\sqrt{2}.$$

In cases (2) to (4), the  $C$  values are larger than all the values (1.0 - 1.84) proposed by other investigators as introduced in Chapter II.

Claesson and Dunand (1983) argued that the equivalent diameter must be smaller than twice the pipe diameter (i.e.,  $C < 2$ ). This was true when two pipes were in direct contact. However, for other cases with greater leg spacing,  $C$ -values could be two or more than two as was true for cases (2) to (4).  $C = 2$  means the heat source area of the equivalent pipe is twice that of a leg. It should be noted that unlike the heat conduction between two parallel planes of equal areas, doubled heat source area does not necessarily mean doubled heat transfer rate. This is explained below.

Let us focus on a homogeneous medium where  $k_1 = k_2$  and thus no backfill boundary exists. With reference to Fig. 4.1(b), the heat transfer rate per unit depth under steady state can be written as

$$Q' = \frac{2\pi k_1 \Delta T}{\ln(r_c/r_a)} \quad (4.7)$$

where  $\Delta T$  is the temperature difference between the heat source and the far-field boundary. Let this heat transfer rate be doubled; then we have

$$2Q' = \frac{2\pi k_1 \Delta T}{\ln\sqrt{r_c/r_a}} = \frac{2\pi k_1 \Delta T}{\ln(r_c/r'_a)} \quad (4.8)$$

where  $r'_a$  denotes an equivalent radius of the heat source in the second case and it can be immediately obtained as

$$r_a' = \sqrt{r_a r_c} = \sqrt{r_a^2 S_c} = r_a \sqrt{S_c} \quad (4.9)$$

Equation (4.9) means that the heat source area must be increased by  $\sqrt{S_c}$  to double the heat transfer rate.  $\sqrt{S_c}$  can be greater than 2. It follows that a  $C$ -value larger than two is possible and reasonable. Nevertheless, the heat transfer rate at the equivalent pipe surface must be smaller than twice that provided by one of two identical legs (including geometry and heat rejection) when it exists alone.

### Errors During Transient Processes

The application of the above expression for  $D_{eq}$  may cause some errors especially within a short time after a heat flux starts, since the expression was derived under steady state. Three cases were examined. Typical leg spacing is around  $2D$ . This value was first taken and so  $D_{eq} = 2D$ .  $H$  and  $G$  values were taken as 1 and 3, respectively (case 1 and case 2). To examine the error with a larger leg spacing, a group of parameters  $L_S = 4D$ ,  $D_{eq} = 2\sqrt{2}D$  and  $H = G = 1$  was also chosen (case 3). Other parameters concerning the soil properties, the geometry of the whole region and the heat transfer rate were the same as with the validation of the analytical solution in Chapter III. The transient temperature rises at the pipe surface of a U-tube were estimated using the classical cylindrical source solution (equation (3.26)) for the homogeneous cases or using the analytical solution (equation (3.25)) for the composite medium. The same superposition method was utilized as stated in assumption 1 in the last section and graphically indicated in Figs. 4.1(b) and (c). The temperature rises at the corresponding equivalent pipes with  $D_{eq}$  given by

equation (4.6) were then calculated.

Figures 4.2 through 4.4 show the temperature increases along with the relative errors (absolute values) for these cases. The maximum errors were about 16%, 14% and 18% in cases 1, 2 and 3, respectively. These figures indicated that the error curves became quite steep near their peaks. It took 54, 75 and 11 minutes respectively for the errors to drop below 5%.

### **Justification Using Conformal Mapping Technique**

The expression for the equivalent diameter was achieved using the assumption of concentricity. How much difference such an assumption would yield becomes a concern at this point. The comparison was made based on *ETR* values. The *ETR* value of the equivalent pipe was easily calculated with equation (4.5). However, the evaluation of *ETR* under the actual non-concentric situation required some modification to the heat transfer system. Assumptions similar to those discussed in the former sections were also used here except that one leg and the far-field boundary were assumed concentric on the origin, but the backfill region was assumed eccentric (Fig 4.5). This new assumption was equivalent to moving the contents within the backfill boundary by a distance equal to the actual eccentricity ( $E$ ) of the leg. It should result in a small difference as long as a large enough far-field boundary was chosen. It was due to this assumption that the conformal mapping technique was utilized. The purpose of the mapping was to transform the whole circular region to a rectangle with its two edges representative of the circumferences of the pipe at the center and the far-field boundary (Fig. 4.6). In this way, the ordinary finite

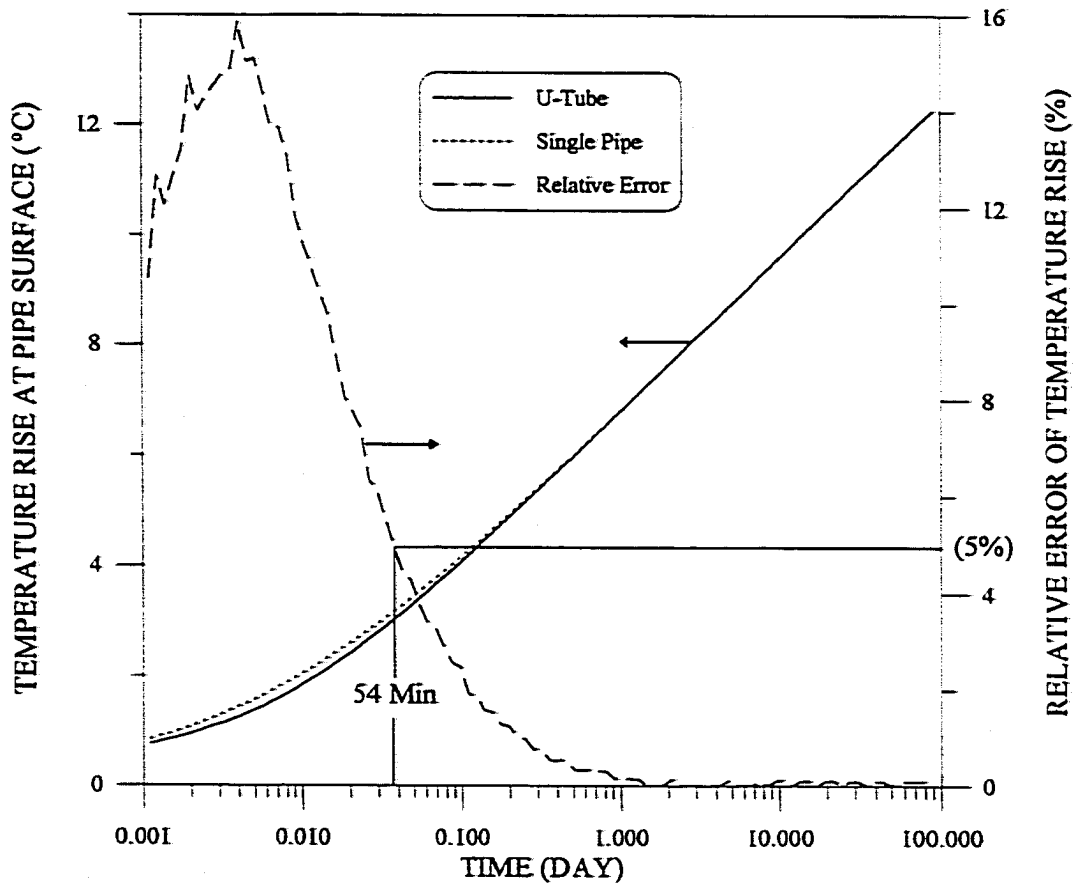


Fig. 4.2 Comparison of the temperature rises calculated for the U-tube and a single pipe with the equivalent diameter  $D_{eq} = 2D$  when  $H = G = 1$

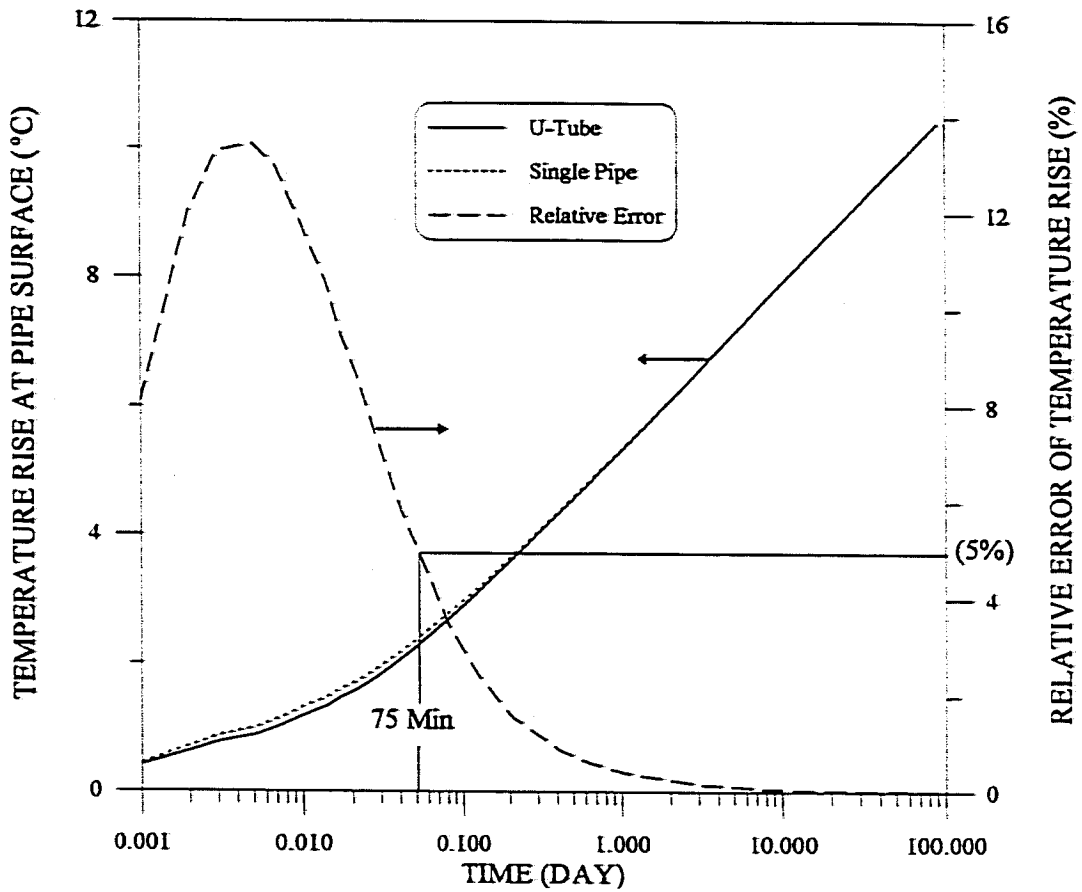


Fig. 4.3 Comparison of the temperature rises calculated for the U-tube and a single pipe with the equivalent diameter  $D_{eq} = 2D$  when  $H = G = 3$

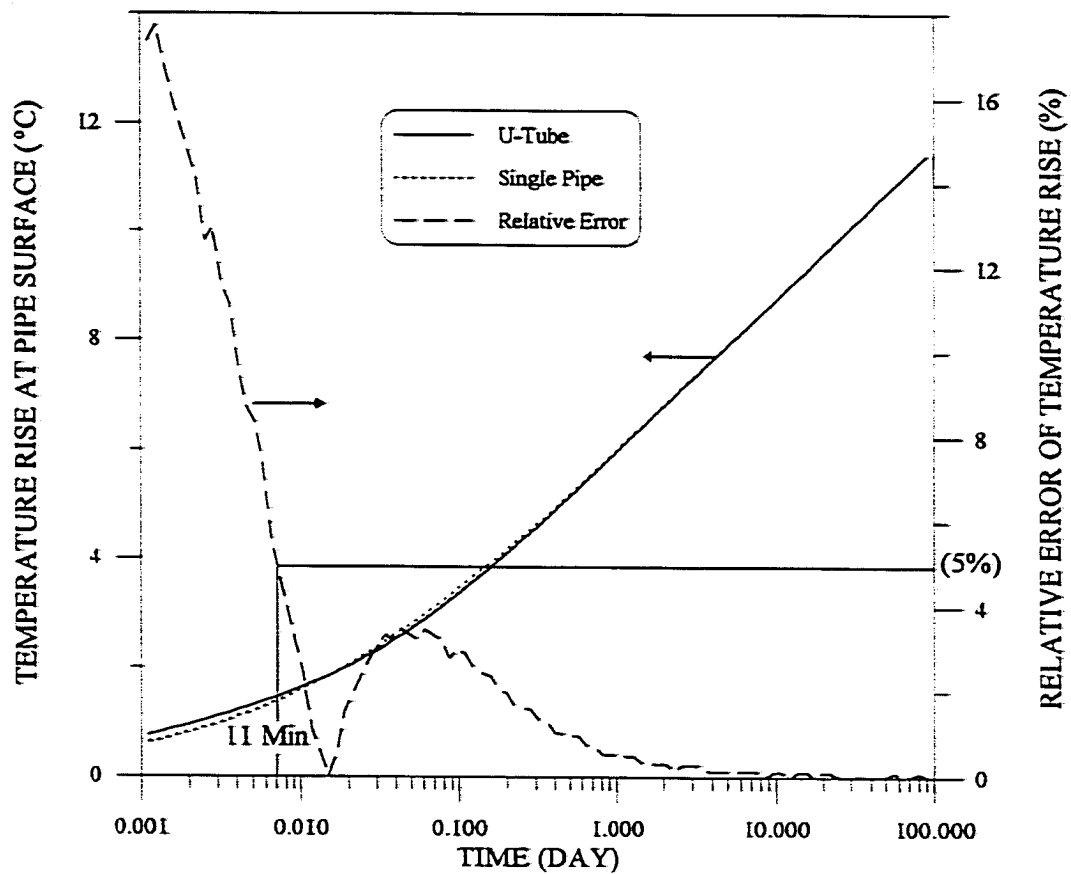
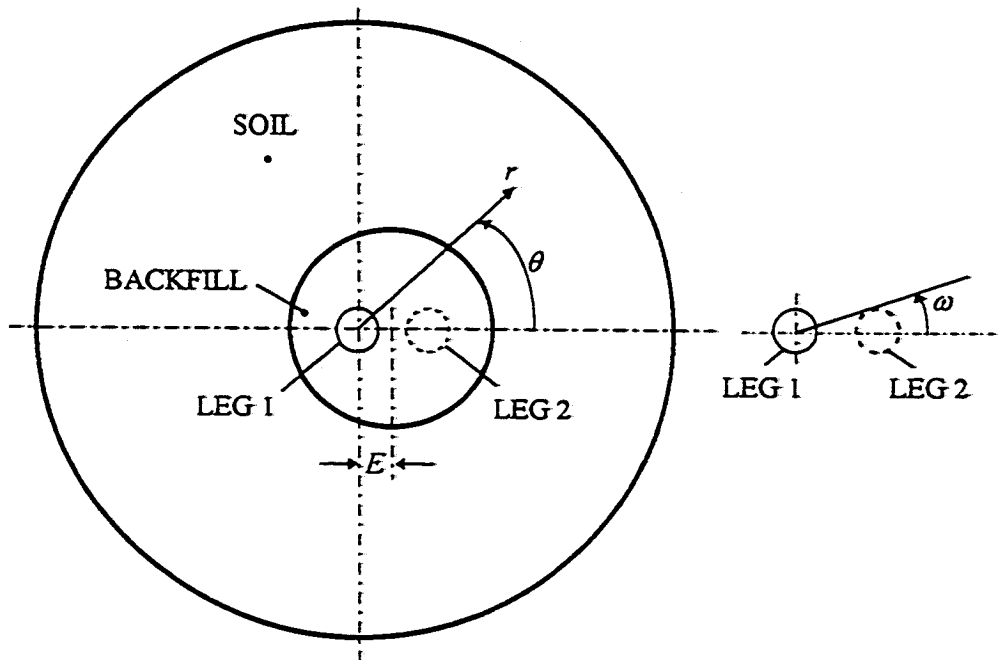


Fig. 4.4 Comparison of the temperature rises calculated for the U-tube and a single pipe with the equivalent diameter  $D_{eq} = 2\sqrt{2}D$  when  $H = G = 1$





**Fig. 4.5 Eccentric assumption of the backfill region for use in the justification applying the conformal mapping technique**

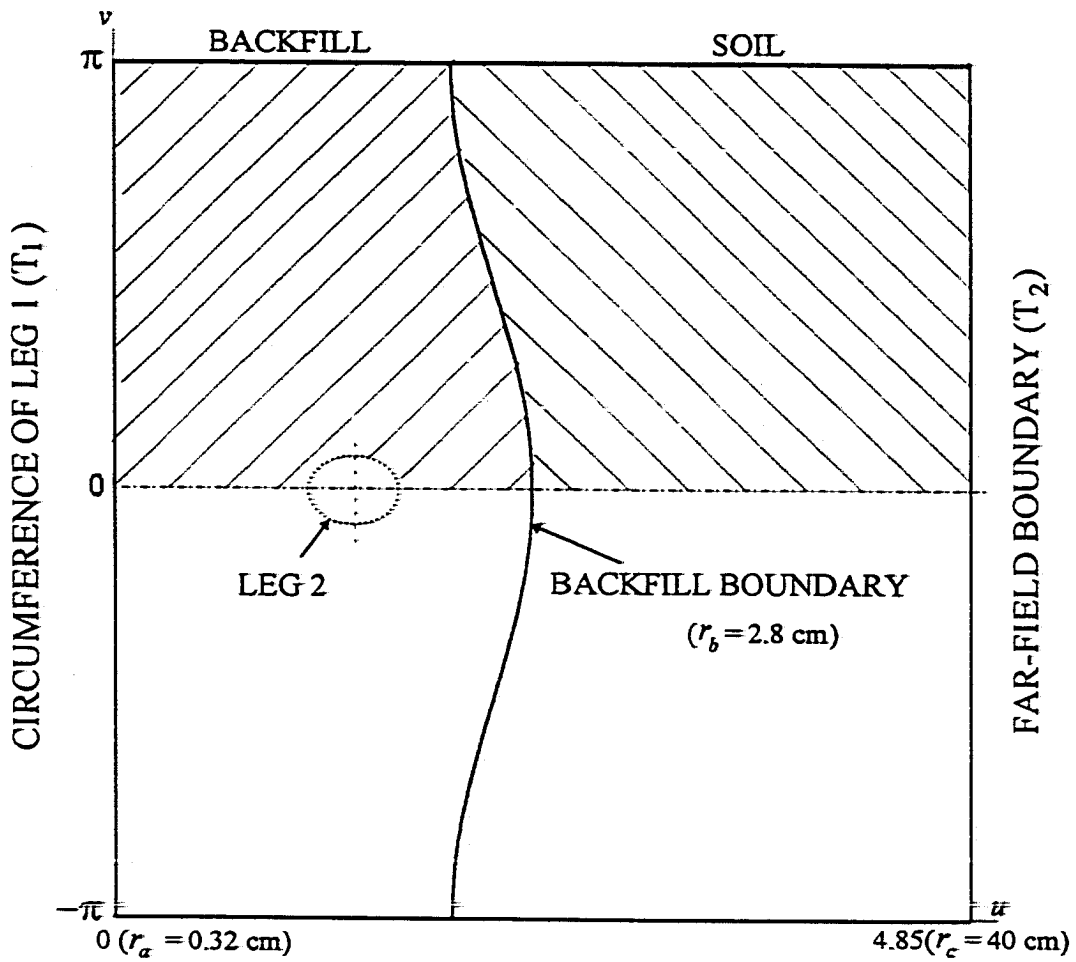


Fig. 4.6 An example of mapped soil and backfill regions using equation (4.12)

difference technique could be readily used to figure out the *ETR* values.

**Conformal Transformations.** Returning to Fig. 4.5, each point on the polar coordinate plane are defined by a complex variable,  $z$ , where

$$z = r e^{j\theta} \quad (4.10)$$

Let a new set of coordinate axes,  $u$  and  $v$ , be built up. Points on this plane are defined by the complex variable  $w$ , where

$$w = u + jv \quad (4.11)$$

If a functional relationship between  $z$  and  $w$  is established, points on the  $x$ - $y$  plane are mapped onto unique points on the  $u$ - $v$  plane. Let the following relationship exist:

$$w = \ln(z) \quad (4.12)$$

By the above conformal transformation, the entire composite region in Fig. 4.5 is mapped onto a rectangle shown in Fig. 4.6.

From the above equations, the mapping functions for  $w$  and  $u$  are

$$w = \ln r + j\theta \quad (4.13)$$

and

$$u = \ln r, \quad v = \theta \quad (4.14)$$

The functions in the original coordinates for different objects shown in Fig 4.5 are given below.

Objects	Functions
perimeter of leg 1	$r = r_a, \quad -\pi \leq \theta \leq \pi$
perimeter of leg 2	$r = E \cos \theta \pm \sqrt{r_a^2 - E^2 \sin^2 \theta}, \quad -\omega \leq \theta \leq \omega$
backfill boundary	$r = E \cos \theta \pm \sqrt{r_b^2 - E^2 \sin^2 \theta}, \quad -\pi \leq \theta \leq \pi$
far-field boundary	$r = r_c, \quad -\pi \leq \theta \leq \pi$

Substituting these functions into equation (4.14) and making the perimeter of leg 1 be cast at the line  $u \equiv 0$  yielded the map shown in Fig. 4.6. Here, the dimension was chosen to be in accordance with the experimental facility in this study. It cannot be overemphasized that  $u$  and  $v$  are non-dimensional coordinates. The height of the rectangle is always  $2\pi$  units, and the width is given by

$$\Delta U = \ln(r_c/r_a) \quad (4.15)$$

The mapping of leg 2 does not need to be known in the calculation because the superposition used here just needs the knowledge of its center's location. Accurately speaking, it is a cylindrical surface instead of a plane, since the upper and lower edges should be connected together to allow heat flow across the edge. The figure is symmetric with respect to both the center line  $v \equiv 0$  and this joined edge or common boundary.

Figures 4.7 and 4.8 display the mapped shapes of the backfill boundary with its different eccentricities and different radii, respectively. In Fig. 4.7, the greater the  $E$  value, the more distorted the curve. The values of  $E = 0$  and  $E = 2.2$  cm are two extreme

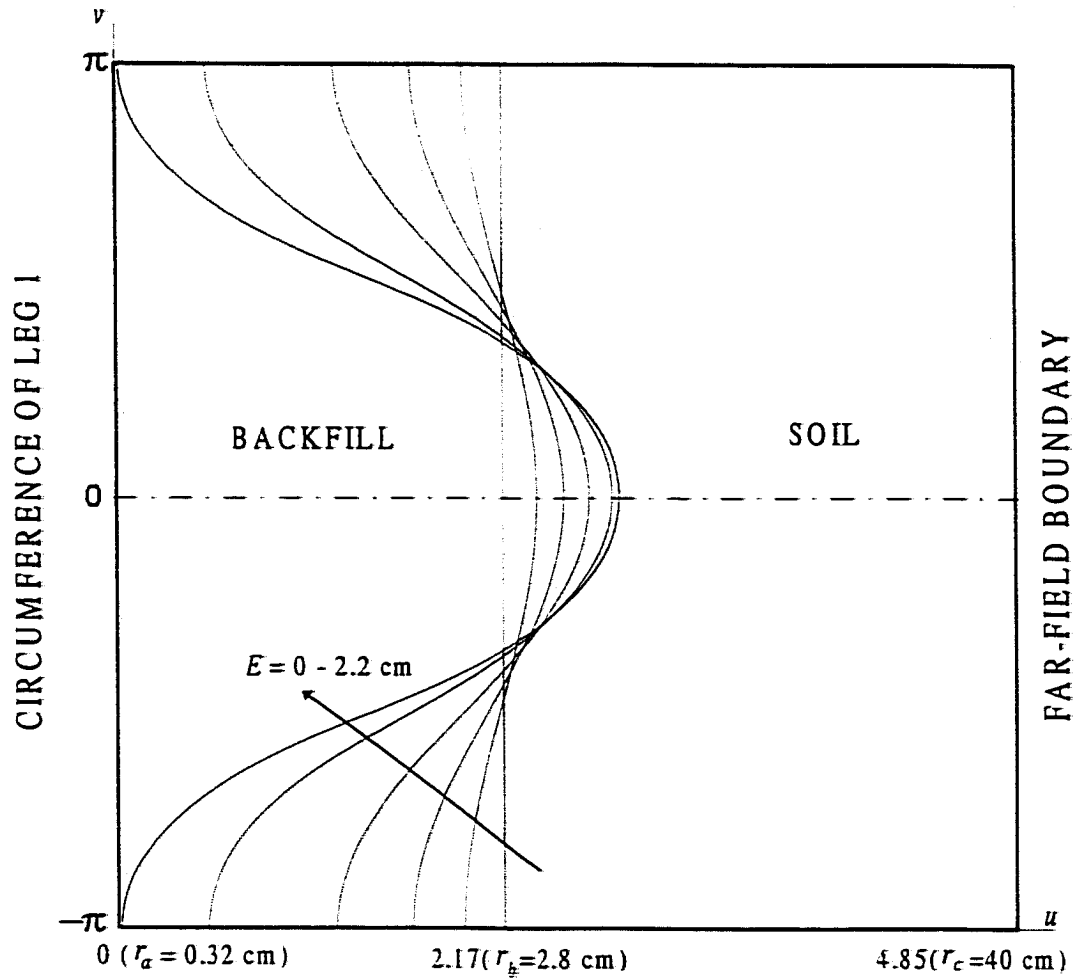


**Fig. 4.7** Varied shapes of backfill boundary after mapping with increased eccentricity

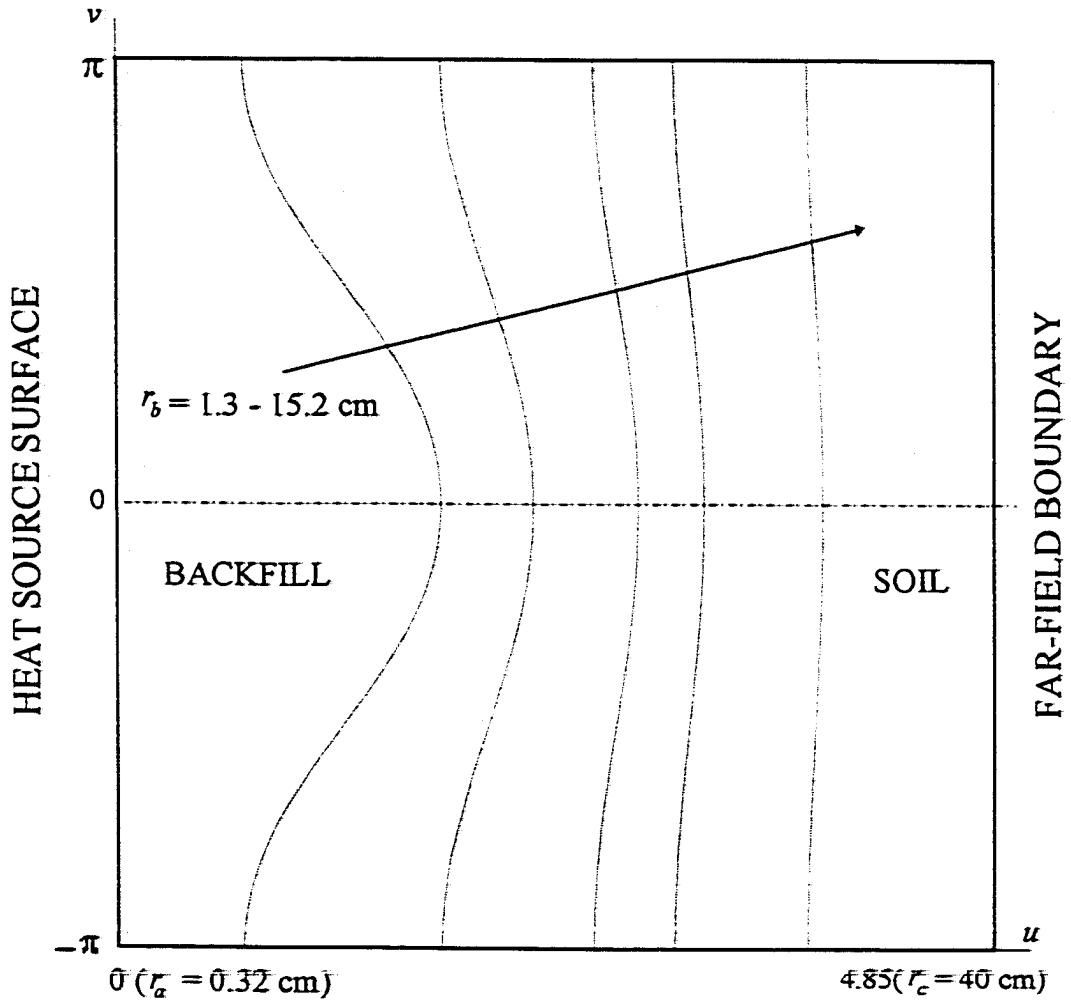


Fig. 4.8 Varied shapes of backfill boundary after mapping with increased radius of backfill region

cases when the boundary is concentric with and internally touches leg I, respectively. In Fig. 4.8, the larger the radius of the backfill boundary, the more straight the curve.

**Numerical Method for *ETR* Calculations.** The heat flow from the pipe surface of leg I to the far-field boundary now becomes two dimensional (Fig. 4.6). The symmetry of the problem yields two advantages. First, only one of the two identical halves, upper or lower, need to be used. Second, because there is no heat flow across the center line and the common boundary, adiabatic boundary conditions can be applied there.

The same superposition method was used here as in the derivation of equation (4.4) to find the *ETR* under the more realistic but still modified condition. The upper half region was taken for the solution as shown in Fig. 4.9. It was represented by a thermal resistive net work having  $(M + 1) \times (N + 1)$  nodes, where  $M$  and  $N$  were any integers (leg 2 ignored). The resistance had values depending on the values of thermal conductivity at their respective locations. Borderline resistances were assigned values determined by how much their length falls on either side of the backfill boundary. For the horizontal and vertical resistances,  $R_u$  and  $R_v$ , completely within the backfill or the soil region, the values per unit depth were

$$\bar{R}_u = \frac{\Delta u}{k_i \Delta v} \quad \bar{R}_v = \frac{\Delta v}{k_i \Delta u} \quad (i = 1, 2) \quad (4.16)$$

where

$$\Delta u = \frac{\Delta U}{M} \quad \Delta v = \frac{\pi}{N} \quad (4.17)$$

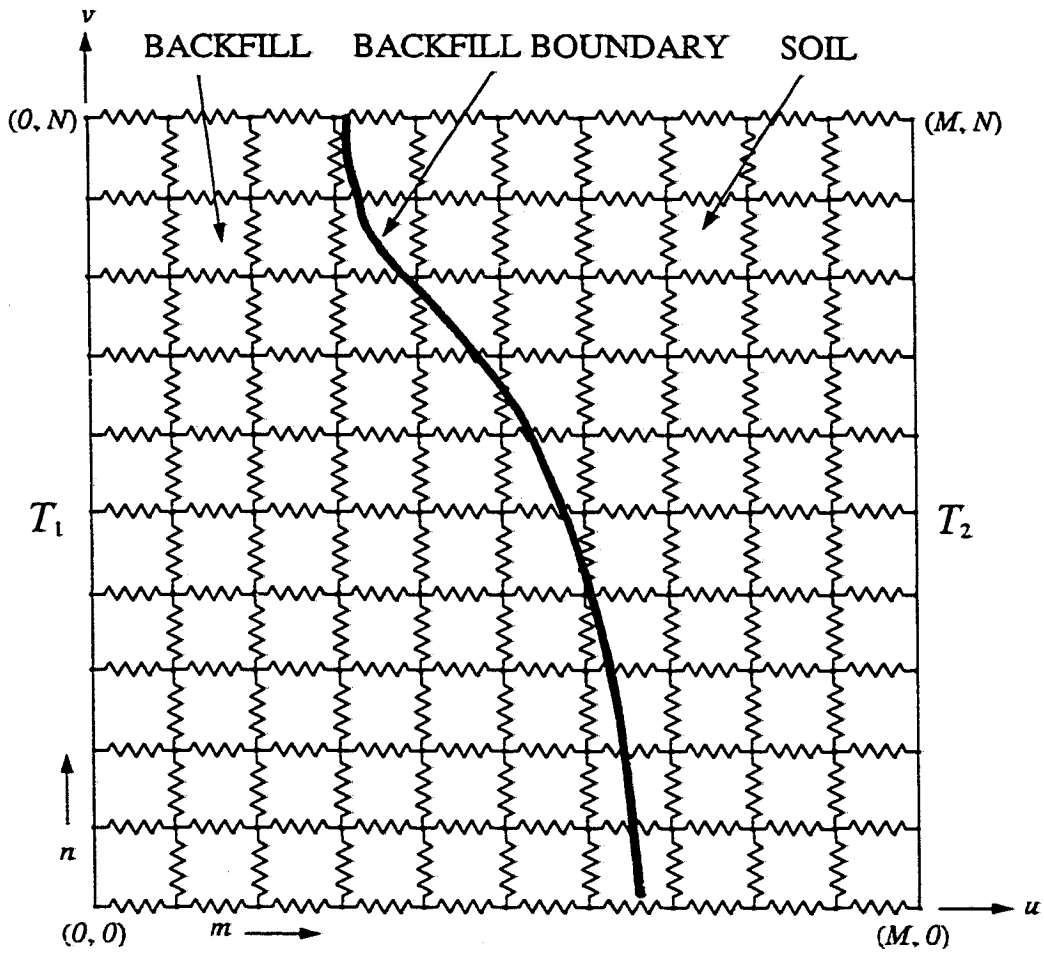


**Fig. 4.9 Schematic of the thermal resistive network for *ETR* analysis under the eccentric assumption**



If, for example, a horizontal resistance had a length of  $\Delta u_1$  falling on the backfill side and  $\Delta u_2$  on the soil side, the resistance value would be evaluated by

$$R_u = \left( \frac{\Delta u_1}{k_1} + \frac{\Delta u_2}{k_2} \right) / \Delta v \quad (4.18)$$

Under steady state, the net heat flowing into a particular node had to be zero except at the heat source and the sink. Thus, if  $(m, n)$  denoted the node number, we had (refer to Fig 4.9)

$$\frac{T_{m-1,n} - T_{m,n}}{R_{u,m}} + \frac{T_{m+1,n} - T_{m,n}}{R_{u,m+1}} + \frac{T_{m,n-1} - T_{m,n}}{R_{v,n}} + \frac{T_{m,n+1} - T_{m,n}}{R_{v,n+1}} = 0$$

$$\text{or } T_{m,n} = \frac{\left( T_{m-1,n}/R_{u,m} + T_{m+1,n}/R_{u,m+1} + T_{m,n-1}/R_{v,n} + T_{m,n+1}/R_{v,n+1} \right)}{\left( 1/R_{u,m} + 1/R_{u,m+1} + 1/R_{v,n} + 1/R_{v,n+1} \right)} \quad \begin{matrix} (m = 1, M-1) \\ (n = 0, N) \end{matrix} \quad (4.19)$$

The columns on the extreme left ( $m = 0$ ) and right ( $m = M$ ) representing the pipe surface and far-field boundary were assigned temperatures of  $T_1$  and  $T_2$ , respectively. The use of adiabatic boundary conditions on the bottom and top rows ( $n = 0$  and  $N$ ) were realized by assuming the existence of a row of vertical resistances  $R_{v,0}$  or  $R_{v,N+1}$  and the corresponding outside nodes ( $n = -1$  and  $N+1$ ), and letting

$$R_{v,0} = R_{v,1} \quad R_{v,N+1} = R_{v,N}$$

and

$$T_{m,-1} \equiv T_{m,1} \quad T_{m,N+1} \equiv T_{m,N-1} \quad (m = 1, M-1)$$

In this way, the net heat flow across these edges would be zero.

The equation system (4.19) was solved using the Gause-Seidel iterative method on the computer. Once all the node temperatures were found, the quantity of the heat

flow rate in the upper half region,  $Q' / 2$ , was then calculated by summing the heat flows through the extreme left- or right-hand resistances. On the other hand, the average temperature rise at the other leg (leg 2 here) could be approximated by finding the nearest node to the central position of the leg. This temperature value plus  $T_1$  gave the total temperature rise at the pipe surface  $(\Delta T)_{\text{tot}}$  when the two legs coexisted. The *ETR* under the eccentric condition was finally obtained as

$$(ETR)_{\text{ecc}} = \frac{(\Delta T)_{\text{tot}}}{2Q'} \quad (4.20)$$

**Results and Discussion.** For the sake of generality, the following properties in wide ranges were chosen with  $D \equiv 0.64$  cm and  $k_2 \equiv 1$  W/m-K:

$$L_S = D \sim 10D \text{ (i.e., } E = L_S / 2 = D / 2 \sim 5D), H = 0.1 \sim 10$$

$$S_b = 2 \sim 100, S_c = 128 \sim 1000$$

The results would vary only with these relative parameters. Their typical values were discussed before and considered in the determination of the ranges.  $S_b = 2$  corresponded to the case in which the backfill boundary touched the two legs in contact.  $S_c = 128$  corresponded to the experimental case discussed in Chapter VI. Nevertheless, the restriction,  $D \leq L_S \leq r_b$ , still held.

A large number of combinations of these parameters was considered in the analysis. The *ETR* values with the equivalent pipe and the eccentric situation were compared. Some of the results for the relative difference are tabulated in Tables 4.1 - 4.3, where  $\Delta ETR$  is defined as

**Table 4.1 Relative error for  $ETR$  ( $S_b = 20$ ,  $S_c = 128$ )**

$H$	LEG SPACING ( $L_s$ )				
	$D$	$2D$	$3D$	$5D$	$10D$
10	1.4%	1.5%	2.0%	3.1%	4.2%
5	1.0%	1.5%	2.4%	3.0%	4.4%
3	1.2%	1.4%	2.3%	2.8%	4.5%
1	0.6%	1.2%	2.5%	2.6%	4.7%
1/3	1.7%	1.6%	2.6%	2.2%	3.2%
1/5	1.5%	1.7%	2.1%	3.1%	3.9%
1/10	1.5%	1.7%	2.8%	3.4%	4.7%

**Table 4.2 Relative error for  $ETR$  ( $L_s = 2D$ ,  $S_c = 128$ )**

$H$	$S_b$				
	4	10	20	50	100
10	2.1%	2.2%	2.5%	2.5%	3.1%
5	2.4%	2.8%	3.3%	2.1%	4.2%
3	2.3%	3.0%	3.7%	1.8%	3.5%
1	2.6%	2.4%	2.5%	2.3%	1.9%
1/3	1.8%	1.1%	1.8%	3.2%	3.5%
1/5	2.9%	1.9%	3.5%	2.8%	1.2%
1/10	2.4%	3.5%	3.3%	2.0%	2.1%

**Table 4.3** Relative error for  $ETR (L_S = 2D, S_b = 8.8)$ 

$H$	$S_c$				
	150	300	500	700	1000
10	1.5%	1.2%	2.4%	3.2%	3.1%
5	1.8%	2.4%	2.3%	3.8%	2.4%
3	1.4%	2.8%	3.3%	3.7%	2.2%
1	1.1%	2.4%	3.1%	3.2%	3.3%
1/3	1.6%	1.1%	2.8%	2.4%	2.8%
1/5	0.9%	1.9%	3.2%	4.1%	3.6%
1/10	1.0%	3.0%	1.6%	3.8%	3.1%

$$\Delta ETR = \frac{(ETR)_{ecc} - (ETR)_{eq}}{(ETR)_{ecc}} \quad (4.21)$$

in which  $(ETR)_{eq}$  and  $(ETR)_{ecc}$  are given by equations (4.5) and (4.20), respectively.

The results show that the discrepancies were all within 5%. The positive values of the discrepancies indicated that  $(ETR)_{ecc}$  was larger than  $(ETR)_{eq}$  under all the conditions.  $\Delta ETR$  increased principally with the increase of leg spacing as shown in Table 4.1 and showed little change with other parameters. However, the calculations could have been affected more or less by the adjustment of the numbers of  $M$  and  $N$  as needed. This was a shortcoming of the numerical method. Take a typical example in which  $L_S = 10D$ ,  $H = 1/10$ ,  $S_b = 20D$  and  $S_c = 128$ , when  $M \times N = 20 \times 20$ ,  $60 \times 60$ ,  $150 \times 150$  and  $200 \times 200$ ,  $\Delta ETR$  were 28%, 23%, 4.9% and 4.7%, respectively. In general, when  $H < 1$ , the lower  $H$  was, the finer a grid had to be to achieve a satisfactory result. This was because the temperature gradient in the backfill region became increasingly larger with a decreasing value of  $H$  and thus required a finer grid when the conductivity of the backfill was lower than that of the soil. However, what we are concerned with is whether or not those discrepancies are all within an acceptable level, say 5 percent. Thus, it does not matter that the error for a specific case is three or four percent.

### Summary

In this chapter, a general expression for the equivalent diameter was derived under the steady state condition. The equivalent diameter ( $D_{eq}$ ) depended on the outer pipe diameter ( $D$ ) and the leg spacing between the two adjacent legs of a U-tube ( $L_S$ ) when the

condition  $D \leq L_s \leq S_b$  was satisfied. Errors during transient processes were examined and the concentric assumption made for the derivation was justified using the conformal mapping technique. Previously suggested  $C$ -values were all smaller than two. However, the calculated  $C$ -values using the expression could be equal to or greater than two if the leg spacing was equal to or larger than  $2D$ . The reason why a  $C$ -value could be over two was clarified.

## CHAPTER V

### SYSTEM MODEL FORMATION

In Chapter III, an analytical solution of a constant cylindrical source was developed for the calculation of the transient temperature profile in the soil. This solution needs to be incorporated into a system model written for the whole U-tube heat exchanger to predict the U-tube performance under various backfill conditions.

The model developed here discretized the ground coil into elements and utilized first-law expressions and the analytical solution for each element to derive a set of fully-implicit finite difference equations (FDEs). Therefore, it can be referred to as a discretized analytical model. This technique has been applied previously by Dobson (1991) for a uniform soil medium and the solution developed below closely follows his derivation. The time-dependent pipe wall temperatures and fluid temperature distribution along the U-tube can be solved directly.

#### Ground-Coil Model Development

Consider the model established for one leg of the U-tube assuming it is at the center of the composite medium. With the definitions for the non-dimensional numbers given in Chapter III, equation (3.25) can be changed to the following form:

$$\begin{aligned} \theta_i(r^*, t) &= \frac{Q'}{2\pi H k_2} \left[ \sum_{n=1}^{\infty} c_n \varphi_{in}(r^*) \exp(-\beta_n^2 \alpha_2 t / r_a^2) - W_i(r^*) \right] \\ &= Q' P_i(r^*, t) \quad (i=1,2) \end{aligned} \quad (5.1)$$

For a given composite medium at a given time and location, the temperature rise in the

soil,  $\theta$ , is proportional to the heat transfer rate per unit depth,  $Q'$ . Clearly, the heat transfer rate varies with both the distance along the U-tube and with time. To handle the variation along the coil, the U-tube was divided into several elements for which the assumption of spatially uniform heat flux was more acceptable.  $Q'$  was calculated for each element and each time step.

To allow for temporal variations in heat transfer rate for each element, the principle of superposition introduced earlier was used. In this way, the temperature rise was estimated as the sum of a series of temperature rises caused by the rectangular heat pulses for each prior time increment. The time value in equation (5.1) was the time since the particular interval began or ended, not the time since the simulation started. This is shown schematically in Fig. 5.1. The methodology can be visualized as imposing a positive heat pulse starting at the beginning of the time interval in conjunction with a negative heat pulse of the same strength beginning at the end of the time interval (Claesson and Dunand, 1983). When applying this methodology to  $m$  consecutive heat pulses, we have

$$\theta_i(r^*, t) = \sum_{i=1}^{m-1} Q'_i [P_i(r^*, t_{i-1}) - P_i(r^*, t_i)] + Q'_m P_i(r^*, t_{m-1}) \quad (i=1,2) \quad (5.2)$$

All the heat pulses are grouped with a difference in  $P$  except the  $m^{\text{th}}$  which continues until the last moment of the simulation. Recalling the discussion in Chapter III, as absolute time increases,  $P$  should change slowly since it approaches the steady state. Thus, the difference in  $P$  which is multiplied by the old values of  $Q'$  tends to zero. This means that "old" heat pulses have decreasing significance as time goes on. When computing



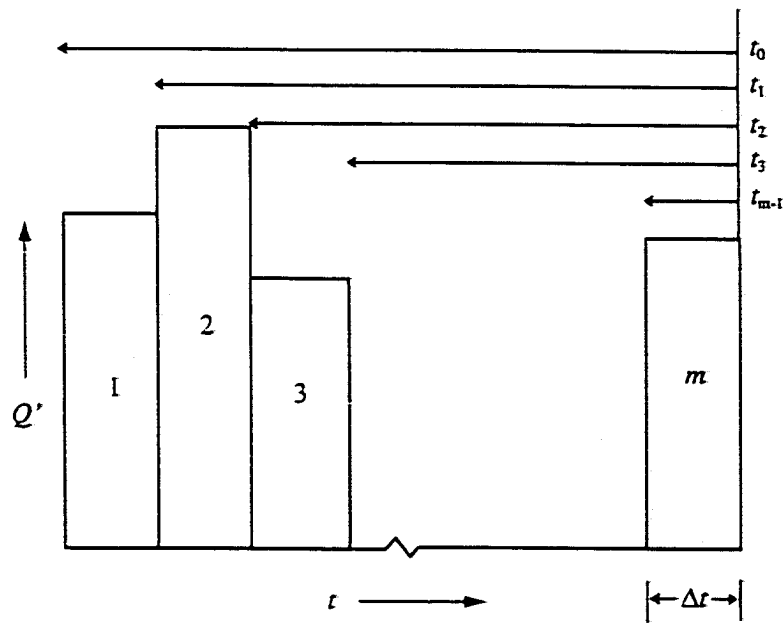


**Fig. 5.1 Superposition of heat pulses for the analytical solution**

temperatures at the outer pipe wall or at a distance equal to the leg spacing,  $L_S$ , simply let  $r^* = 1$  or  $r^* = L_S / r_o$ .

Now that a method for calculating the temperatures in the composite medium is in place, the task of developing the FDEs to solve for the fluid temperature inside the pipe remains. Figure 5.2 illustrates a schematic of the computational domain and the unknown temperatures. This is helpful in deriving the governing equations. In the following derivation, the temperatures are subscripted as follows:

$f$  - fluid

$w$  - inner wall of the pipe

$s$  - outer pipe surface

$ff$  - far-field

The temperatures are superscripted as follows:

$p$  - value at the current time step

$p+1$  - value at the next time step

The bulk temperature for each element was represented by an average of the fluid temperatures at the ends of the element

$$\bar{T}_{fj} = \frac{T_{fj-1} + T_{fj}}{2} \quad (5.3)$$

The major assumptions made for each element include:

1. Thermal short-circuiting between the adjacent legs of the U-tube was treated using either superposition or the equivalent diameter approach.
2. The initial temperature was uniform everywhere including the pipe and the fluid,

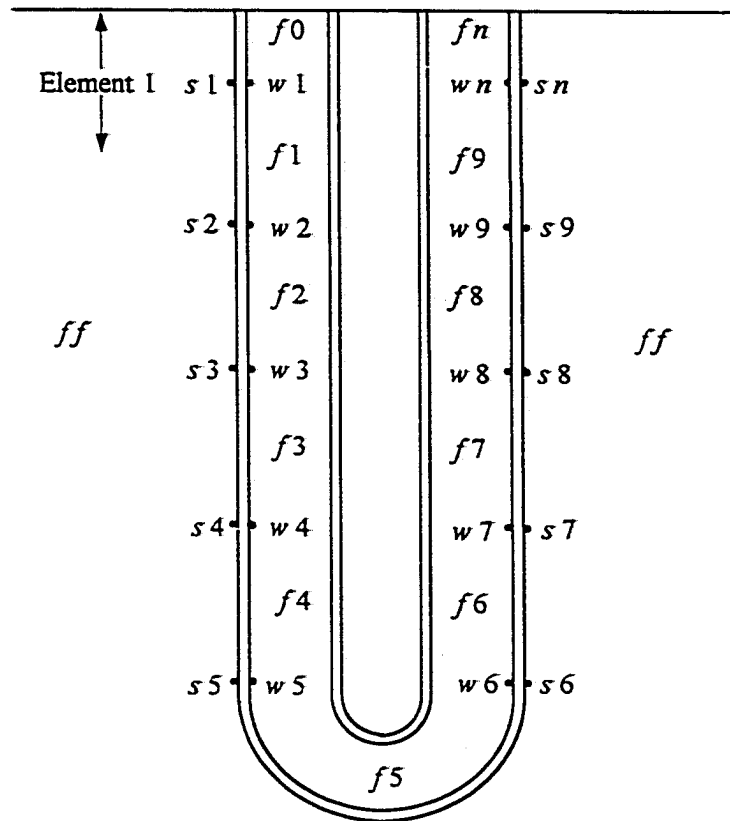


**Fig. 5.2 Schematic of computational domain and unknown temperatures**

and was equal to the far-field temperature which was constant both spatially and in time.

3. The thermal storage capacity of the pipe wall was negligible.
4. Heat conduction was one dimensional in  $r$ .
5. Axial conduction inside the fluid was negligible.
6. Radial temperature gradients inside the fluid were ignored.
7. All the thermal properties and the convective coefficient were constant.

Still, the thermal contact resistance at both pipe-to-backfill and soil-to-backfill interfaces are not considered in the present model.

**On-Cycle.** Subject to the above assumptions, the application of the first law to each fluid element yielded

$$\dot{m}c_f \Delta t (T_{f,i} - T_{f,i}^{p+1}) - hU\Delta L \Delta t (\bar{T}_{f,i} - T_{w,i}) = (\rho c)_f A_c \Delta L (\bar{T}_{f,i}^{p+1} - \bar{T}_{f,i}^p) \quad (5.4)$$

Equation (5.4) states that the internal energy increment within an element for a time step was equal to the net energy entering the element by advection minus the energy leaving the element by convection. The fully implicit technique demanded all terms on the left-hand side of equation (5.4) be evaluated at time  $p+1$ . This method was chosen in the current study since it was unconditionally stable.

In rearranging equation (5.4), the following dimensionless variables were defined:

$$\chi = \frac{\dot{m} \Delta t}{\rho_f A_c \Delta L} = \frac{u \Delta t}{\Delta L}$$

$$\delta = \frac{2h\Delta t}{(\rho c)_f r_{in}}$$

Introducing these to equation (5.4) and separating terms in  $p$  and  $p+1$ , one obtained

$$T_{f_{j-1}}^{p+1}(1-2\chi+\delta) + T_{f_j}^{p+1}(1+2\chi+\delta) - 2\delta T_{w_i}^{p+1} = T_{f_{j-1}}^p + T_{f_j}^p \quad (5.5)$$

If  $n+1$  denotes the number of fluid temperatures and  $n$  the number of wall temperatures, equation (5.5) provides  $n$  equations and  $2n+1$  unknowns. However, IWT, which was denoted here by  $T_{f_0}$ , was always used as an input parameter during the on-cycle and thus the number of the unknowns was reduced to  $2n$ .

The heat carried away by convection at any time equaled the heat conducted away through the pipe wall, neglecting the thermal capacity of the pipe. Therefore, the following relation held for each element:

$$hU(\bar{T}_{f_j} - T_{w_i})^{p+1} = \frac{(T_{w_i} - T_{s_j})^{p+1}}{R} \quad (5.6)$$

where

$$R = \frac{\ln(r_o/r_{in})}{2\pi k_{pipe}}$$

$T_{s_j}$  in equation (5.6) could be solved by employing the analytical solution in the form of equation (5.2). At the outer pipe wall where  $i = 1$ , representing the backfill region,

$$\theta_{1j} = T_{s_j} - T_{ff} \quad r^* \equiv 1$$

Substituting this into equation (5.2) gave

$$T_{s_j}^{p+1} = T_{ff} + \sum_{l=1}^{m-1} Q_{jl} [P_1(t_{l-1}, 1) - P_1(t_l, 1)] + Q_{jm} P_1(t_{m-1}, 1) \quad (5.7)$$

In the above equation,  $l$  was used to subscript the prior heat pulses for element  $j$ , with the  $m^{\text{th}}$  being the last one. The  $l^{\text{th}}$  heat pulse for the  $j^{\text{th}}$  element was written as

$$Q'_{jt} = hU(\bar{T}_{fj}^{p+1} - T_{wI}^{p+1}) \quad (5.8)$$

With equation (5.8),  $Q'_{jt}$  for each time increment were calculated using the temperature values at time  $p+1$ . The quantity  $Q'_{jm}$ , however, involved unknown fluid and inner wall temperatures at time  $p+1$ .

Substituting equation (5.8) into equation (5.6) and grouping terms in  $p+1$  yielded

$$T_{fj}^{p+1}(-\varepsilon) + T_{fj+1}^{p+1}(-\varepsilon) + T_{wI}^{p+1}(1+2\varepsilon) = T_{ff} + \sum_{i=1}^{m-1} Q'_{ji}[P_i(t_{i-1}, 1) - P_i(t_i, 1)] \quad (5.9)$$

where

$$\varepsilon = \frac{P_1(t_{m-1}, 1)hU + hUR}{2}$$

which was also a dimensionless variable. Equation (5.9) added  $n$  equations to the  $n$  equations previously written, thereby closing the problem. In equation (5.9), the subscripts on  $t$  refer to the time values to be used.

In the above mathematical model, equation (5.9) was true only if one leg existed alone and had to be modified to account for the effect of the other leg of the U-tube. Either the method of superposition or the equivalent diameter approach can be utilized. They are described below.

When applying the method of superposition, both legs were alternatively assumed at the center of the composite medium as illustrated in Figs. 4.1(b) and (c). The presence of the other leg was ignored when considering the thermal field produced by one leg. By restriction  $D \leq L_S \leq r_b$ , the U-tube was still within the backfill region when one leg moved to the center. The added temperature to element  $j$  by its "thermal interference partner", element  $k$  at the end of the  $m^{\text{th}}$  heat pulse can be written as

$$\Delta T_{\varepsilon_j} = \sum_{i=1}^{m-1} Q_i [P_i(t_{i-1}, L_S/r_a) - P_i(t_i, L_S/r_a)] + Q_{km} P_i(t_{m-1}, L_S/r_a) \quad (5.10)$$

Adding equation (5.10) to equation (5.7) and substituting the resulting right-hand side for  $T_{\varepsilon_j}$  in equation (5.6), equation (5.9) became

$$\begin{aligned} & T_{f_{j-1}}^{p+1}(-\varepsilon) + T_{f_j}^{p+1}(-\varepsilon) + T_{w_j}^{p+1}(1+2\varepsilon) + T_{f_{k-1}}^{p+1}(-\phi) + T_{f_k}^{p+1}(-\phi) + T_{w_k}^{p+1}(2\phi) \\ & = T_f + \sum_{i=1}^{m-1} Q_i [P_i(t_{i-1}, 1) - P_i(t_i, 1)] + Q_{ki} [P_i(t_{i-1}, L_S/r_a) - P_i(t_i, L_S/r_a)] \end{aligned} \quad (5.11)$$

where

$$\phi = \frac{P_i(t_{m-1}, L_S/r_a) h U}{2}$$

was a dimensionless variable.

When applying the equivalent diameter approach, the form of equation (5.9) remained the same because the equivalent pipe was a single pipe assumed at the center. However, because the pipe size ( $D_{eq}$ ) was enlarged when estimated using equation (4.6), the radius ratios  $S_b$  and  $S_c$  defined earlier were also changed accordingly and so the coefficients  $C_n$ , eigenvalues  $\beta_n$  and eigenfunctions  $\varphi_n$  in equation (5.1) had to be different. Therefore, the function  $P_i$  in equation (5.9) had to be re-evaluated by replacing  $r_a$  with  $r_{eq}$ . In all other related equations,  $r_a$  was also replaced with  $r_{eq}$ . The use of  $D_{eq}$  merely assures approximately the same ETR values per unit length. To achieve the same heat dissipation rate across the whole pipe under the equal average temperature difference between the water inside the pipe and the far-field boundary, three other modifications had to be made. First, the internal thermal resistance of the pipe had to be the same. Neglecting the fouling factors, the resistance included conductive resistance of the pipe wall and convective

resistance of the fluid. For the two legs in parallel with a U-tube, the resistance per unit depth could be written as

$$R_t = \frac{1}{2} \left[ \frac{1}{2\pi r_{in} h} + \frac{\ln(r_a/r_{in})}{2\pi k_{pipe}} \right] = \frac{1}{2\pi(2r_{in}h)} + \frac{\ln(r_a/r_{in})}{2\pi(2k_{pipe})} \quad (5.12)$$

For the equivalent pipe, the resistance was given as

$$R_t' = \frac{1}{2\pi(r_{in}'h')} + \frac{\ln(r_{eq}'/r_{in}')}{2\pi k_{pipe}'} \quad (5.13)$$

where the prime denoted the quantities associated with the equivalent pipe. Comparing equation (5.13) with (5.12), it is clear the values of the internal thermal resistance were equal only if the following relations were satisfied:

$$r_{in}'h' = 2r_{in}h, \quad r_{eq}'/r_{in}' = r_a/r_{in}, \quad k_{pipe}' = 2k_{pipe} \quad (5.14)$$

or

$$r_{in}' = \frac{D_{eq}}{D} r_{in}, \quad h' = \frac{2r_{in}}{r_{in}'} h, \quad k_{pipe}' = 2k_{pipe} \quad (5.15)$$

Second, the temperature drop per unit depth would not be the same unless the mass flow rates were equal. This yielded

$$\frac{u'}{u} = \left( \frac{D}{D_{eq}} \right)^2 \quad (5.16)$$

where  $u'$  was the flow velocity of the fluid inside the equivalent pipe.

Last, the total thermal capacity of the water inside the tube had also to be the same. This required

$$(\rho c A_c L)' = (\rho c A_c L) \quad (5.17)$$



Substituting the following:

$$A'_\xi = \left(\frac{D_{eq}}{D}\right)^2 A_\xi, \quad L' = \frac{L}{2} \quad (5.18)$$

one obtained

$$(\rho c)' = 2 \left(\frac{D}{D_{eq}}\right)^2 (\rho c) \quad (5.19)$$

The development of the expression for  $D_{eq}$  involved the same implementation of superposition as in the derivation of equation (5.11). The difference was in that the use of an equivalent diameter made the calculation more straightforward while it might lose some accuracy since the expression was obtained under steady state. Equation (5.5) coupled with equation (5.9) or (5.11) formed a system of  $2n$  equations. All coefficients of the  $p+1$  terms were time invariant, provided that the same time step was used throughout the simulation. Thus, the  $2n \times 2n$  coefficient matrix could be decomposed following the  $LU$  decomposition method (Golub et al., 1983) before simulation began and then the system could be solved with the subsequent right-hand side vector at each time step by backsubstitution. This was considerably faster than decomposing a new coefficient matrix and solving the system at each step.

**Off-Cycle.** A GCHP cycles on and off to meet the cooling load on the building. During the off-cycle, the advection term in equation (5.4) vanishes (i.e.,  $\chi = 0$ ) and the forced convection turns into free convection. If the vertical motion of the fluid due to gravitation and the vertical temperature gradient inside an element are negligible, there

should be no difference between  $T_{f,t}$  and  $T_{fj}$  for each element. Furthermore, IWT was no longer an input parameter since no water was supplied to the U-tube. Consequently, the fluid temperatures were evaluated in terms of the bulk temperatures and equation (5.4) became

$$-hU\Delta L\Delta t(\bar{T}_{fj}^{p+1} - T_{wj}^{p+1}) = (\rho c)_f A_e \Delta L (\bar{T}_{fj}^{p+1} - \bar{T}_{fj}^p) \quad (5.20)$$

By rearranging equation (5.20), equation (5.5) was replaced by

$$(1 + \delta)\bar{T}_{fj}^{p+1} + (-\delta)T_{wj}^{p+1} = \bar{T}_{fj}^p \quad (5.21)$$

In equation (5.21),  $\delta$  had to be re-evaluated with the free convection coefficient.

Likewise, when the bulk temperatures appeared as the unknowns, equation (5.9) became

$$(-2\varepsilon)\bar{T}_{fj}^{p+1} + (1 + 2\varepsilon)T_{wj}^{p+1} = T_{fj} + \sum_{l=1}^{m-1} Q_{jl} [P_l(t_{l-1}, 1) - P_l(t_l, 1)] \quad (5.22)$$

and equation (5.11) became

$$\begin{aligned} & (-2\varepsilon)\bar{T}_{fj}^{p+1} + (1 + 2\varepsilon)T_{wj}^{p+1} + (-2\phi)\bar{T}_{fk}^{p+1} + (2\phi)T_{wk}^{p+1} \\ & = T_{fj} + \sum_{l=1}^{m-1} Q_{jl} [P_l(t_{l-1}, 1) - P_l(t_l, 1)] + Q_{kl} [P_l(t_{l-1}, L_S/r_a) - P_l(t_l, L_S/r_a)] \end{aligned} \quad (5.23)$$

In equations (5.22) and (5.23),  $\varepsilon$  and  $\phi$  also needed re-evaluation with the free convection coefficient. Equation (5.21) in conjunction with equation (5.22) or (5.23) also provided  $2n$  equations for solving for  $2n$  unknowns. Again, the coefficient matrix was time invariant. When applying the equivalent diameter approach during the off-cycle, equations (5.15) and (5.19) could be used.

### Time Intervals and Number of Elements

In principle, all the prior heat pulses needed to be stored for the computation of the right-hand side in equation (5.9), (5.11), (5.22) or (5.23) at each following time step. However, one immediate problem was encountered. If a one-minute time step and a ten-element grid were chosen, 14,400 heat pulses needed to be stored by the end of the first day. Their effect must be re-estimated at each time step because the difference in  $P$  associated with particular heat pulses change step by step. No doubt, it would result in large memory requirements and extremely slow calculation process when the simulation for a GCHP was made for weeks, months or even years. The solution to this problem included two aspects. On the one hand, it was not necessary to store the "old" heat pulses in one-minute intervals while such a small time step was necessary to capture the start-up or shutdown characteristics. Actually, after some time (qualitatively speaking), the effect of a varying heat dissipation was nearly equivalent to that of a constant heat dissipation with the same mean value. This was pointed by Claesson and Dunand (1983) and demonstrated by Dobson (1991). Dobson designed three different time intervals to store the heat pulses. The options used in his verification runs were: (1) sixty one-minute time intervals, (2) twelve two-hour time intervals, and (3) the remainder stored in one-day time intervals. The two longer time intervals carried with them average heat transfer rates. This combination provided the same IWT to within one decimal place as using all one-minute data for a one-day simulation.

On the other hand, "old" heat pulses have diminishing effect on the computational results as time goes on. Therefore, the heat pulses "old enough" may be dropped to

reduce the memory and computational requirements. How “old” is enough depends on the accuracy desired and the history of heat dissipation including the magnitude and duration. The determination of time intervals is given in Chapter VII for the experimental verification and in Chapter VIII for the parametric studies, respectively.

The choice of element length largely depends on how fast the fluid temperature varies along the U-tube heat exchanger. Or more precisely, it depends on the temperature gradient per element. The greater the gradient, the finer the grid should be. Dobson (1991) divided a 232 m coil into ten elements in his study where the total temperature drop across the U-tube was less than 3 °C. Thus, the average gradient defined above was less than 0.3 °C per element. He also tried twenty- and thirty-element grids but achieved outlet water temperature predictions over a one-day simulation within 0.1 °C. The results were not as sensitive to the element length as to the time intervals. The U-tube heat exchangers were divided into ten elements throughout the current investigations.

## CHAPTER VI

### EXPERIMENTAL SET-UP AND PROCEDURES

This chapter describes the experimental set-up and outlines the test procedures used to verify the analytical model for the U-tube heat exchanger. This chapter is divided into four sections: experimental set-up, soil preparation, backfill preparation, and experimental procedures.

#### Experimental Set-Up

A small-scale simulator of the vertical U-tube heat exchanger system was built as shown in Fig. 6.1. Heat was added to the circulating water in a water heater and rejected to the soil in a metal tank through the small-scale U-tube. The inlet water temperature (IWT) to the heat exchanger was controlled by means of a Proportional-Integral-Differential (PID) controller and adjusted as needed. The flow rate of the water was set with the combination of a hand valve and a by-pass valve, and was measured through a float flow meter. Temperatures along the U-tube and in the soil were taken by T-type thermocouples. An Acurex AutoCalc data acquisition system was connected to a microcomputer to display and record the temperature data. The data acquisition system could provide up to 100 channels. It also provided amplification and cold junction compensation for each thermocouple input. IWT would be used as input data in the simulation program and the outlet water temperature (OWT) would be used as the parameter for comparison with the calculated results. The thermocouples at these two locations were inserted into the tubes to improve the accuracy of the water temperature readings. Other thermocouples along the U-tube were welded to the wall and the welded

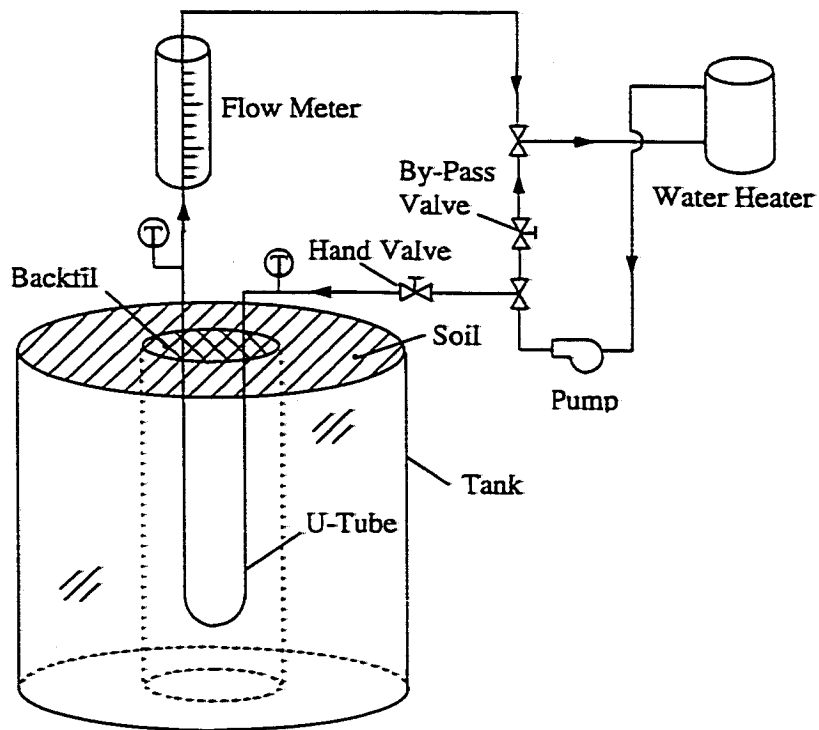


**Fig. 6.1 Schematic diagram of the U-tube test facility**

joints were insulated with silicone glue and then wrapped with teflon tape to get close readings to the in-tube water temperatures. These temperature readings were used to obtain the water temperature profile along the U-tube during on-times.

Figures 6.2 and 6.3 show the major dimensions of the set-up and the thermocouple locations. Thermocouples were also buried in the soil at radial locations from the U-tube and at two different depths. Those locations were evenly distributed between the backfill boundary and the tank wall. The two groups of thermocouples (i.e., TC #11 to #15 and TC #16 to #20) were arranged at locations 180 degrees from each other as indicated in Fig. 6.3. These were used to examine if the initial temperature distribution was uniform. Two additional thermocouples were inserted in the backfill region during the installation of the U-tube for the same reason. The U-tube was made of 0.64 cm OD (outer diameter) copper tubing with each leg being 120 cm long. This length was determined based on the expectation of a water temperature drop ( $\Delta T$ ) of at least two degrees Celsius across the U-tube during the whole test to guarantee the accuracy of measurement of  $\Delta T$ . The two legs were coupled by a U-bend welded at the bottom. Three small wooden spacers were attached to maintain proper spacing between the two legs. A round rubber stopper at the top and several wooden sticks bound along the U-tube served to ensure the central position of the heat exchanger inside the hole.

The tank diameter was 80 cm which provided an  $S_c$  value of 128. This ratio would allow nearly ten hours' simulation without affecting the temperature at the tank wall according to the results given in Fig. 3.3. The top of the tank was covered with a piece of insulation to reduce vaporization of the moisture from the top of the soil. It also

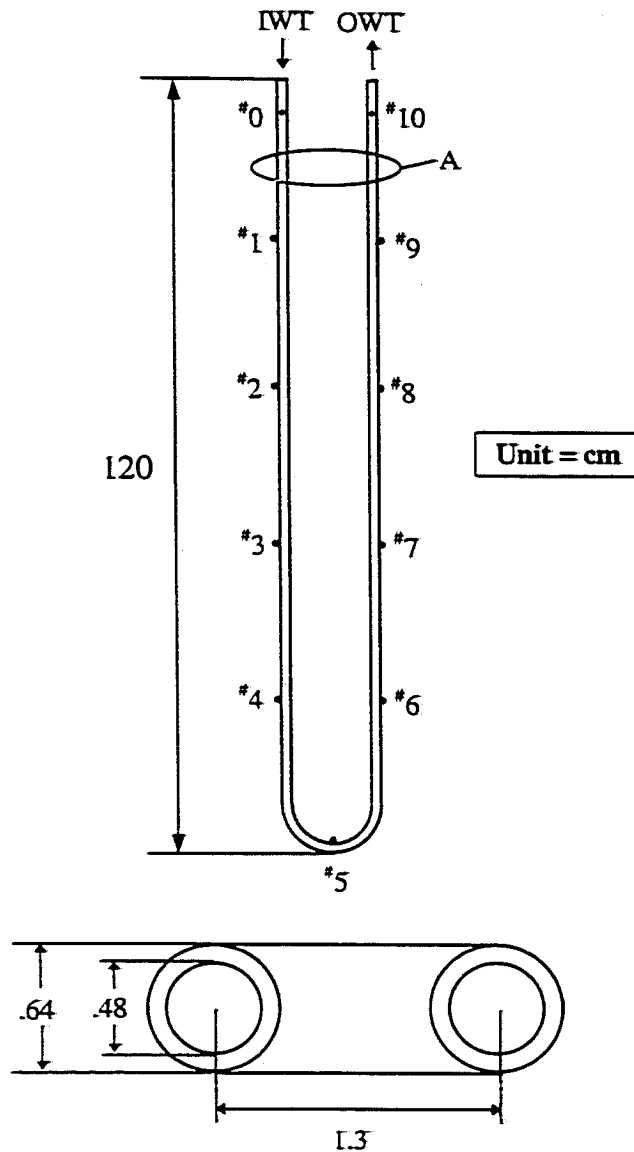


Fig. A Cross section of the U-tube

**Fig. 6.2 U-tube heat exchanger and thermocouple locations used in the small-scale simulator**



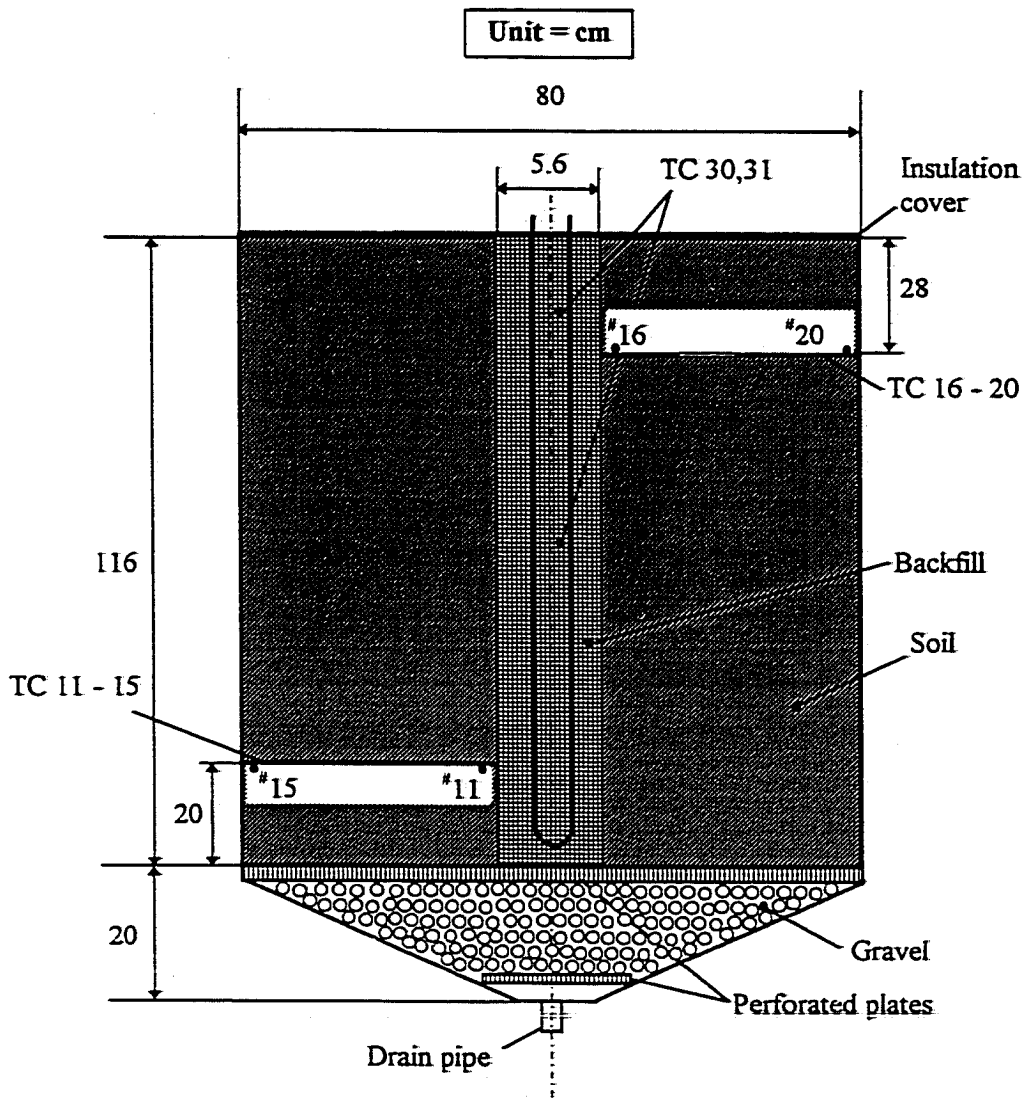


Fig. 6.3 Cross-section of the tank and the contents used in the simulator

provided an adiabatic boundary condition to reduce the end effect on the U-tube heat transfer.

The input cards of the data acquisition system were calibrated by immersing the thermocouples into an ice bath (using distilled water) at 0 °C and turning the adjusting screw to get temperature readings as close to 0 °C as possible. A standard glass thermometer of 0.01 °C-graduation was used to check the triple point in the ice bath. Those readings had a maximum bias error of  $\pm 0.3$  °C and had fluctuations within  $\pm 0.2$  °C. Furthermore, five thermocouples were selected to determine their response time to temperature change. These thermocouples were initially at  $24.5 \pm 0.2$  °C and were suddenly immersed into the ice bath. Within 5 seconds, their temperatures dropped to  $0 \pm 0.2$  °C. In other words, the average response was as fast as 5 °C per second. However, the most rapid change in water temperature inside the U-tube turned out to be less than 1 °C per second in the experiment. Thus, the use of these thermocouples were reliable.

The flowmeter was calibrated with water before the test. The range of the flowmeter was 0 ~ 1000 ml /min. The calibrated values agreed very well with those provided by the manufacturer especially near the central section. The manufacturer-determined average bias error was  $\pm 2\%$ . During the tests, flow fluctuations were within  $\pm 2.5\%$  which was the random error. The water temperature during the calibration was 27 °C, while the maximum OWT during the tests was 57.5 °C. The flowmeter was located downstream of the test section (Fig. 6.1). This temperature difference could cause a difference in fluid density and thus would lead to an error in reading of the volumetric flow rate. Therefore, the volumetric flow rate was corrected by the following:

$$\bar{V} = \bar{V}_0 \frac{\rho_0}{\rho} \quad (6.1)$$

where the subscript 0 denotes the state of calibration. However, the maximum error at 57.5 °C was estimated to be only 1.3% using equation (6.1). The heat transfer rate along the U-tube heat exchanger was implicitly involved in the system model discussed in Chapter V. The uncertainty in its evaluation is described in Appendix B.

Before the experiment, it was considered that water could be poured from the top to let it down to get more uniform soil structure. The bottom part of the tank was in a cone shape and was filled with gravel to allow the water to drain easily through a small hole at the bottom. However, this scheme was not implemented because it would take a long time for the water to drain away and it would be hard to control moisture content in the soil. Instead, some water was added from both the top and bottom to keep the soil wet with about 14% moisture content (MC) during the four-month experiment. The water was added at the top with a pot and to the bottom through a hose connected with a water tank put on the top. The average moisture content of the soil was measured once during and after the end of the experiment, respectively. Soil samples of 5 g each were randomly taken from different locations and were oven-dried for 24 h at 110 °C to obtain the average value of MC. The uncertainty of moisture measurement was about 2%.

The use of such a laboratory facility had the following major advantages over that of a real system for the purpose of verification:

- I. In the facility, the length dimensions in radial direction of a typical full-scale system were reduced by a factor of 4.5. The dimensionless solution of  $T^*$  given

earlier was a function of  $r^*$  and  $Fo$ . The characteristic length,  $r_c$ , did not appear in equation (3.25). At equal values of  $Fo$  and  $r^*$  in the same composite medium with the same thermal properties, the time scale was proportional to the square of the length scale. Therefore, a reduction of the length of 1/4.5 gave a 1/20 reduction of real time. This allowed a day to be simulated in about one hour, and three weeks to be simulated in about one day.

2. The analytical solution required that the initial temperature distribution be uniform throughout the whole composite region. This condition, however, was difficult to meet once the GCHP system had been in operation. One had to either stop the system and wait for a long time for the ground temperature to recover to its undisturbed state or had to determine the initial temperature profile using all the previously recorded heat transfer data before starting the simulation (see Dobson, 1991). It was fairly easy to meet such demand with the laboratory facility since it was small and just took about two days to return to a uniform temperature distribution after several hours' running.
3. The soil inside the tank could be made more uniform by careful preparation and proper compaction after being filled in the tank. The backfill materials could be changed readily. The IWT and the water flow rate could be varied as required to obtain appropriate heat transfer rates and temperature drop across the coil. The operation of the simulator would not be subject to other conditions associated with cooling or heating loads inside a building.

For the first seven tests, a thin wall steel tube was used to load the backfill

materials along with the U-tube. It was intended for convenient change of the backfills and for preventing the loss of water content in the backfill. The outer diameter of the tube was just a little smaller than the bore of the hole and it could easily be inserted or removed from the hole without effort. A layer of thin mud was applied to the tube wall when inserting it into the hole to reduce the contact resistance between the tube and the soil.

Initially, tests were run with the steel tube holding the backfill. However, simulation results indicated that the contact resistance had a significant influence on the performance of the ground heat exchanger. Thermal conductivities which were attributable to the backfill/steel tube and used in the simulations were 40% lower than the values measured by the TAMU (Texas A&M University) Heat Transfer Laboratory. Actually, the wall of the borehole was not smooth and even had small indentations in places. Thus, the test setup was modified by removing the steel tube. Tests without the steel tube proved to be successful, although there arose two attendant limitations. One was the inconvenience of changing backfills. A bucket auger was used to clean out the backfills. The diameter of the borehole could become larger due to the repeated use of the auger. The other was the potential drying, shrinking and cracking of the backfills with high percent bentonite (compared to field use) after a long time heating. Contact resistance was ignored in simulations without the steel tube. Conservatively speaking, only the data within the first several hours were believed to be reliable. Up to seven hours' data from the scale simulator (equivalent to about six days for a typical GCHP) were used for the verification of the model.

Test facilities for vertical coils were more difficult to build than those for horizontal ones. They required a much thicker soil layer and presented difficulties in changing backfills and in inspecting the heat exchanger or the backfilling condition deep inside the hole. It might be for this reason that few investigations have reported laboratory studies of vertical ground heat exchangers.

### **Soil Preparation**

It was decided that a soil common to Texas, like silty loam and sandy loam, should be used for the experiment. Silty loam from the Brazos river bed was chosen primarily for its availability. The moist soil was spread onto the floor and air-dried for two weeks. During this period, the soil was turned over regularly to speed its drying and large lumps were removed. Other impurities such as leaves, grass and stone, etc., were also removed. The dried soil was then machine-crushed to fine particles in preparation for the experiments.

The average moisture content of the dry soil was measured at 3%. The dry soil density was found to be  $1125 \text{ kg/m}^3$ . The soil composition was determined using the hydrometer method. It consisted of 52% silt, 26% clay and 22% sand, which is classified as a silty loam soil.

The dry soil and water were weighed out and mixed uniformly to reach a moisture content of approximately 14% (dry basis). It had been suggested that silt loam with a moisture content of this percentage would be compacted most easily. The processed soil was packed in the tank every 5 cm in thickness (after compaction) to gain a uniform and

proper degree of compaction. About 900 kg of the soil was required to fill the tank. The soil density acquired in this manner was  $1695 \text{ kg/m}^3$  which was within the range for common Texas soils. Its thermal conductivity and specific heat were measured in the TAMU Heat Transfer Laboratory and found to be at  $1.3 \text{ W/m-K}$  and  $2079 \text{ J/kg-K}$ , respectively.

### **Backfill Preparation**

**Fluidized Backfills Using Bentonite.** Commonly used backfill materials were introduced earlier in the literature survey. Fluidized mixtures are suitable for vertically-oriented heat exchangers. Before the emergence of this kind of material, cement, wax, some chemicals as well as soil-type materials (native or compacted soil) were utilized. However, these backfills demanded good compaction, and a uniform, quality backfilling was not ensured. The fluidized backfills were first proposed for use in electrical cable installations. After solidification (settling and hardening), they form a low thermal resistance and mechanically strong envelope for cables or pipes. A typical composition for such backfill consists of:

- 1) natural mineral aggregates to make up the bulk of the volume, such as crushed stone or stone screenings, gravel and sand,
- 2) cementitious materials to give the interparticle bond and strength, e.g., cement,
- 3) fluidizer to provide a homogeneous fluid consistency for ease of placement, as fly ash and bentonite, and

- 4) additives to improve thermal properties, such as metal filings, masonry sand, limestone, iron ore, magnetite dust and quartzite.

The choice of the aggregates and the cementing material are usually based on their general availability. Sand can serve as both the aggregate and the additive.

Bentonite, which is commercially available in powder form, is a swelling montmorillonite clay, and when mixed with water, expands and becomes a gel. In its gel form, it acts as a lubricant or fluidizer for the mix. Bentonite is applied in drilling operations as a lubricant, in hydraulic structures as a water seal, and in excavations as a stabilizer. It is now widely used in GCHP applications for its ready availability and its water retention property. However, it can shrink and crack upon drying, and swell when rewetted. Cement could not be used in this experiment because the backfill material in the hole needed to be changed easily without damaging the U-tube.

Remund and Lund (1993) analyzed the thermal conductivity of the bentonite grouts alone and bentonite mixed with various selected additives. The results showed that thermal conductivities of the bentonite grouts were relatively low compared to common soils under conditions normally found in the field. The measured data were around 0.75 W/m-K in comparison with the range from 0.35 W/m-K for light, dry soil to 2.42 W/m-K for heavy, saturated soil. They also investigated improving the thermal properties of bentonite mixed with the respective additives: clay, iron ore, limestone, masonry sand and quartzite. The percent additive was in the range of 0 to 70 % for each case and the percent bentonite varied from 3 to 36%. The rest was water. Remund and Lund concluded that at 70% additive level, quartzite provided grout mixtures with



conductivities of as high as 2.35 W/m-K. At that same additive level, sand, limestone and iron ore provided thermal conductivities of 1.79, 1.56 and 1.46 W/m-K. At 50% additive level, the quartzite, sand, limestone iron ore and clay produced thermal conductivities of 1.65, 1.35, 1.26, 1.175 and 1.13 W/m-K, respectively. Clay would not be a good choice because of its poor workability when adding more than 30 percent to the grout as well as the small improvement in conductivity. The mixtures became too thick and difficult to mix for additives over 50 percent. Also, for bentonite content higher than about 36%, the mixtures would be too thick to flow into the borehole. For very low bentonite content, the mixtures were too thin and the additives tended to settle to the bottom of the sample container. Bentonite-additive combinations near 20 percent produced the most uniform mixture and were easiest to mix. Therefore, the maximum net increase in thermal conductivity with the quartzite additive would be 100 percent.

**Backfills Used for the Experiments.** Two kinds of fluidized backfill materials were chosen for the experimental verification: (i) bentonite + masonry sand, and (ii) bentonite + copper powder. Backfills were chosen that would have higher conductivities than those of the soil and were also easy to install in the borehole.

The first backfill was a masonry sand blended with bentonite. After reviewing Remund and Lund's (1993) results, a composition of 12.5% bentonite, 25% sand and 62.5% water was used. It should be noted that different brands of bentonites from different suppliers may affect the workability of the mixture significantly. If the blend is too thin, the backfill will lose water quickly when placed into the hole due to initial water

infiltration to the surrounding soil.

The weighed bentonite had to be mixed thoroughly with the water first in a bucket with an electric mixer. Then the masonry sand was poured slowly into the bucket while the mixer was still running. The backfill was poured into the borehole and the U-tube was inserted gradually to avoid producing air bubbles. The density of the backfill was 1092 kg/m<sup>3</sup>. Its thermal conductivity and specific heat values were measured at 1.6 W/m-K and 3960 J/kg-K, respectively. The uncertainties in the conductivity and specific heat measurement (also for the soil) were 12%. The analysis of the experimental uncertainty associated with the measurement of these thermal properties ( $\rho$ ,  $c$  and  $k$ ) are included in Appendix B.

The second backfill material was composed of 10% bentonite, 25% copper powder and 65% water. The particle size of the powder was in the range of 100 to 355 microns. Although copper powder is cost prohibitive for field applications, it was used to evaluate the improvement on the U-tube heat exchanger performance with a high-conductivity backfill. Because of cost constraints, the thermal properties were not measured directly. The density was measured at 1205 kg / m<sup>3</sup>. However, the increase in thermal conductivity was not as large as expected, as indicated by the experiment. This phenomenon may be ~~attributed to the very small particle size of the powder and the use of too much bentonite.~~ It was found that the particles were enveloped by the slurry, forming an insulative layer around each to reduce the heat transfer between the high-conductivity particles. Use of slightly larger copper particles may have led to a greater increase in thermal conductivity of the mixture. The mixing procedure was exactly the same as described before.

### Experimental Procedures

Two tests were designed for the verification. One was a test with the bentonite/sand backfill (Test A). The other was a test with the bentonite/copper powder backfill (Test B). Before the start of each test, water was pumped into the circulation system to exclude air and to flush the inner wall of the U-tube to reduce the fouling resistance. The water flow rate was pre-adjusted to the expected value of 400 ml/min. The pump was then switched off when the heater was turned on to raise the water temperature inside the heater to a preset value (near 60 °C). It took approximately two hours for this process.

The supply water temperature from the heater could be maintained by the temperature controller. When this temperature reached the set value, the data acquisition system and the computer were switched on to scan the temperatures at all the sensor locations. The temperature distribution inside the soil and the backfill was checked for uniformity. Once the distribution was uniform, the pump was started and the data collection began.

For approximately the first hour, the scan interval was set at ten seconds to keep up with the fast changes of water temperatures inside the U-tube. The interval varied from 30 seconds to 3 minutes for the rest of time. ~~Each test was run for several hours.~~ Meanwhile, the pump was paused twice for five to seven minutes each time to simulate on/off cycles in a real GCHP system. IWT was also intentionally cycled up and down at times during on-cycle periods to better simulate cycling in GCHPs. The procedure could

be divided into three phases for each test and these phases are illustrated in Figs. 6.4 to 6.6 for Test A and in Figs. 6.7 to 6.9 for Test B. In these plots, the types, properties and sizes ( $D \times H$  = outer diameter  $\times$  height) of the soil and backfills as well as the range of the ambient air temperature are also provided. During the first phase, IWT increased from an initial value to a relatively stable state (Figs. 6.4 and 6.7). The initial water temperature was close to the initial soil temperature and the relatively stable state was around 60 °C. Next, the pump was switched off and then on twice to simulate on/off cycles in GCHPs (Figs. 6.5 and 6.8). In this phase, large temperature jumps in IWT occurred at the moments when the pump was turned on right after an off-cycle. This is because the water suddenly flushing into the U-tube was much hotter than the already cooled water inside during the preceding off-cycles and raised the IWT rapidly. Finally, IWT experienced fairly large fluctuations (Figs. 6.6 and 6.9) to simulate cycling in GCHPs. Such fluctuations were made by turning off and on the water heater repeatedly, or even by adding some cold water into a bucket to mix with the hot water from the heater, as was in Test B. The fluctuations were as large as 12.8 °C (in Test B). Table 6.1 provides detailed information about the on/off times and the range of variations in IWT for both tests. Test results during the second and third phases were used to examine whether the calculated results could still track the experimental data well during the on/off cycles and oscillations.

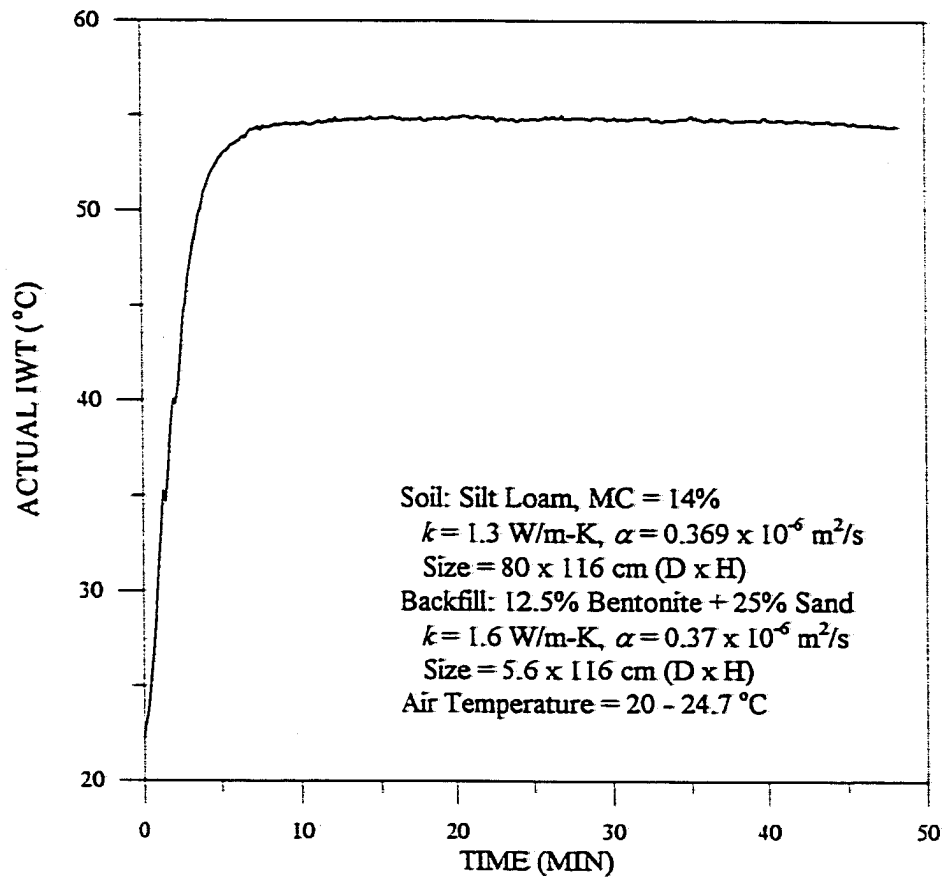


Fig. 6.4 Variation of IWT from start-up to steady state (0 - 48 min) in Test A

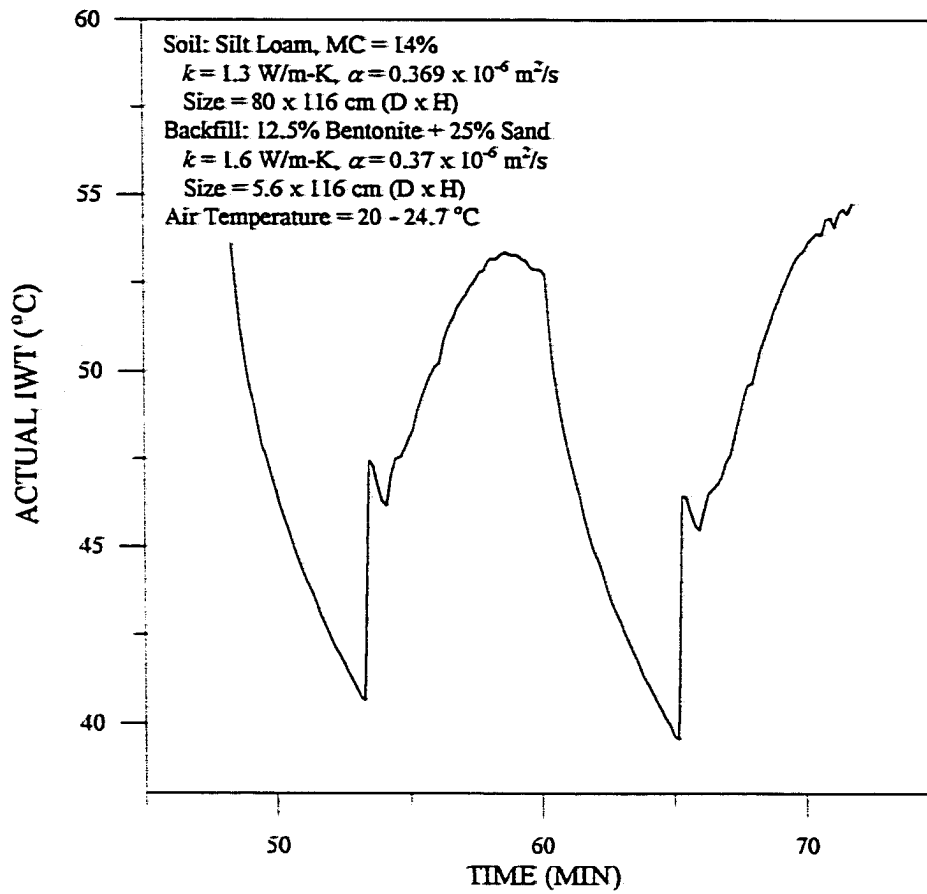


Fig. 6.5 Variation of IWT during the two on/off cycles (48 - 65 min) in Test A

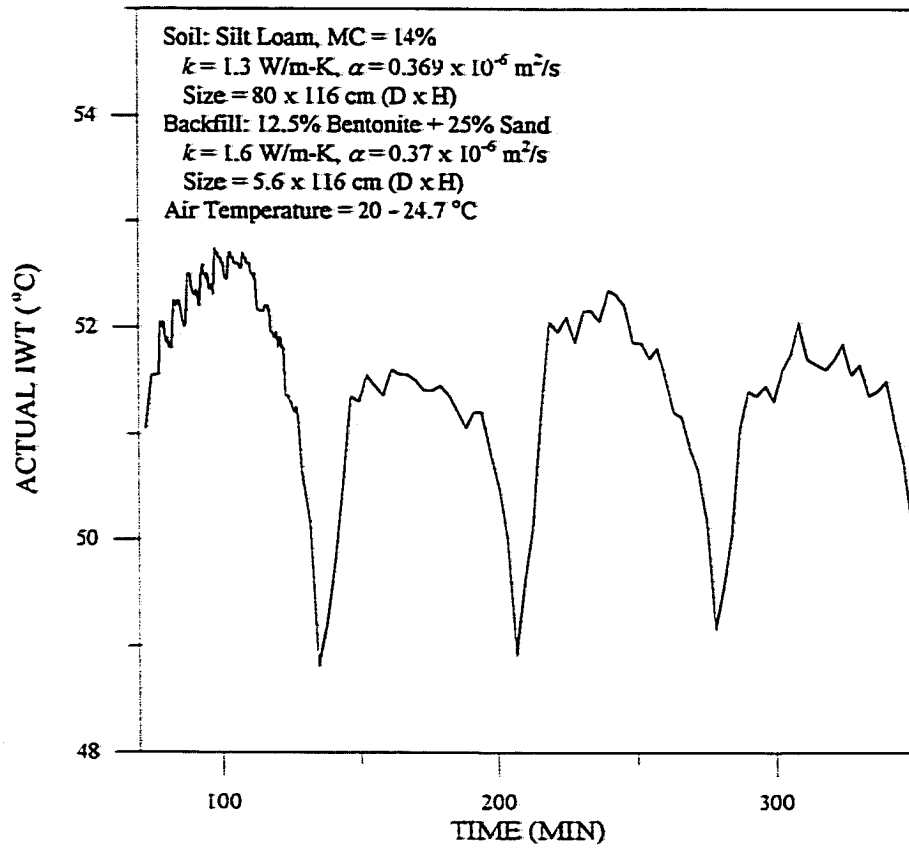


Fig. 6.6 Oscillation of IWT during the last phase (65 - 350 min) in Test A

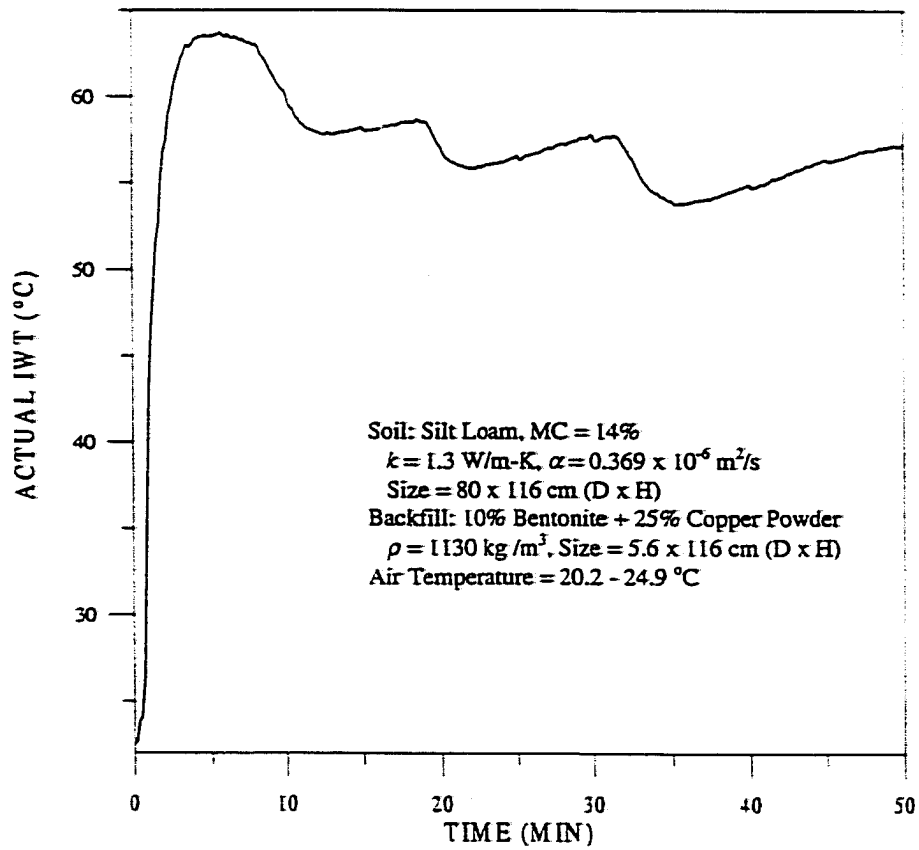


Fig. 6.7 Variation of IWT during the first phase (0 - 50 min) in Test B



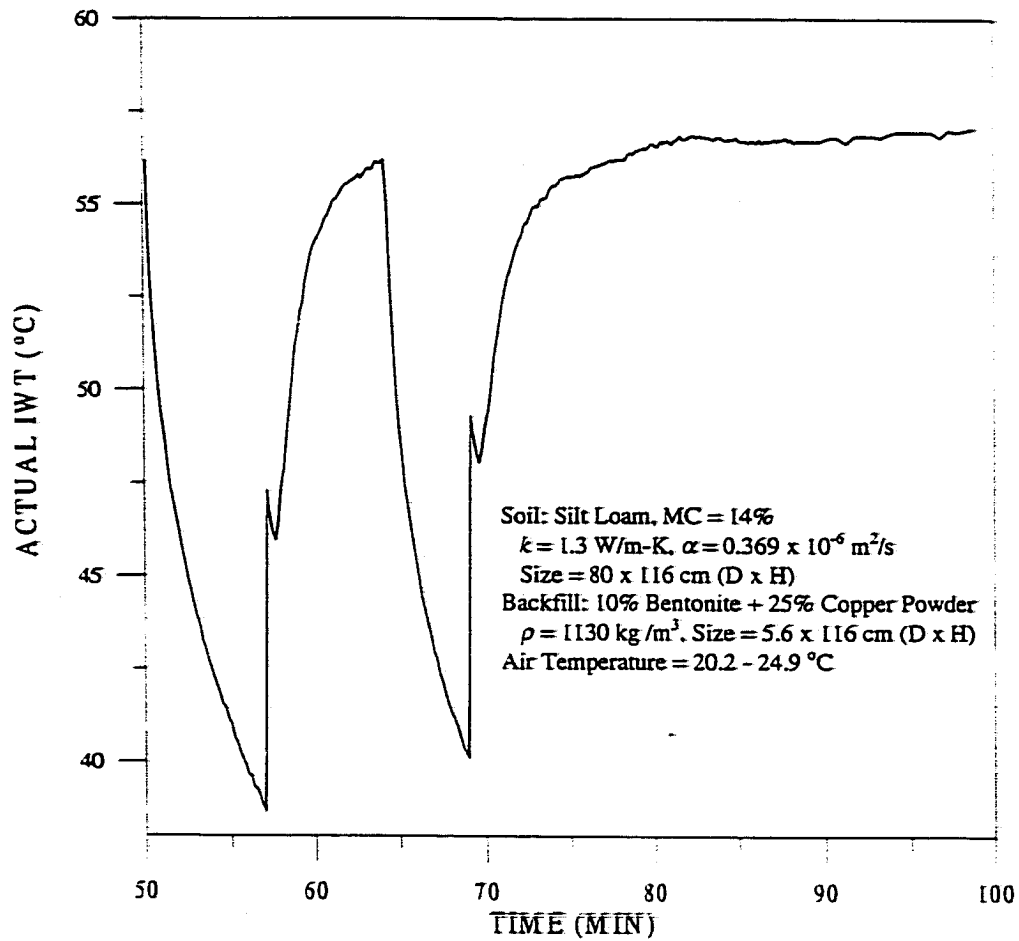


Fig. 6.8 Variation of IWT during the two on/off cycles (50 - 69 min) in Test B

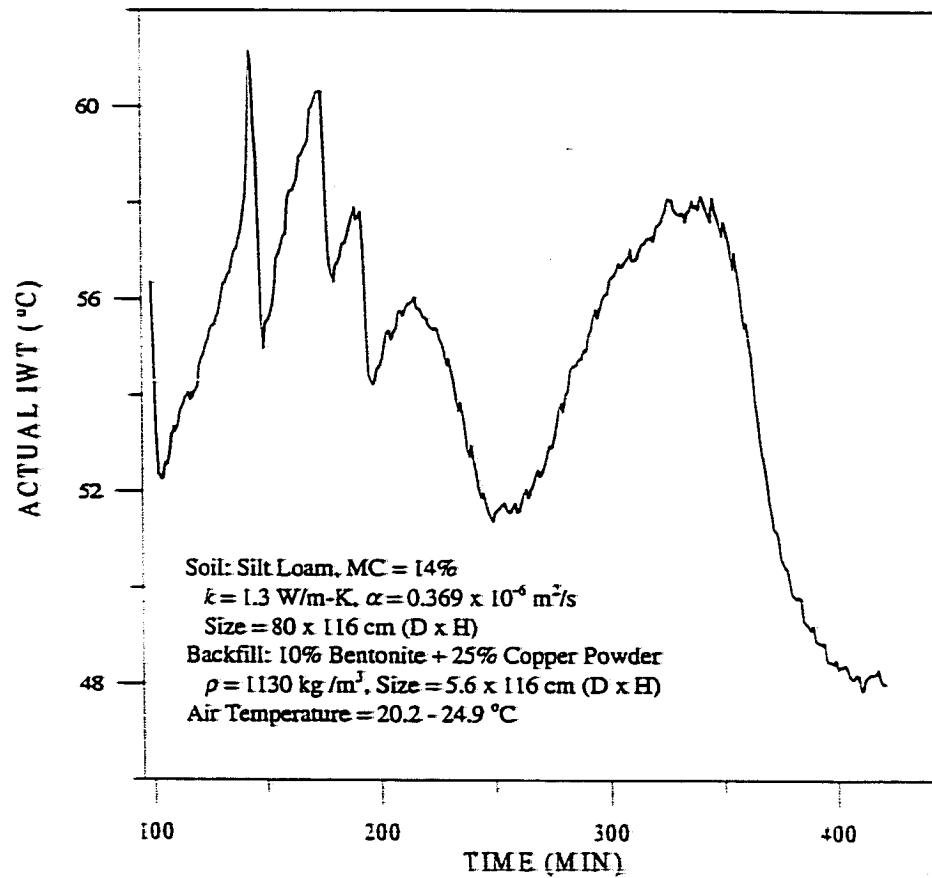


Fig. 6.9 Oscillation of IWT during the last phase (69 - 420 min) in Test B

**Table 6.1 Variation of IWT with time and on/off modes in Test A and Test B**

TEST A			TEST B		
Time (min)	On/Off	IWT (°C)	Time (min)	On/Off	IWT (°C)
0 - 48	On	22.2 - 55.0	0 - 50	On	22.5 - 63.7
48 - 53	Off	55.0 - 40.7	50 - 57	Off	63.7 - 38.7
53 - 60	On	40.7 - 53.4	57 - 64	On	38.7 - 56.2
60 - 65	Off	53.4 - 39.6	64 - 69	Off	56.2 - 40.1
65 - 350	On	39.6 - 56.6	69 - 420	On	40.1 - 60.9
350	Stop		420	Stop	

## CHAPTER VII

### COMPARISON OF MODEL AND EXPERIMENTAL RESULTS

The model developed in Chapter V was verified against experimental data from Test A and Test B defined in the last chapter. Major input parameters used in the simulation program are discussed below.

I. The mean temperature of the soil and bentonite/sand backfill during the whole process of Test A were 24 °C and 29 °C, respectively. Their thermal conductivity, specific heat as well as density were measured as

$$\text{Soil: } k = 1.3 \text{ W / m-K, } c = 2079 \text{ J / kg-K, } \rho = 1695 \text{ kg / m}^3.$$

$$\text{Backfill: } k = 1.6 \text{ W / m-K, } c = 3960 \text{ J / kg-K, } \rho = 1092 \text{ kg / m}^3.$$

From the above data, the thermal diffusivities ( $\alpha = k / \rho c$ ) were obtained at  $0.369 \times 10^{-6} \text{ m}^2/\text{s}$  for the soil and  $0.37 \times 10^{-6} \text{ m}^2/\text{s}$  for the backfill. Thermal properties for the bentonite/copper powder were not available. The same data as the above were applied to see how much difference it would make with the potential increase in conductivity.  $S_b$  and  $S_c$  were taken as 8.8 and 909, respectively.

2. During the on-cycle, the volumetric flow rate was fixed at 400 ml/min, which yielded a flow velocity of 0.37 m / s. The Reynolds number, defined as  $Re_d = u d_m / \nu$ , was 3169 which was within the transition flow regime. Kavanaugh (1984) discussed the evaluation of heat transfer coefficients for the transition regime and gave the following correlation:

$$h = \frac{J(\rho c)_f u}{Pr^{2/3} (\mu_w / \mu_f)^{0.14}} \quad (7.1)$$

where

$$J = \left[ .0044 - .0012 \exp\left(\frac{2200 - Re_d}{1300}\right) \right] - \left( 1.4 - \frac{Re_d}{5000} \right) \left( \frac{L/d_{in} - 50}{8.7 \times 10^{10}} \right)^{1/3} \quad (7.2)$$

The convection coefficient was calculated to be 1624 W/m<sup>2</sup>-K using the above equations.

Kavanaugh also reviewed correlations for free convection inside a vertical tube and presented one developed by Martin and Cohen (1954). It is modified in form and given below.

$$Nu = \frac{Gr_r Pr r_{in}}{892 L} \quad 10^3 \leq Gr_r Pr \leq 10^{5.2} \quad (7.3)$$

where  $Gr_r$  is the Grashof number determined by the characteristic length,  $r_{in}$ . The scope of the product of the Grashof number and the Prandtl number (i.e., Raleigh number) was met during the off-cycles. The free convection coefficient was calculated to be 33.9 W/m<sup>2</sup>-K using equation (7.3). However, a value of 30 W/m<sup>2</sup>-K was finally chosen to achieve reasonable agreement with the measured data. This lower value might have included the fouling factor inside the tube.

3. An in-tube fouling resistance was included in the part of the water-side resistance because the inside wall of the pipe might not be perfectly clean after a few trial tests. A recommended value of .00055 m<sup>2</sup>-K/W by Yang (1980) for water at 50 °C was selected for the on-cycle.

4. The effective heat transfer length of the U-tube was determined by the height to which the backfill material was filled. It was observed that the backfill could sink up to two centimeters after the test, probably due to a decrease in its water content. This led to

about 2% reduction in heat transfer area. The wooden spacers and the teflon tape wrapping around the welded thermocouple joints also contributed to the reduction. As a result, an effective heat transfer length was taken as 112 cm measured from the bottom of the U-tube heat exchanger. The entire U-tube was divided into ten elements and thus the length of each element was 22.4 cm.

In the verification runs, two time intervals were chosen. They were (1) sixty ten-second time intervals, and (2) the rest stored in three-minute intervals. As a comparison, these are equivalent to about three-minute and seventy-five-minute intervals for a typical GCHP. Temperature data were continuously collected at time intervals of ten seconds to three minutes. The ten-second data scan intervals were used for approximately the first hour including all the start-up and off-cycles.

Although the spacers were used, the leg spacing was not constant along the U-tube because the designed small spacing could not be obtained near the bottom with a commercially available "U" coupling to join the two legs together. The average value was taken as 1.4 cm which nearly corresponded to  $L_S = 2D$ .

Figures 7.1 to 7.3 show the comparisons of the experimental and simulated OWT using the superposition and equivalent diameter techniques in Test A. The actual OWT profiles are presented while the predicted data are represented by their curve-fits. In Fig. 7.1, the actual OWT increased from the initial value of 22.2 °C to a steady state value of 52 °C. Figure 7.2 shows the comparison of OWT values during the on/off cycles in the second phase. In Fig. 7.3, there were fluctuations up to 4 °C in OWT caused by the

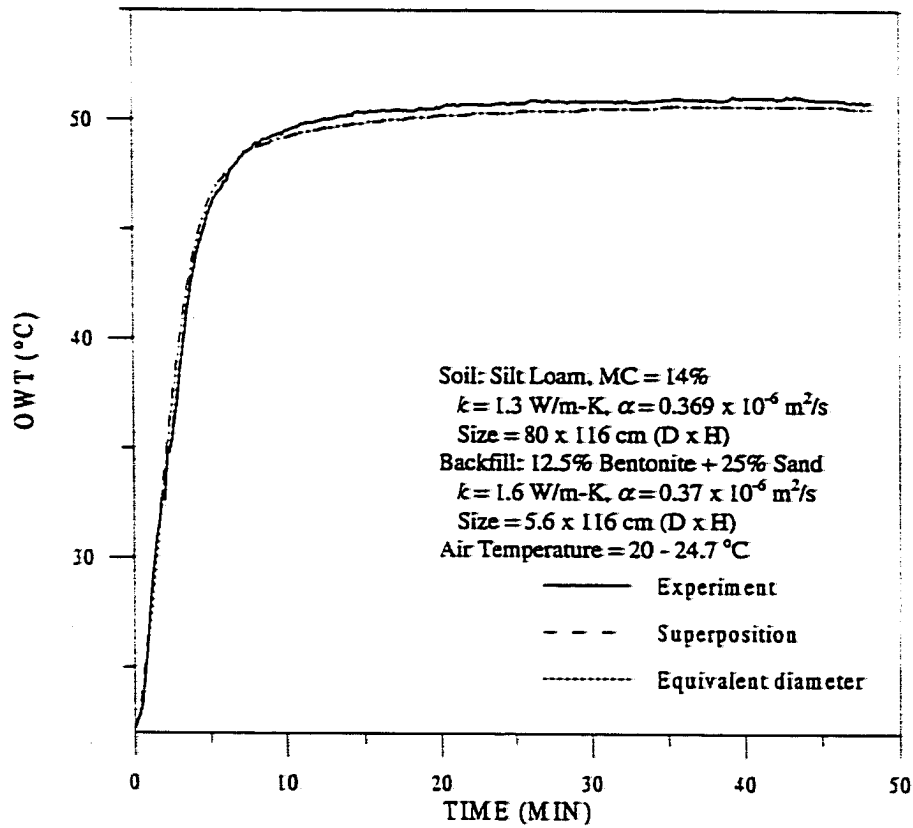


Fig. 7.1 Comparison of OWT during the first phase in Test A

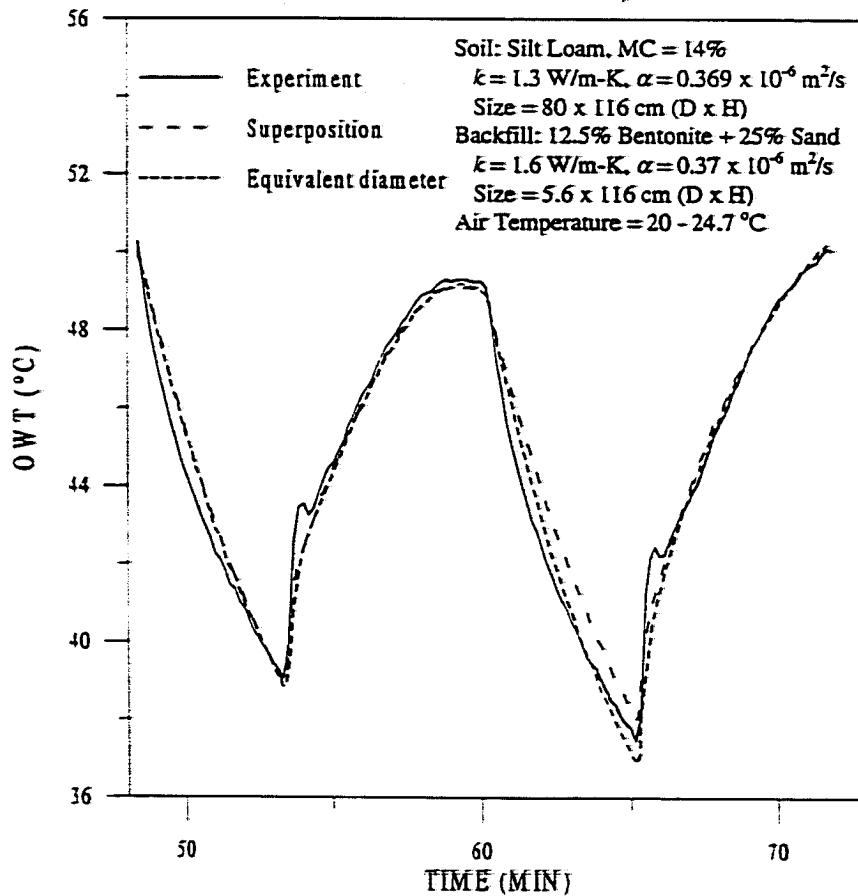


Fig. 7.2 Comparison of OWT during the second phase in Test A



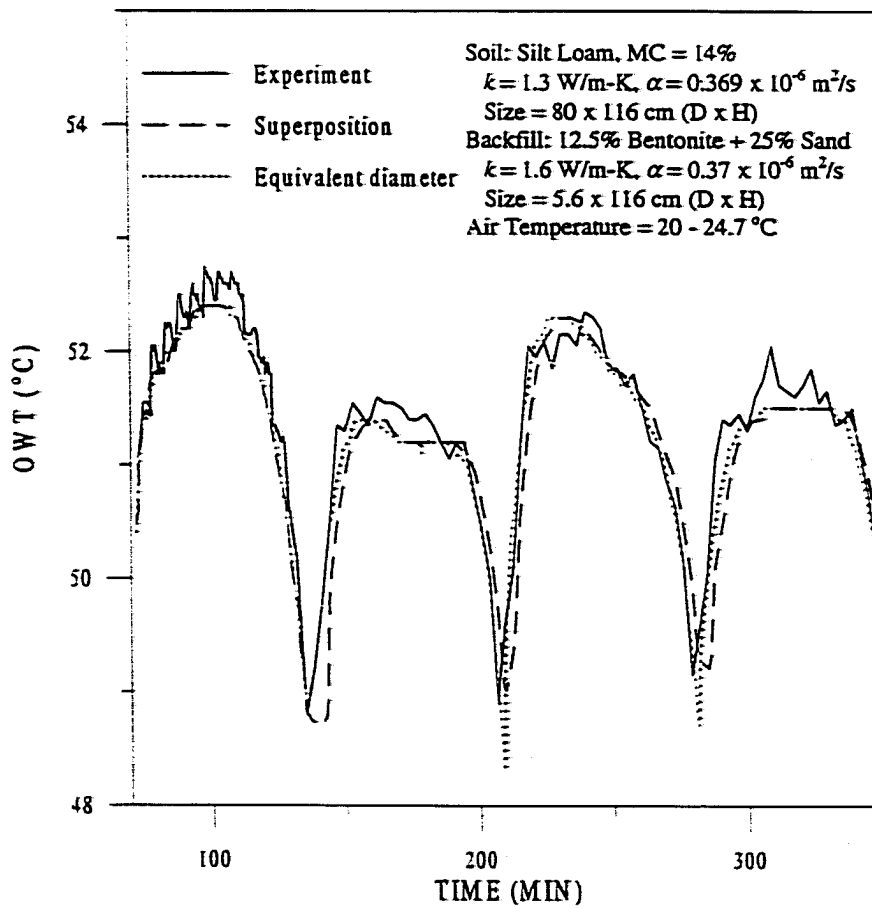
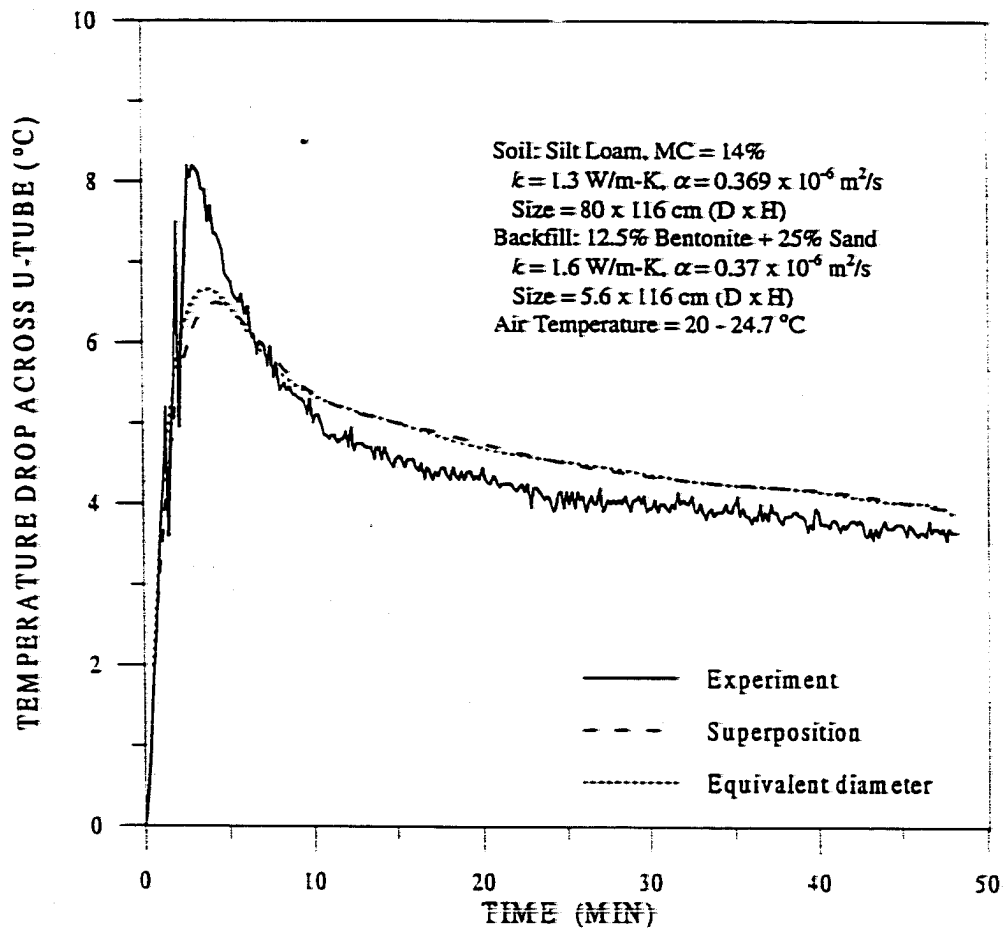


Fig. 7.3 Comparison of OWT during the third phase in Test A

manmade oscillations in IWT described earlier. The model generally underestimated OWT over the six hours' simulation but was within 0.5 °C most of the time. It also tracked the trends in OWT reasonably well during the start-up and off-cycles. Predictions with the superposition and the equivalent diameter approaches achieved results with discrepancies of less than 0.25 °C on average.

The corresponding temperature drop across the U-tube heat exchanger ( $\Delta T$ ) are shown in Figs. 7.4 to 7.6. In these figures, the difference between the experimental and predicted results are made more clear. During the initial start-up in Fig. 7.4, the pipe wall was heated up gradually due to its thermal capacity. This capacity was neglected in the model and thus the wall temperature attained a higher value almost immediately in the simulation. The predicted temperature drop was considerably smaller than the measured for the first four minutes because of the reduced temperature difference between the water and the pipe wall. As the pipe and backfill increased in temperature,  $\Delta T$  went down quickly. The two jumps right after the off-cycles in Fig. 7.5 were caused by the suddenly raised temperature difference between the inlet and outlet when the hot water from the inlet hose was pumped into the U-tube. On average, the measured  $\Delta T$  was approximately 4 °C for the first two hours and 3.2 °C for the rest of time. The simulations with both thermal short-circuiting models overpredicted  $\Delta T$  by approximately 0.5 °C over the whole time range.

Similar comparisons were made and presented in Figs. 7.7 through 7.12 for Test B. The cyclic behavior varied from that shown before and the temperature level was higher. There were also two off-cycles, but larger on-time fluctuations occurred. The



**Fig. 7.4 Comparison of temperature drop across the U-tube heat exchanger during the first phase in Test A.**

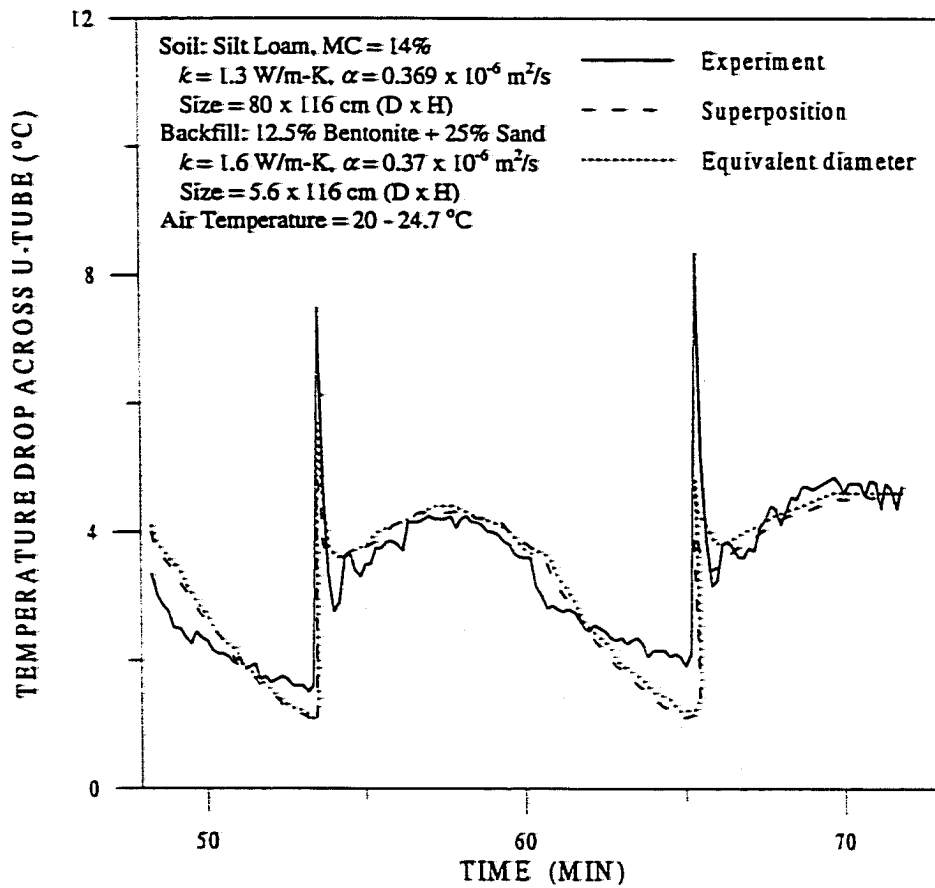


**Fig. 7.5 Comparison of temperature drop across the U-tube heat exchanger during the second phase in Test A**

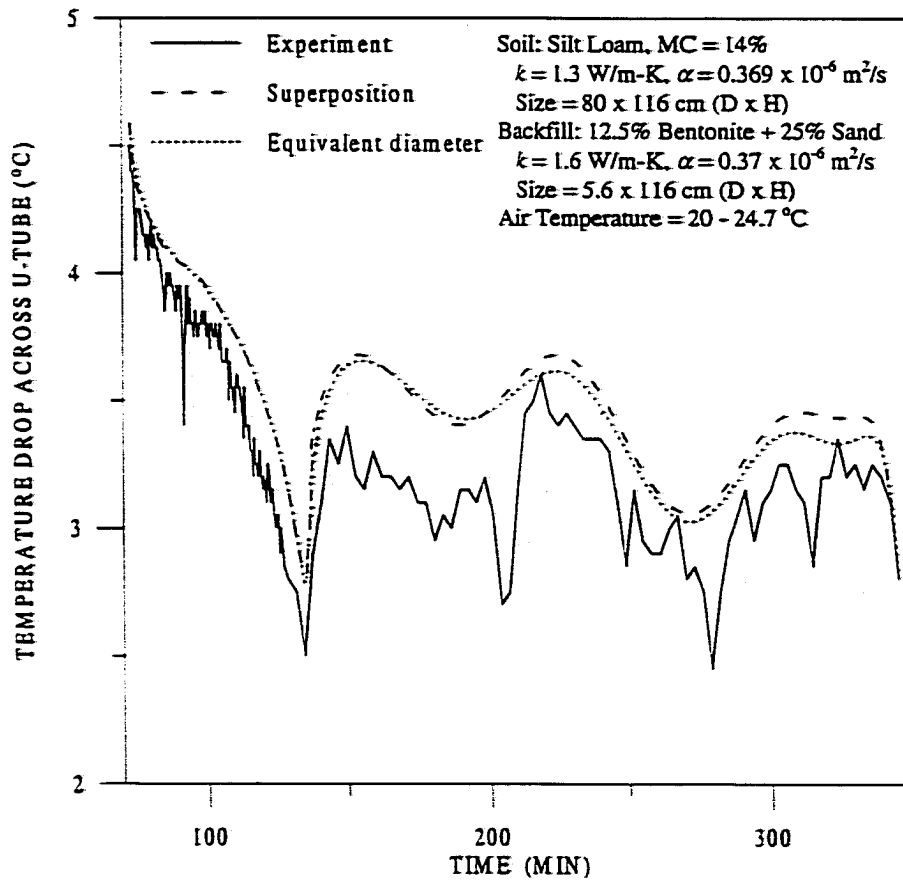


**Fig. 7.6 Comparison of temperature drop across the U-tube heat exchanger during the third phase in Test A**

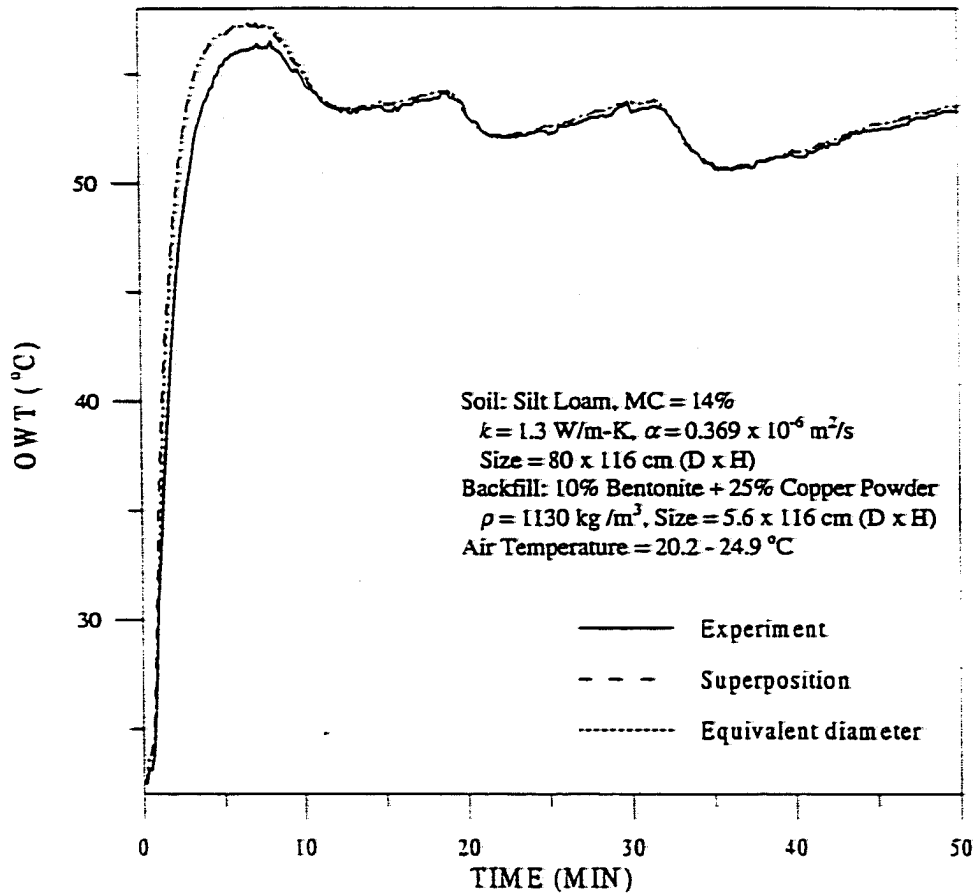


Fig. 7.7 Comparison of OWT during the first phase in Test B

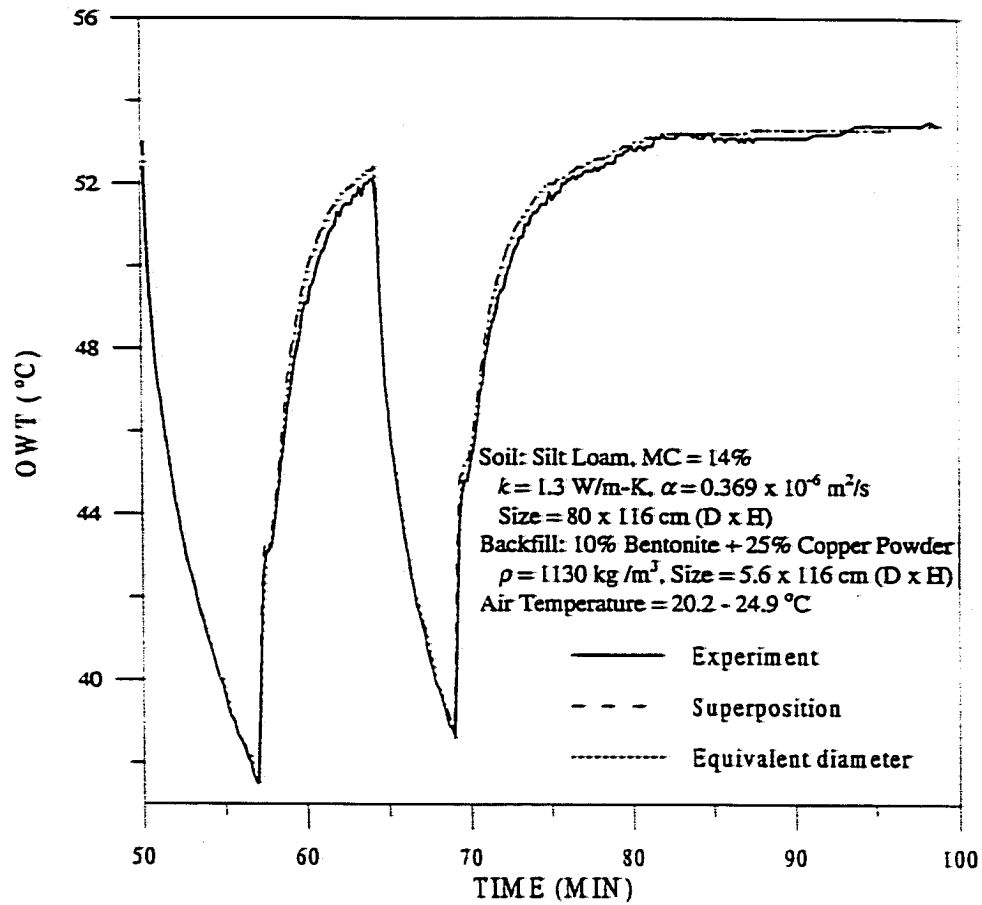


Fig. 7.8 Comparison of OWT during the second phase in Test B

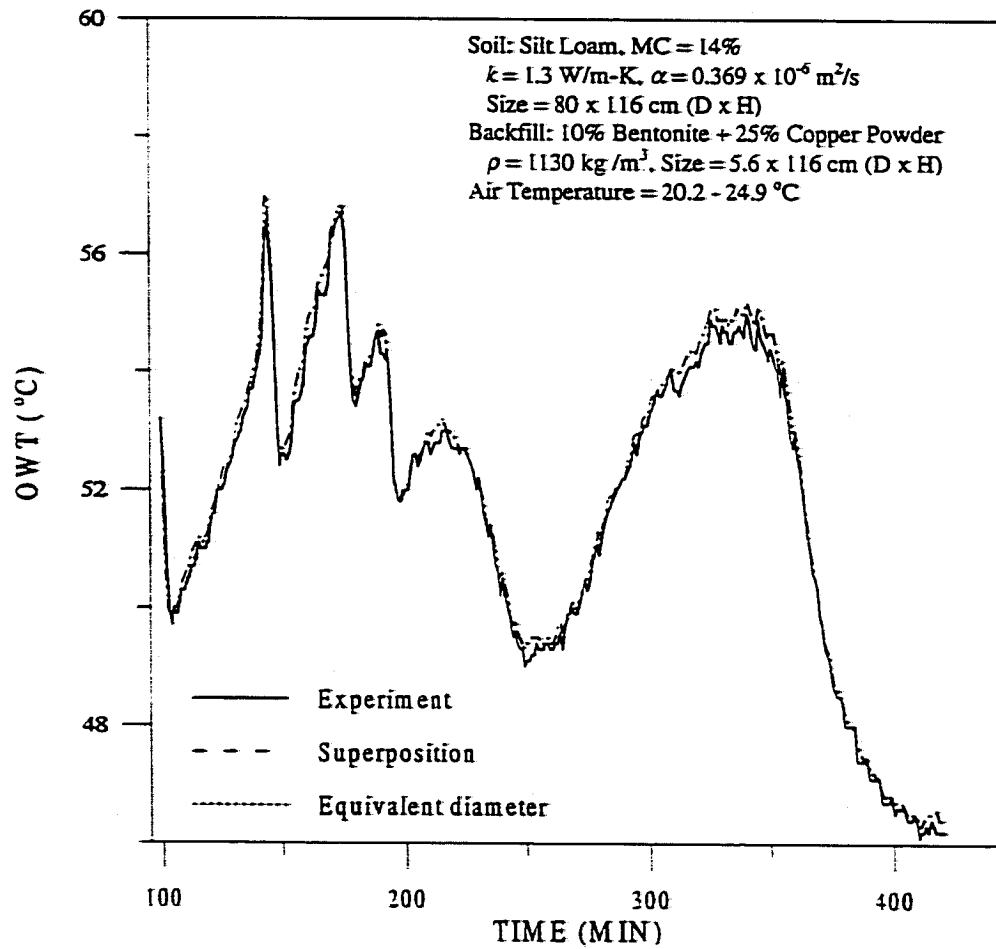
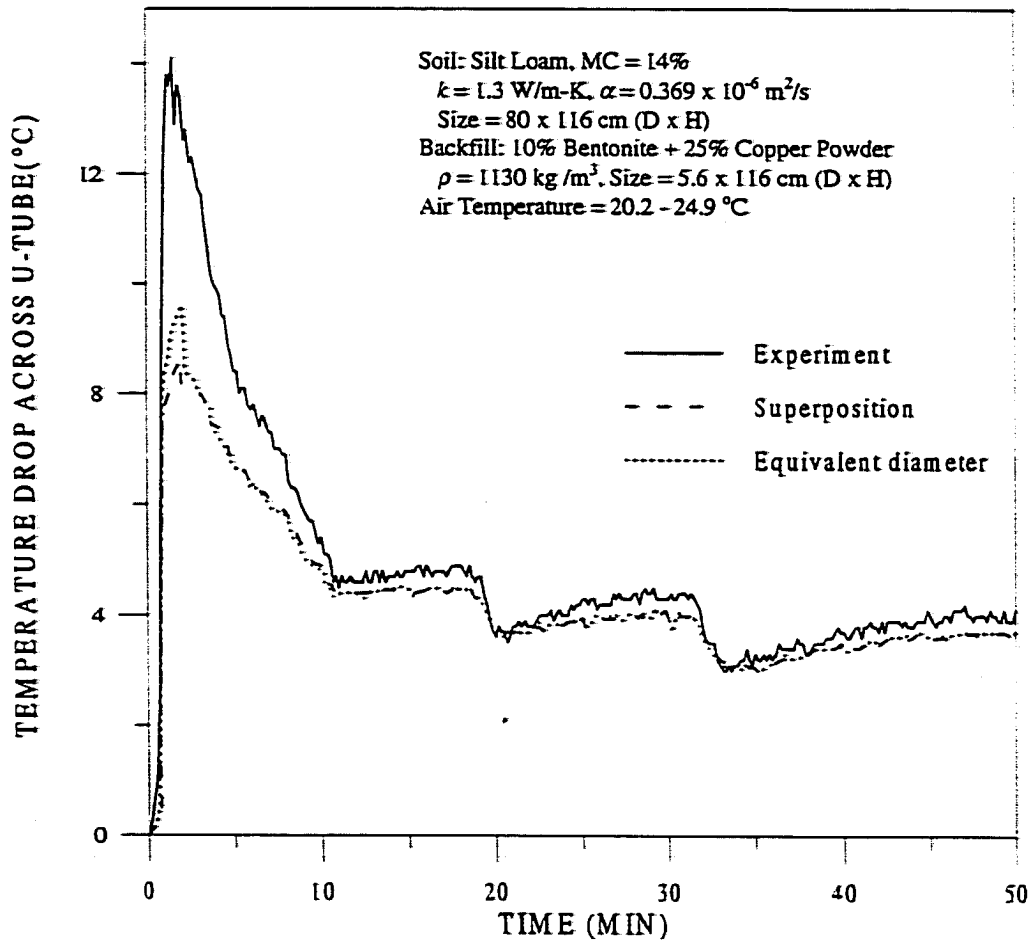
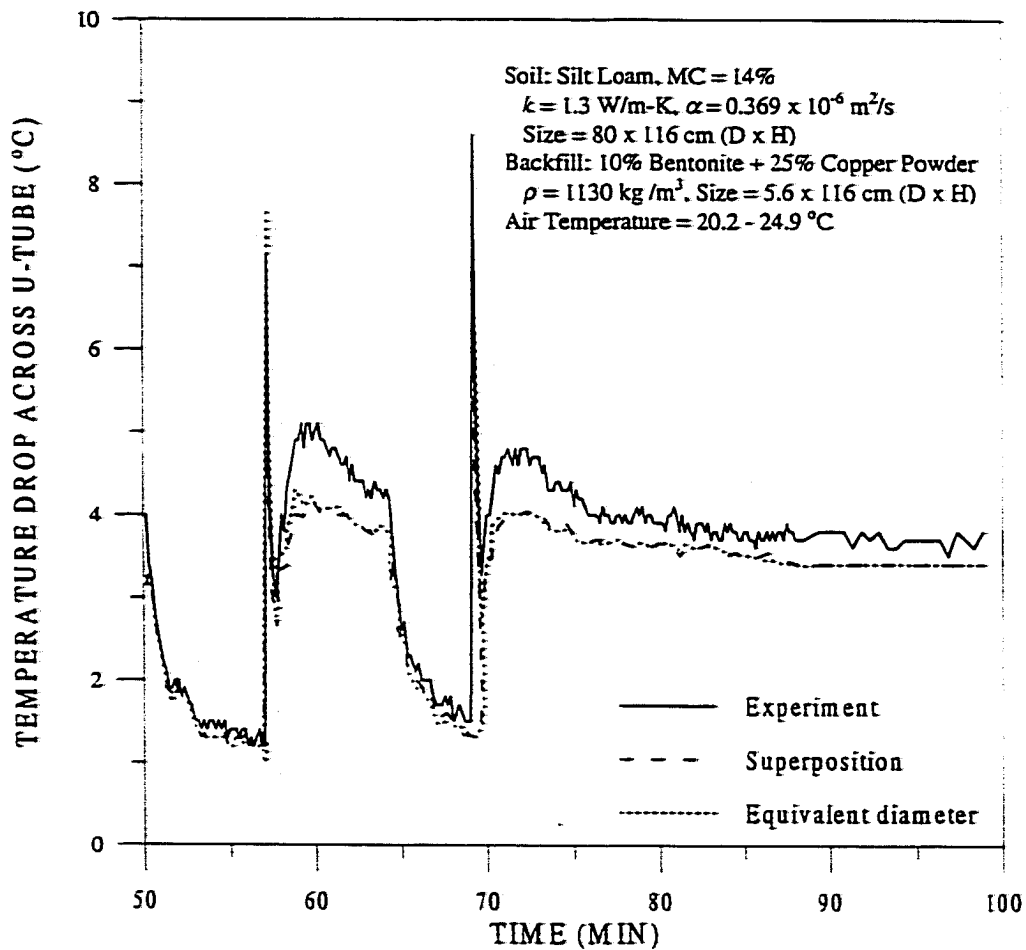


Fig. 7.9 Comparison of OWT during the third phase in Test B





**Fig. 7.10 Comparison of temperature drop across the U-tube heat exchanger during the first phase in Test B**



**Fig. 7.11 Comparison of temperature drop across the U-tube heat exchanger during the second phase in Test B**

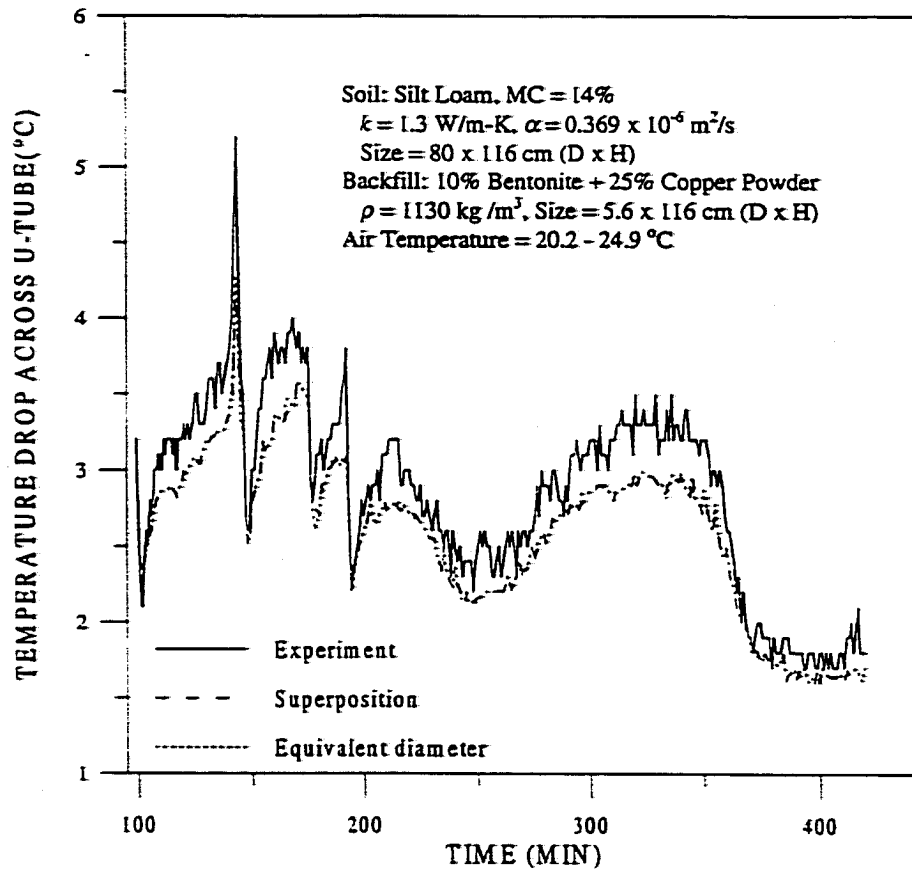


**Fig. 7.12 Comparison of temperature drop across the U-tube heat exchanger during the third phase in Test B**

major distinction from the previous simulation results was that OWT was generally overestimated within 0.5 °C, while the temperature drop was underestimated by 0.5 °C on average. It could be inferred that with the bentonite/copper powder backfill in place of the bentonite/sand backfill, OWT would decrease or  $\Delta T$  would increase by up to 1 °C if the average temperature level is maintained. The total heat rejection would increase by 25 - 30 percent based on the constant mass flow rate.

Figures 7.13 and 7.14 show the variations of the ambient air and the tank wall temperatures. Although the air temperature exhibited large fluctuations, the tank wall temperature had relatively stable values. The ambient air temperature near the tank varied from 20 to 24.7 °C during Test A and from 20.2 to 24.9 °C during Test B. Such big temperature fluctuations in a conditioned room probably attributed to the fact that the tank was set immediately under the supply air vent. Accordingly, the tank wall temperature ranged from 21.2 to 22.9 °C for Test A and from 21.8 to 23.3 °C for Test B. For most of the time, the air temperatures were varying periodically with a period of nearly 100 minutes. The tank wall temperature was obviously affected by such a pattern of variation and displayed small fluctuations which somewhat lagged behind those of the air temperature. However, both had about the same average value. The amplitudes of the air temperature oscillations in Test A and Test B were both 4.7 °C and those for the tank wall temperatures were 1.7 °C and 1.5 °C, respectively.

To better understand temperature variations in the soil, Tables 7.1 and 7.2 provide every hour's soil temperature data from the beginning to the end of the simulations at various thermocouple locations. Unfortunately, TC #17 had been broken even before the

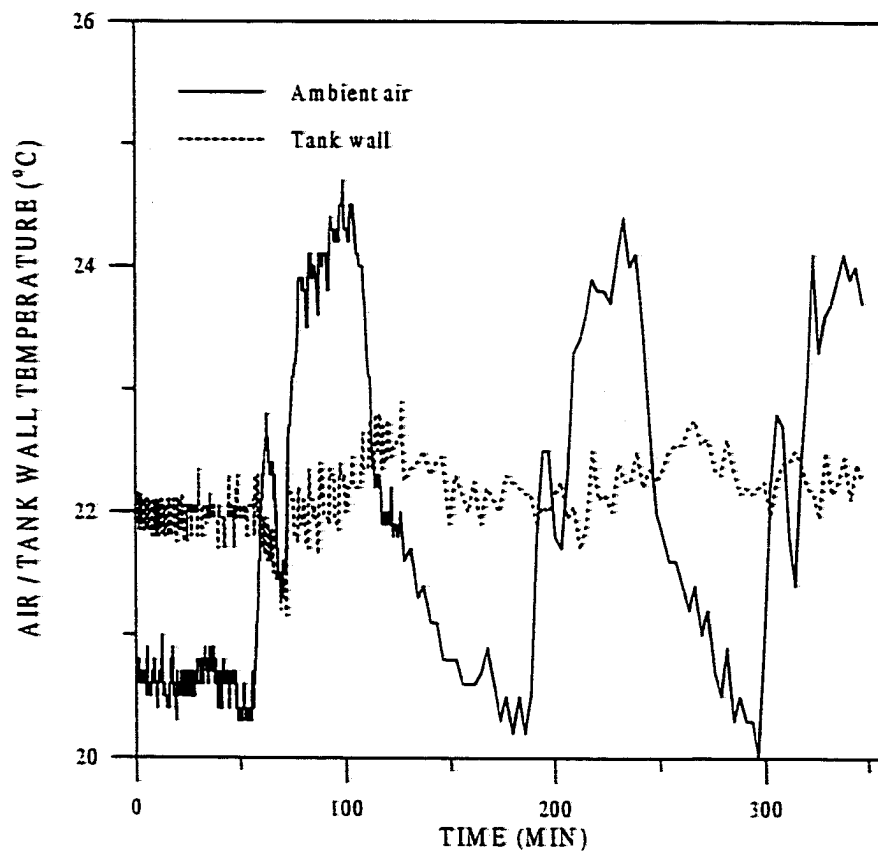
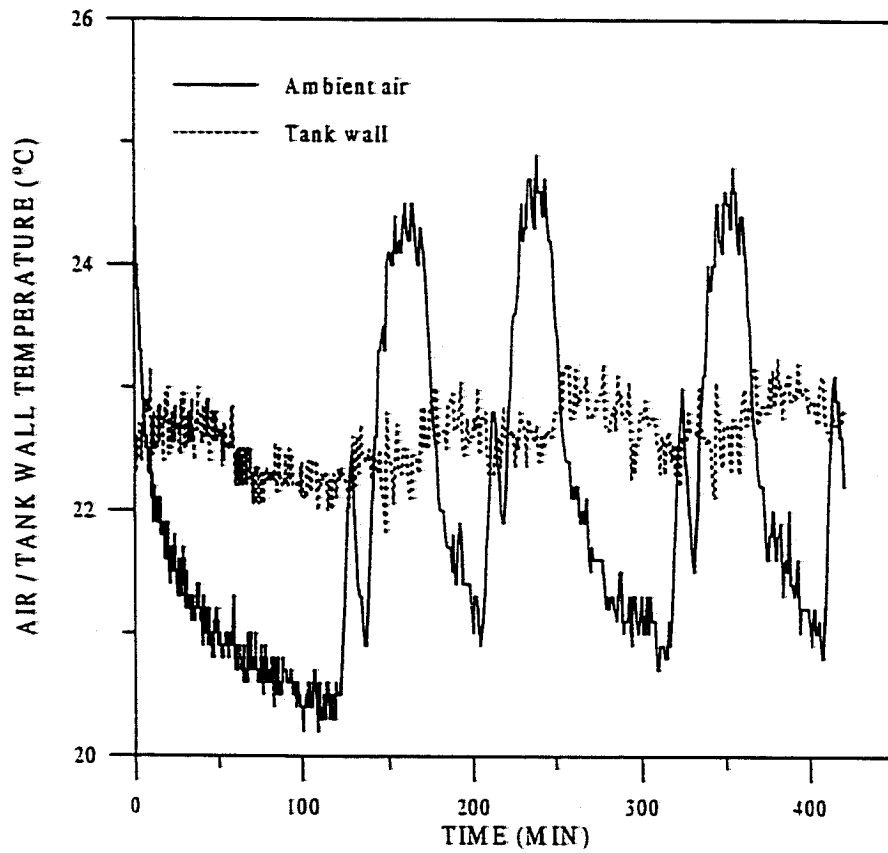


Fig. 7.13 Variations of ambient air and tank wall temperatures during Test A



**Fig. 7.14** Variations of ambient air and tank wall temperatures during Test B

**Table 7.1 Variation of soil temperature distribution with time in Test A**

Time (h)	Soil Temperature (°C)									
	#11	#12	#13	#14	#15	#16	#18	#19	#20	Ave.
0	22.6	22.8	22.5	22.5	22.4	22.8	22.8	22.6	22.3	22.6
1	22.9	22.9	22.7	22.7	22.5	24.1	23.0	22.6	22.3	22.9
2	23.8	23.4	22.9	22.9	22.9	25.4	23.2	23.0	23.0	23.4
3	24.0	23.6	22.7	22.6	22.3	26.3	23.5	22.8	22.3	23.3
4	24.4	24.1	22.7	22.6	22.3	27.0	23.8	23.0	22.8	23.6
5	24.9	24.3	22.8	22.5	22.3	27.5	24.0	23.1	22.3	23.7
6	25.2	24.7	23.0	22.6	22.6	27.8	24.3	23.3	22.9	24.0

(Average initial backfill and water temperatures were 22.5 °C and 22.2 °C, respectively.)

**Table 7.2 Variation of soil temperature distribution with time in Test B**

Time (h)	Soil Temperature (°C)									
	#11	#12	#13	#14	#15	#16	#18	#19	#20	Ave.
0	21.5	20.9	21.4	21.0	21.0	21.8	21.5	21.2	22.4	21.4
1	21.9	21.1	21.6	21.1	21.2	23.3	21.5	21.6	22.5	21.8
2	22.3	21.4	21.7	21.0	20.9	24.5	21.8	21.7	22.2	21.9
3	23.0	21.9	21.5	20.9	21.1	25.6	22.1	21.6	22.5	22.2
4	23.4	22.3	21.6	20.8	20.8	26.4	22.5	21.6	22.8	22.5
5	24.1	22.9	22.1	21.3	21.2	26.9	23.1	22.2	22.6	22.9
6	24.3	23.1	22.2	21.2	21.3	27.4	23.2	22.2	22.5	23.0
7	24.1	22.9	22.0	21.2	21.2	26.8	23.0	22.2	22.7	22.9

(Average initial backfill and water temperatures were 22.4 °C and 22.5 °C, respectively.)

first trial test began. The average initial temperatures for the backfills and the water inside the U-tube are also given in these tables. The average initial temperatures of the composite media were used as input data in the simulations.

Tables 7.1 and 7.2 show that there was a nonuniformity of 0.5 °C and 1.5 °C respectively in the initial temperature distribution in the composite media. This would contribute to the experimental error when the comparison was made to the simulation in which a uniform initial temperature distribution was assumed. Because TC #16 through #20 were buried on the same side as the “hot” leg where the hot water entered the U-tube, their temperature readings were higher than those taken from TC #11 through #15 at their corresponding radial locations. The average soil temperature on the “hotter” side were as much as 0.96 °C and 1.4 °C higher than that at the opposite side during Test A and Test B, respectively. However, these temperature differences might have been affected by the non-uniform thermal properties due to uneven compactness of the soil.

These tables also show that soil temperatures closest to the tank wall (i.e., TC #15 and #20) had small fluctuations within  $\pm 0.3$  °C around the initial values. This guaranteed a fixed far-field temperature condition as prescribed in the development of the analytical solution. The average soil temperatures were subject to both the heat dissipation from the U-tube heat exchanger and the environment. Therefore, it was not surprising that the calculated average soil temperature could decrease as the experiment proceeded from two hours to three hours in Table 7.1, and from six hours to seven hours in Table 7.2. However, the soil temperatures nearby the heat exchanger were always increasing as time went on.



Another interesting phenomenon was observed in the tests. During the off-cycles, the wall temperatures along the U-tube (denoted by TC #1 to #9 in Fig. 6.2) always achieved the lowest value at the bottom (i.e., TC #5). This phenomenon is clearly shown in Table 7.3 when compared to a typical on-cycle wall temperature distribution. The bottom temperature could be as much as 4.6 °C lower than the two adjacent ones (TC #4 and #6) at about 2.5 minutes after the shutdown. This was believed to be caused by the end effect that the bottom part of the U-tube not only rejected heat in radial direction but also to the bottom of the tank where the bulk temperature was relatively lower due to less heat dissipation to it. This phenomenon became almost undetectable during the on-cycle because the water ran through the bottom of the U-tube very quickly and had little time to transfer heat to the surrounding medium. It could also be observed in a real GCHP system as described in Chapter II when Dobson's (1991) work was reviewed.

**Table 7.3 Typical wall temperature distribution along the U-tube in Test A**

Operation Mode	Wall Temperature (°C)								
	#1	#2	#3	#4	#5	#6	#7	#8	#9
On-Cycle	56.4	55.4	54.9	54.6	<u>53.8</u>	53.6	53.4	53.0	52.8
Off-Cycle	47.6	46.6	46.1	45.9	<u>41.3</u>	45.6	45.6	46.0	45.9

## **CHAPTER VIII**

### **PARAMETRIC STUDIES**

Some parameters related to the geometry of the U-tube, the size of the backfill region as well as the thermal properties of the soil and backfill have a direct effect on the performance of the U-tube heat exchanger. The geometric parameters include the length of the U-tube, the diameter of the leg and the leg spacing. To focus on the effect of backfill materials, the diameter of the leg, the length of the U-tube and soil properties were fixed in this study.

#### **Parameter Selection**

A typical U-tube heat exchanger for a GCHP was considered. A U-tube configuration similar to that simulated by Dobson (1991) was chosen except the length of the U-tube was changed. In Dobson's study, there were three coils of the same size arranged in parallel with each approximately 67 m long. In this study, only one coil with a length of 134 m was used. With this length, the temperature drop between the inlet and outlet of the U-tube during the on-time could still maintain a value of nearly 5 °C after 30 days of operation under the assumed homogeneous-medium condition. This temperature difference would be desirable for a GCHP system. The U-tube was made of 2.68 cm OD polyethylene pipes. The volumetric flow rate of the circulating water used by Dobson was 11.36 l /min and this value was used here. Both forced and free convection coefficients are also the same as those in Dobson's simulation. All input data are included in Appendix A.

Suppose a GCHP supplied water at a constant temperature of 35 °C at the inlet of the U-tube heat exchanger for 30 minutes, then was cycled off for 30 minutes, and this process was repeated each hour for 30 days. The far-field ground temperature was assumed at 22 °C. The equivalent diameter approach was utilized for the parametric studies. The coil was divided into ten elements and the time intervals were determined as (1) 60 six-minute time intervals, (2) 100 one-minute time intervals, and (3) the remainder stored in twelve-hour time intervals.

The thermal conductivity and diffusivity of the soil were taken as 1.732 W/m-K and  $0.96 \times 10^{-6}$  m<sup>2</sup>/s, respectively.  $S_c$  was fixed at 909. The parameters were divided into three groups for the investigations on effects of: (1) backfill to soil thermal property ratios,  $H$  and  $G$ , (2) the size of the backfill region represented by the ratio,  $S_b$ , and (3) the leg spacing,  $L_s$ . As shown in Table 8.1,  $H$  equals  $G$  and both varied from 0.2 to 5 in Group I. In Group II,  $S_b$  was in a range of 5 to 20 with the leg spacing being  $2D$ , and in Group III,  $L_s$  varied from  $D$  to  $10D$  with  $S_b = 40$ . In both Group II and III,  $H$  and  $G$  were taken as 2 and 0.5, respectively for each  $S_b$  and  $L_s$  variation. These combinations provided twenty cases altogether for the simulation. The first case in Group I was selected as the base case for comparison since it was a homogeneous medium and closest to Dobson's (1991). The magnitude of the parameters used in the three groups might be beyond those in typical applications. However, the results were useful for analyzing the potential achievements with variations of individual parameters. In most field applications,  $H$  and  $G$  values are smaller than 2 and low values could appear when the backfill gets dry and shrinks or cracks, while the leg spacing and  $S_b$  are nearly  $2D$  and 5, respectively.

Table 8.1 List of cases in the three groups used for parametric studies

GROUP I			GROUP II			GROUP III		
$D = 2,68 \text{ cm}, L = 134 \text{ m}$ $L_s = 2D, S_b = 5$			$D = 2,68 \text{ cm}, L = 134 \text{ m}$ $L_s = 2D$			$D = 2,68 \text{ cm}, L = 134 \text{ m}$ $S_b = 40$		
Case No.	$H, G$		Case No.	$S_b$	$H, G$	Case No.	$L_s$	$H, G$
1	1.0		1	5	2.0	1	$D$	2.0
2	1.5		2	10	2.0	2	$2D$	2.0
3	2.0		3	20	2.0	3	$4D$	2.0
4	3.0		4	5	0.5	4	$10D$	2.0
5	5.0		5	10	0.5	5	$D$	0.5
6	0.5		6	20	0.5	6	$2D$	0.5
7	0.3					7	$4D$	0.5
8	0.2					8	$10D$	0.5

## Results and Discussion

The temperature drop across the U-tube during the on-time ( $\Delta T$ ) and the heat rejection from the heat exchanger to the earth are two important parameters for the evaluation of the U-tube heat exchanger performance. Therefore, the results were plotted in the following forms:

1. Comparison of the temperature drop,  $\Delta T$ , at the end of the last on-cycle for each day during the 30-day simulation.
2. Comparison of the daily energy exchange between the soil and coil,  $Q_d$ , for 30 days.
3. Comparison of the cumulative energy exchange between the soil and coil,  $Q_{acc}$ , over 30 days' operation.

Figures 8.1 through 8.3 show the above comparisons for varied parameters in Group I. In Fig. 8.1,  $\Delta T$  decreased quickly and then leveled off with time for all cases. For the base case,  $\Delta T$  decreased from 6.5 °C to 4.9 °C during the 30-day simulation. For a given time,  $\Delta T$  increased as  $H$  and  $G$  increased. If  $H$  and  $G$  were both lowered or raised by the same percentage relative to the base case, the time-averaged  $\Delta T$  would decrease faster than it would increase. For example, when  $H$  and  $G$  doubled or decreased by a factor of 2, the average  $\Delta T$  increased by about 11% or decreased by 18%, respectively. The highest and lowest values of the average  $\Delta T$  achieved in cases  $H = G = 5$  and  $H = G = 0.2$  were 6.4 °C and 2.5 °C, respectively. Figure 8.2 showed similar variations and nearly the same percent increase or decrease in average daily energy exchange ( $Q_d$ ) from case to case. An average value of 54 kWh was obtained in the base case. Figure 8.3

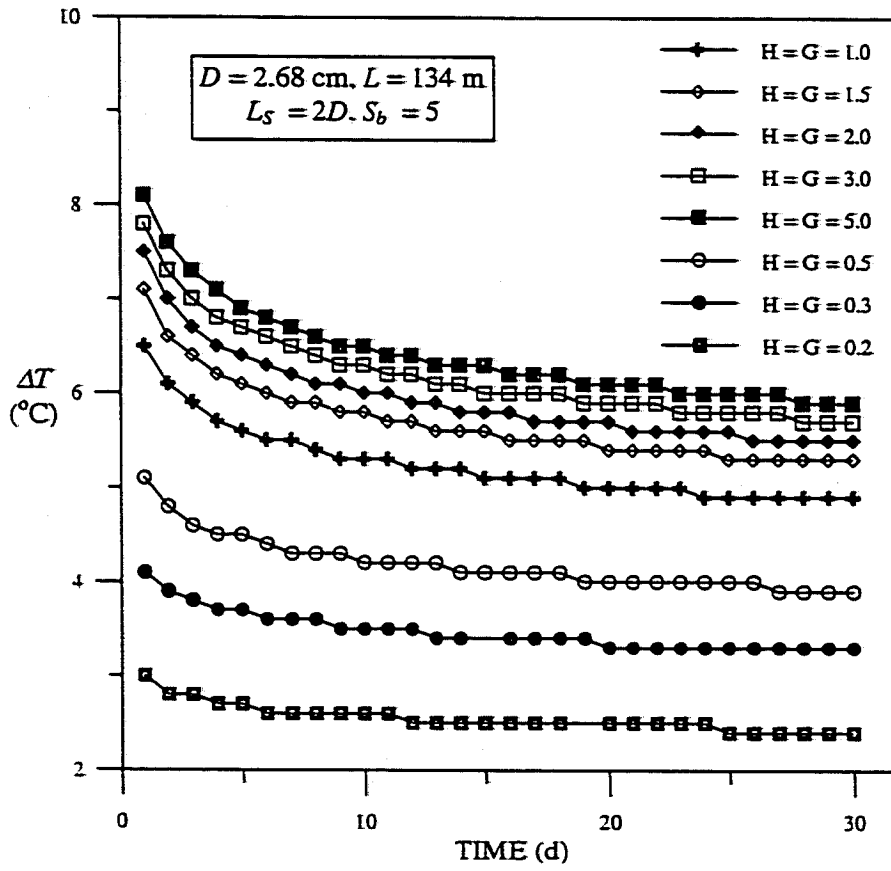


Fig. 8.1 Comparison of  $\Delta T$  during 30-day simulation for Group I

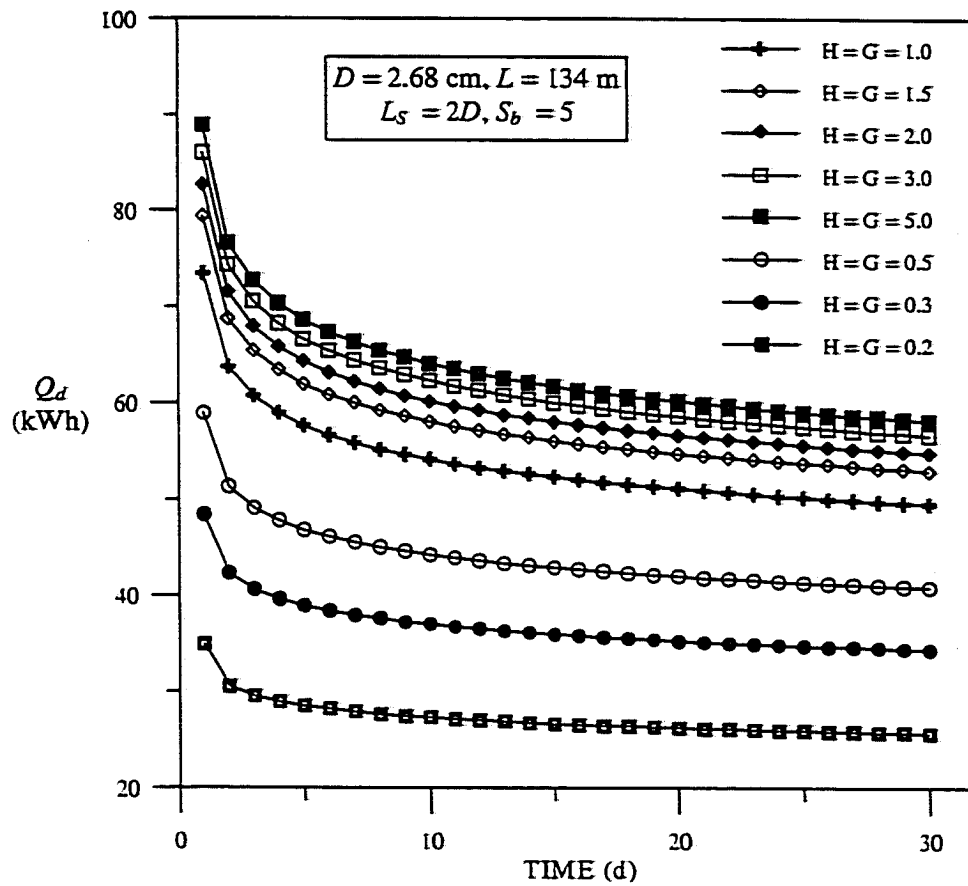
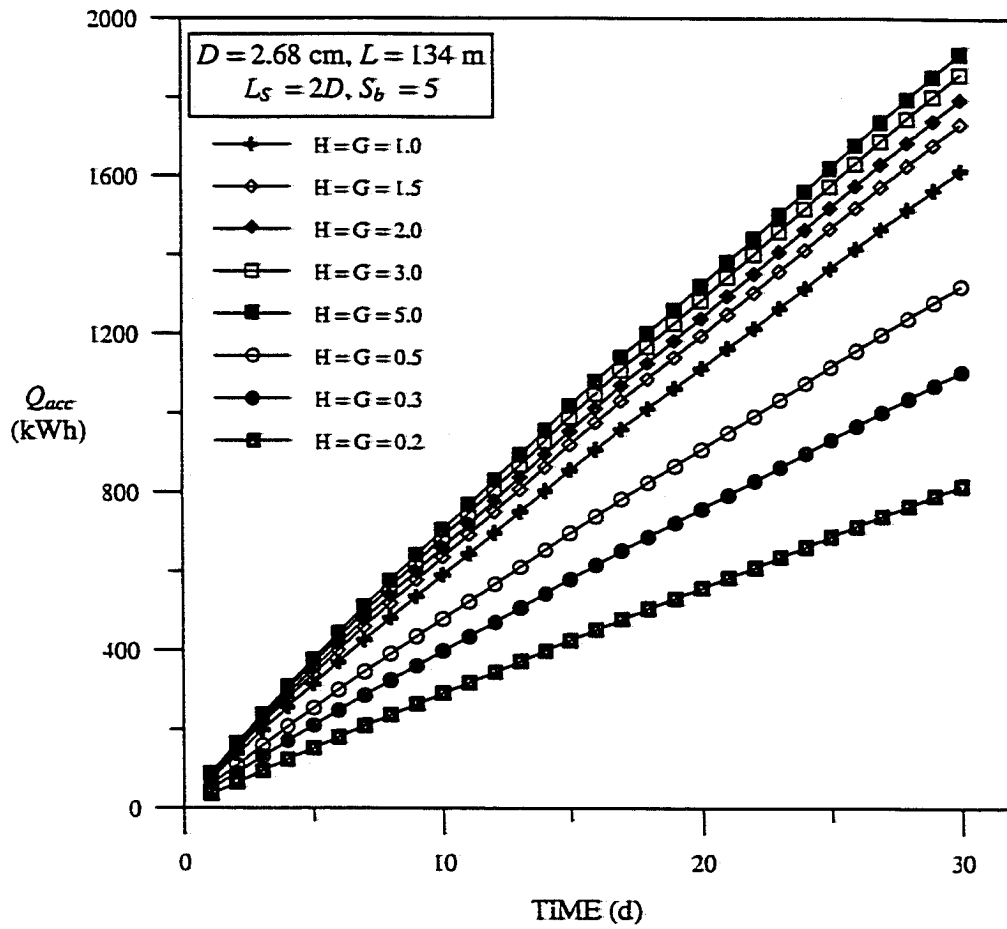


Fig. 8.2 Comparison of daily energy exchange between the soil and coil during 30-day simulation for Group I





**Fig. 8.3 Comparison of cumulative energy exchange between the soil and coil over 30-day operation for Group I**

provides the comparison of the cumulative energy exchange ( $Q_{acc}$ ) for the eight cases. All these curves displayed approximately linear relationships between the heat dissipation and time.

Figures 8.4 through 8.6 give the comparison for different dimensions of the backfill region in Group II.  $\Delta T$  and  $Q_d$  both increased with the increase of  $S_b$  for  $H = G = 2$  but with the decrease of  $S_b$  for  $H = G = 0.5$ . Note that for a homogeneous medium where  $H = G = 1$ , there would be no difference with the change of  $S_b$  since the backfill boundary disappeared. The difference should become larger when  $H$  and  $G$  values deviate more from unity. The set of curves for the two different  $H$  and  $G$  values were clearly separated from each other. The percent change in average  $\Delta T$  or  $Q_d$  was larger with lower  $H$  and  $G$  values. In Fig. 8.6,  $Q_{acc}$  increased almost linearly with time.

Figures 8.7 through 8.9 present the comparisons for varied leg spacing. As in Group II, two non-homogeneous media ( $H = G = 2$  and  $H = G = 0.5$ ) were chosen. Generally speaking,  $\Delta T$ ,  $Q_d$  and  $Q_{acc}$  all increased with expanded leg spacing for all the cases due to reduced thermal interference between the legs.

### Backfill Effectiveness

Couvillion and Cotton (1990) defined a dimensionless backfill effectiveness ( $BE$ ) in the following form:

$$BE = \frac{\sum |Q' / k|}{\sum |T_c - T_m|} \quad (8.1)$$

where  $k$  is conductivity of the soil,  $T_c$  the temperature at the heat source and  $T_m$  the mean

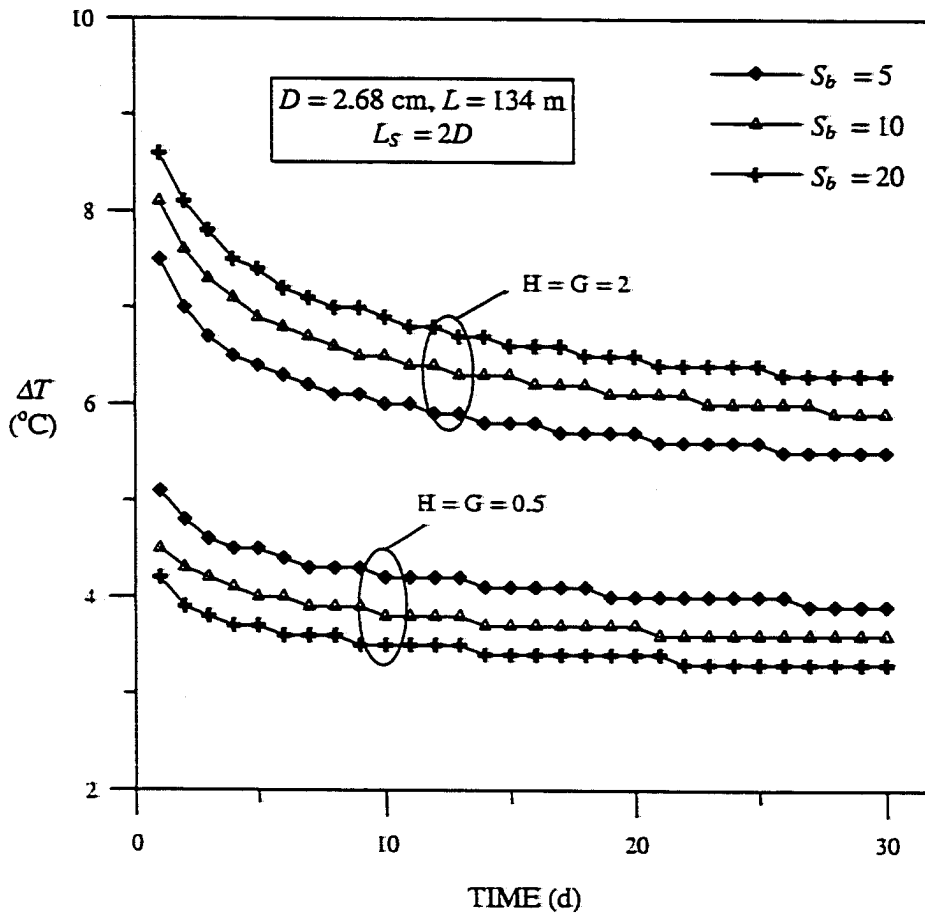
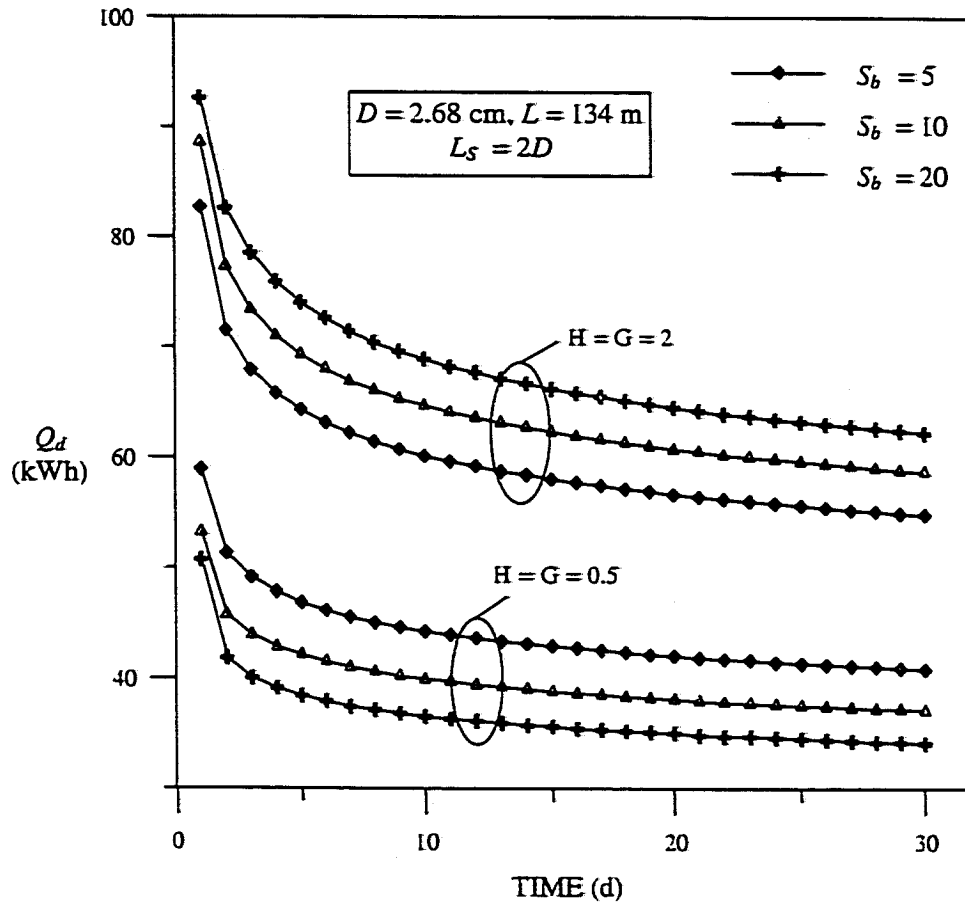
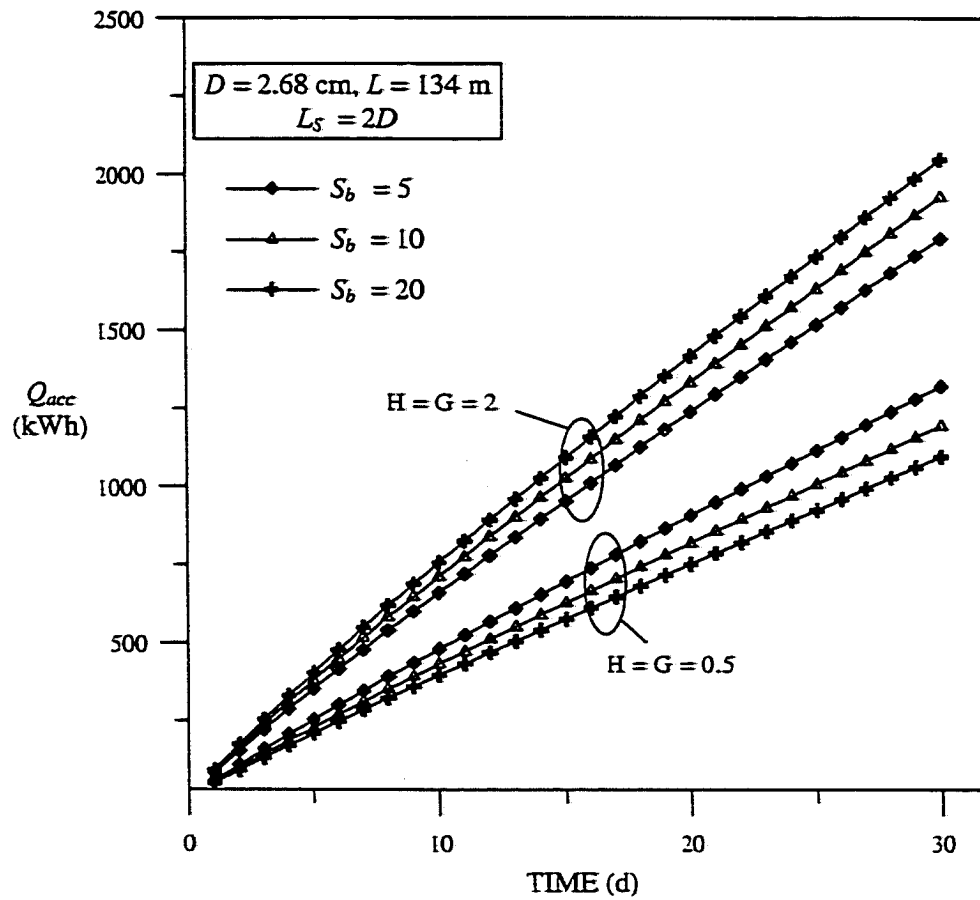


Fig. 8.4 Comparison of  $\Delta T$  during 30-day simulation for Group II



**Fig. 8.5 Comparison of daily energy exchange between the soil and coil during 30-day simulation for Group II**



**Fig. 8.6 Comparison of cumulative energy exchange between the soil and coil over 30-day operation for Group II**

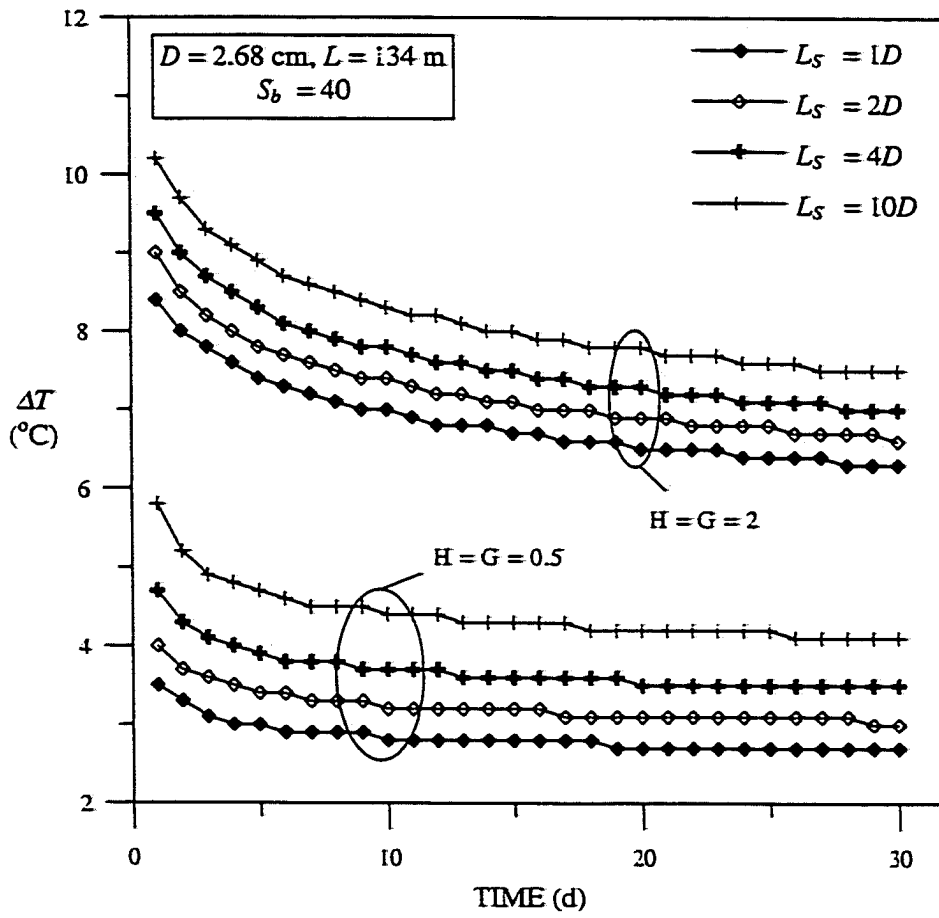
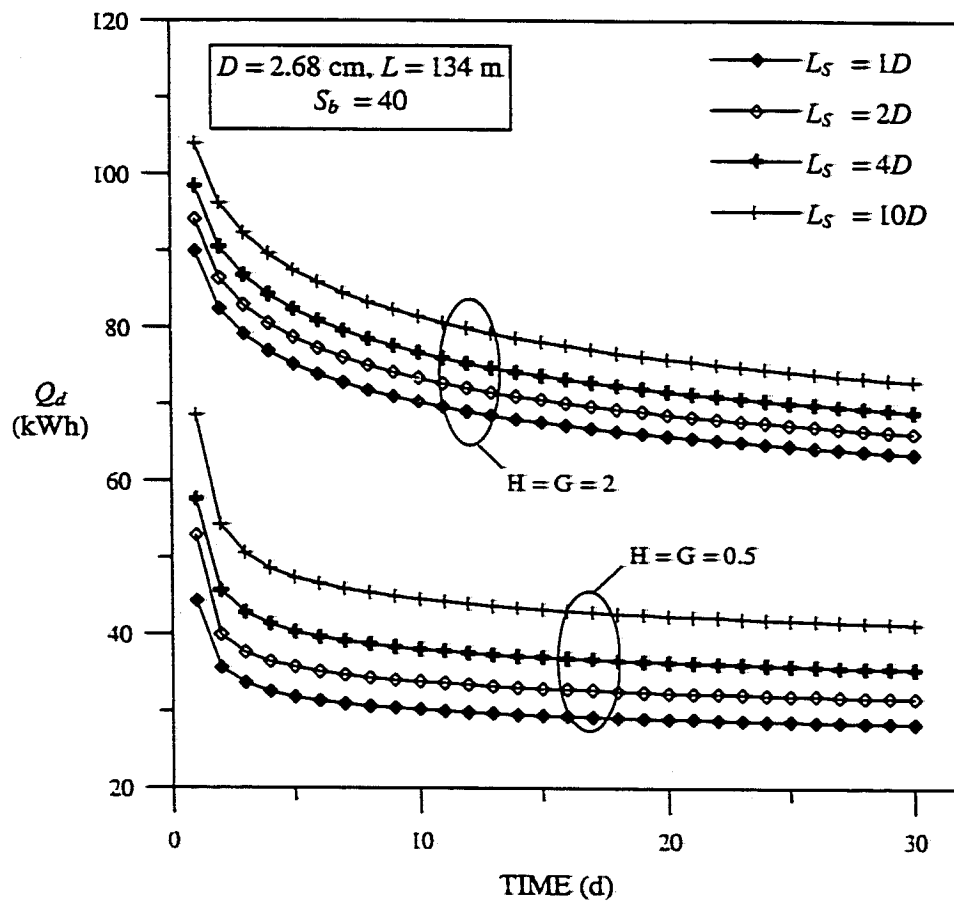


Fig. 8.7 Comparison of  $\Delta T$  during 30-day simulation for Group III



**Fig. 8.8 Comparison of daily energy exchange between the soil and coil during 30-day simulation for Group III**

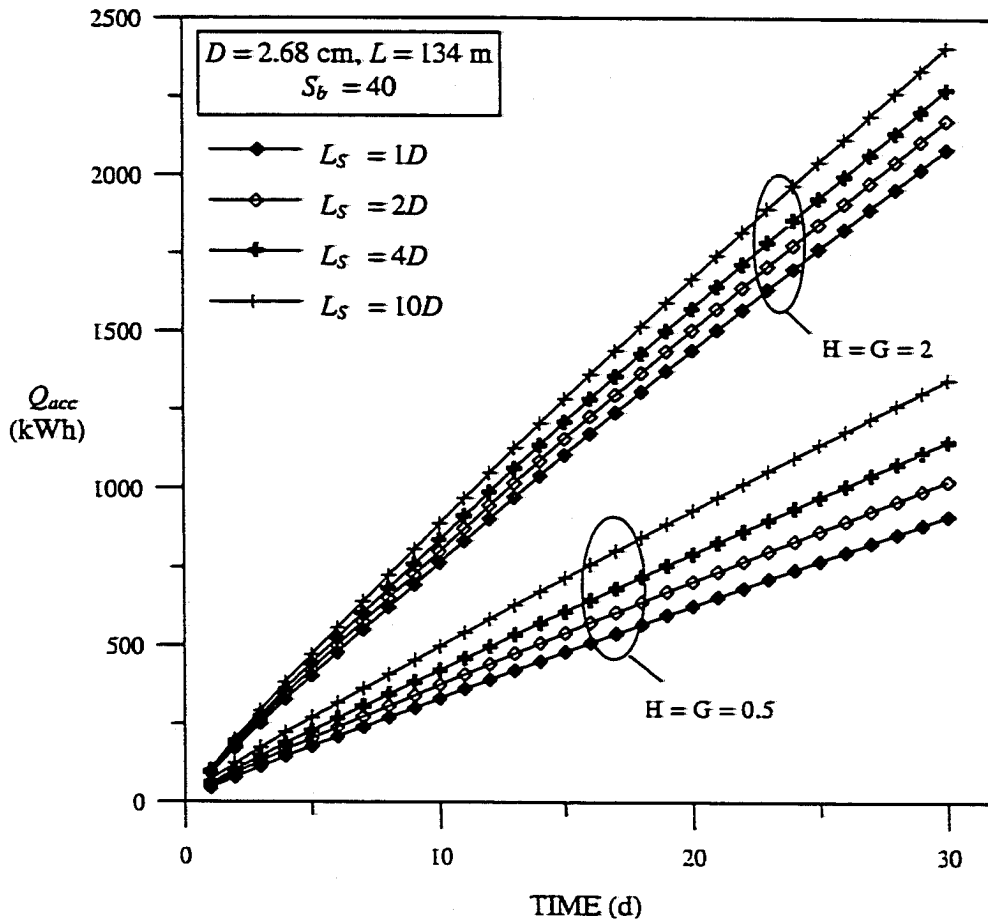


Fig. 8.9 Comparison of cumulative energy exchange between the soil and coil over 30-day operation for Group III



ground surface temperature. The summation is over all time intervals during the simulation. They used equation (8.1) in their model for a horizontal ground coil to calculate  $BE$  and compared the results with the experimentally determined values using another expression similar in concept but different in form from this equation. Physically, this definition is equivalent to an averaged value of the reciprocal of the dimensionless temperature,  $T^* = k_2 \theta / Q'$ , defined in Chapter III. Therefore, the greater the  $BE$ , the lower the average  $T^*$ , and thus the better the backfill for a given soil. However, equation (8.1) was not used in this parametric study for the following two reasons:

1. The quantities,  $k$  and  $T_{sm}$  in equation (8.1), were both constants. The heat transfer rate tended to increase as IWT increased, even though the thermal properties of the soil and backfill were unchanged. This was because the increase in IWT could cause the temperature difference,  $T_c - T_{sm}$ , to increase and thus enhanced heat dissipation. IWT varied in different ways from test to test in Couvillian and Cotton's experiment. Therefore, they included the term  $T_c - T_{sm}$  in the denominator in equation (8.1) to offset the increase in  $Q'$  due to the increase in IWT. However, IWT and the operation mode in present parametric studies were all fixed. The soil conductivity was also constant. ~~Thus, the inclusion of a temperature difference and the thermal conductivity~~ were unnecessary and would only complicate the calculation.
2. The definition in equation (8.1) has a drawback in that it would only provide an independent value of  $BE$  and could not give a straightforward result to show

how much improvement or degradation it generated with the use of a particular backfill compared to the homogeneous case with soil everywhere.

Based on the above rationale and recognizing that the criterion for comparison of backfills should be nothing but the ability of heat dissipation from a ground heat exchanger, a backfill effectiveness was defined as follows:

$$BE = \frac{Q}{Q_{Base} |_{30 \text{ days}}} \quad (8.2)$$

In words, equation (8.2) accounted for the ratio of total 30-day accumulated energy exchange between any case and the base case. This expression seemed simplest to calculate and allowed one to know immediately by what percent the heat rejection increased or decreased with the use of a backfill material. How many days' value of the cumulative energy exchange was chosen would make no difference if the curve for this energy exchange was linear. In fact, the ratios between 30-day and 15-day accumulated energy exchange for all the cases ranged from 1.88 to 1.92. It followed that the curves for accumulated energy exchange were nonlinear and the slopes decreased slowly, because this ratio should be equal to two for a linear function. However, if the definition was made based on a 15-day simulation, the resulting discrepancy would be negligible. Take a typical example, for case 6 in Group III, the value of  $BE$  was calculated to be 0.633 using equation (8.2), while it would become 0.632 if 15-day result was chosen. The difference was less than 0.2 %.

Table 8.2 provides the backfill effectiveness ( $BE$ ) for all the twenty cases divided into the three groups. For the base case,  $BE$  was equal to 1. Of all the cases, case 4 in the

**Table 8.2 Backfill effectiveness for all the twenty cases divided into three groups**

	BACKFILL EFFECTIVENESS							
	Case 1	Case 2	Case 3	Case 4	Case 5	Case 6	Case 7	Case 8
GROUP I	1.000	1.073	1.112	1.152	1.184	0.818	0.684	0.505
GROUP II	1.112	1.195	1.270	0.818	0.740	0.679		
GROUP III	1.290	1.348	1.408	1.492	0.565	0.633	0.712	0.834

third group achieved the highest  $BE$  (1.492) due to an assumed large backfill region composed of a high-conductivity material. The last case in Group I had the lowest  $BE$  (0.505) because the lowest  $H$  and  $G$  values had been used. As an example, it is easy to find out that the total heat rejection over the 30-day operation would increase by 11.2% for case 3 in Group I and decrease by 18.2% for case 6 in the same group compared to the base case.

### Summary

Three groups of parameters provided a total of twenty combinations for the investigations of the U-tube heat exchanger performance.  $H$ ,  $G$ ,  $S_b$  and  $L_S$  were selected as variables. Comparisons of  $\Delta T$  across the U-tube heat exchanger, daily energy exchange ( $Q_d$ ) and 30-day cumulated energy exchange ( $Q_{acc}$ ) were presented graphically. The simulation showed reasonable results applying the composite-medium analytical solution and the equivalent diameter expression developed in this study.

Instead of the definition of backfill effectiveness ( $BE$ ) made by Couvillion and Cotton (1990), a more suitable one was made here for the evaluation of  $BE$  for all the cases concerned. The results were tabulated and the percent increase in energy exchange between the coil and soil could be obtained immediately compared to the homogeneous case.

## CHAPTER IX

### CONCLUSIONS AND RECOMMENDATIONS

In this study, an approximate analytical solution to the transient heat-conduction problem in an infinite composite medium was developed and validated by comparing it with the homogeneous cylindrical solution and the numerical solutions. A general expression for the equivalent diameter was derived based on the steady-state heat conduction and the concentric assumption. The discretized analytical model for the U-tube heat exchanger was then established and verified against the laboratory experiments on the backfill materials. Finally, a parametric study concerning the effects of the backfill's thermal properties, the leg spacing and the dimension of the backfill region was accomplished, and a backfill effectiveness was proposed and different values were analyzed. These studies resulted in the following conclusions:

1. The analytical solution was an extended application of the orthogonal expansion technique to transient heat transfer with a cylindrical source in an infinite composite medium. The solution was given in non-dimensional form and effects of the four essential dimensionless variables,  $H$ ,  $G$ ,  $S_b$  and  $S_c$ , were investigated. In the validation, results typically agreed well with either the homogeneous cylindrical solution or the numerical solutions except for long time intervals (greater than one year). Larger values of  $S_c$  would have to be chosen to extend the results of this solution for larger time increments. Furthermore, this solution was dependable only if the Fourier number was above 0.35 because there were oscillations in the solution with lower Fourier

numbers.

2. The equivalent diameter expression was derived for a range of leg spacing with values between  $D$  (pipe diameter) and  $r_b$  (radius of the backfill region). The value of an equivalent diameter depended on the pipe diameter and the leg spacing. For the case of two pipes in direct contact, the coefficient ( $C$ ) was exactly the same as obtained by Claesson and Dunand (1983). For a leg spacing equal to or larger than  $2D$ ,  $C$ -values were greater than all those proposed by previous investigators. The application of this expression for a transient process and the non-concentric situation with a U-tube configuration was justified by comparison with the superposition method and by means of the conformal mapping technique, respectively. Furthermore, its application in the system model written for the whole U-tube heat exchanger was validated experimentally along with the superposition method. The parametric studies using this method achieved reasonable results.
3. A small-scale simulator was built up for the verification of the system model. Two kinds of backfill materials were used: bentonite/masonry sand (Type A) and bentonite/copper powder (Type B) mixtures. The verification runs last for up to seven hours, equivalent to nearly five days' operation for a typical GCHP. The experimental data showed that the model generally under- or over-estimated OWT within  $0.5\text{ }^{\circ}\text{C}$  most of the time for Type A or Type B, respectively. On the other hand, the corresponding temperature drop across the U-tube heat exchanger was over- or under-predicted within  $0.5\text{ }^{\circ}\text{C}$  for

Type A or Type B. Predictions with the superposition and equivalent diameter methods differed from each other by less than 1%. The model tracked the trends in OWT quite well during the start-up and off-cycles. However, the predicted temperature drop was considerably smaller than the actual within the initial four minutes because the thermal capacity of the pipe wall was neglected in the model.

4. During the off-cycles of the tests, an interesting phenomenon was observed. The pipe wall temperature at the bottom of the U-tube achieved the lowest value immediately after the water pump was shut off. This temperature could be as much as 4.6 °C lower than those measured at the two adjacent thermal couple joints. This phenomenon could also be observed in a real GCHP system as used by Dobson (1991) and it might have been caused by the end effect as depicted in Chapter VII.
5. The parametric studies showed that the application of the analytical solution combined with the equivalent diameter approach led to reasonable results over wide ranges of the major parameters which would have direct effects on the GCHP performance. With backfill effectiveness defined in this study, it would be easy to predict by what percent the total heat exchange between the coil and soil will increase or decrease with the use of a particular backfill.

From this study, the author recommend the following for the future studies:

- Potential techniques for reducing the number of terms in the series to obtain an analytical solution to  $T^*$  should be investigated. As described earlier, up to

one thousand terms had to be used to reduce the oscillations in the solution to an acceptable level for small values of  $Fo$ .

- This study did not take the moisture migration into account. Therefore, effort should be made to develop a model in which a mass transfer equation can be incorporated with the analytical solution derived in this study to better describe the coupled mass and heat transfer process in the composite medium.
- Further experimental verification is needed for the equivalent diameter expression in a wide range of  $L_S$  and  $r_b$  as well as  $H$  and  $G$ .
- The U-tube system model should be incorporated into a GCHP utility program to predict the heat pump performance with a non-homogeneous medium in both cooling and heating seasons.



## REFERENCES

- Beach, H. L., 1967, "The Application of the Orthogonal Expansion Technique to Conduction Heat Transfer Problems in Multilayer Cylinders," M.S. Thesis, North Carolina State University, Raleigh.
- Boggs, S. A., Chu, F. Y., Radhakrishna, H. S., and Steinmanis, J. E., 1981, *Underground Cable Thermal Backfill*, Pergamon Press, Toronto, Canada, pp. 34-53.
- Boo, J., 1984, "Influence of Vapor Mass Flux on Simultaneous Heat and Mass Transfer in Moist Porous Media," M.S. Thesis, Georgia Institute of Technology, Atlanta.
- Bose, J. E., Parker, J. D., and McQuiston, F. C., 1985, *Design/Data Manual for Closed-Loop Ground-Coupled Heat Pump Systems*, American Society of Heating, Refrigerating, and Air-Conditioning Engineers, Inc., Atlanta, Georgia, pp. 2.15, 2.35.
- Bulavin, P. E., and Kascheev, V. M., 1965, "Solution of the Non-Homogeneous Heat Conduction Equation for Multilayered Bodies," *Int. Chem. Eng.*, Vol. 5, pp. 112-115.
- Carslaw, H. S., and Jaeger, J. C., 1959, *Conduction of Heat in Solids*, 2nd ed., Oxford University Press, New York, pp. 327-339.
- Claesson, J., and Dunand, A., 1983, "Heat Extraction From the Ground by Horizontal Pipes - A Mathematical Analysis," Document D1, Swedish Council for Building Research, Stockholm.
- Coogan, C. H., Jr., 1949, "Heat Transfer Rates: Experimental Determination for Heat-Absorbing Coils Buried in the Earth," *Mechanical Engineering*, Vol. 71, pp. 495-498.
- Couvillion, R. J., and Cotton, D. E., 1990, "Laboratory and Computer Comparisons of Ground-Coupled Heat Pump Backfills," *ASHRAE Transactions*, Vol. 96, Part 1, pp. 643-651.
- Couvillion, R. J., 1981, "Heat and Mass Transfer in a Semi-Infinite Moist Soil With a Drying Front Present," Ph.D. Dissertation, Georgia Institute of Technology, Atlanta.
- Dobson, M. K., 1991, "An Experimental and Analytical Study of the Transient Behavior of Vertical U-Tube Ground-Coupled Heat Pumps in the Cooling Mode," M.S. Thesis, Texas A&M University, College Station.

Fink, L. H., and Smerke, J. J., II, 1958, "Control of the Thermal Environment of Buried Cable Systems - Part II," presented at the AIEE Winter General Meeting, New York, Feb. 2-7.

Fischer, R. D., and Stickford, G. H., 1983, "Technical and Economic Feasibility of Horizontal, Multiple Shallow-Well and Deep-Well Ground Coupling," ORNL/Sub/80-7800/3&06, Oak Ridge National Laboratory, Oak Ridge, Tennessee.

Goldenberg, H., 1969, "External Thermal Resistance of Three Buried Cables in Trefoil Touching Formation. Restricted Application of Superposition," *Proc. IEE*, Vol. 116, pp. 1885-1890.

Golub, Gene, H., Loan, V., and Charles, F., 1983, *Matrix Computations*, Johns Hopkins University Press, Baltimore, Maryland, Chapter 4.

Guenther, R. B., and Lee, J. W., 1988, *Partial Differential Equations of Mathematical Physics and Integral Equations*, Prentice Hall, Englewood Cliffs, New Jersey, p. 223.

Hartley, J. G., 1987, "Coupled Heat and Moisture Transfer in Soils: A Review," In: *Advances in Drying*, Vol. 4, Hemisphere, New York, pp. 199-248.

Hartley, J. G., and Black, W. Z., 1981, "Transient Simultaneous Heat and Mass Transfer in Moist, Unsaturated Soils," *ASME Journal of Heat Transfer*, Vol. 103, pp. 376-382.

Hopkins, P. L., 1983, "Performance of a Vertical Heat Pump Ground-Coupled Device," M.S. Thesis, Oklahoma State University, Stillwater.

Ingersoll, L. R., Zobel, O. J., and Ingersoll, A. C., 1954, *Heat Conduction With Engineering, Geological, and Other Applications*, McGraw-Hill, New York, pp. 250-251.

Jackson, K., 1980, "Enhancement of Thermal Energy Transport Through Granular Media," Ph.D. Dissertation, Georgia Institute of Technology, Atlanta.

Jaeger, J. C., 1942, "Heat Flow in the Region Bounded Internally by a Circular Cylinder," *Proc. of the Royal Society of Edinburgh*, Vol. 61, pp. 223-228.

Johnson, W. S., McGraw, B. A., Baugh, R. N., and Griffith, W., 1987, "Final Report: 1984-1985 Annual Performance Testing and Analysis of Two Horizontal Coil Ground-Coupled Heat Pump Systems," ORNL/Sub/81-7685/4892, Oak Ridge National Laboratory, Oak Ridge, Tennessee.

Kavanaugh, S. P., 1984, "Simulation and Experimental Verification of Vertical Ground-Coupled Heat Pump Systems," Ph.D. Dissertation, Oklahoma State University, Stillwater.

Lei, T. K., 1993, "Development of a Computational Model for a Ground-Coupled Heat Exchanger," *ASHRAE Transactions*, Vol. 99, Pt. 1, pp. 149-159.

Margo, R. E., 1992, "An Experimental Study of Heating Performance and Seasonal Modeling of Vertical U-Tube Ground Coupled Heat Pump," M.S. Thesis, Texas A&M University, College Station.

Martin, B. W., and Cohen, H., 1954, "Heat Transfer by Free Convection in an Open Thermosyphon Tube," *British Journal of Applied Physics*, Vol. 5, pp. 91-95.

Mei, V. C., 1991, "Heat Transfer of Buried Pipe for Heat Pump Application," *ASME Journal of Solar Energy Engineering*, Vol. 113, pp. 51-55.

Mei, V. C., 1987, "Effect of Backfilling Material on Ground Coil Performance," *ASHRAE Transactions*, Vol. 93, Part 2, pp. 1845-1857.

Mei, V. C., and Baxter, V. D., 1986, "Performance of a Ground-Coupled Heat Pump With Multiple Dissimilar U-Tube Coils in Series," *ASHRAE Transactions*, Vol. 92, Part 2A, pp. 30-42.

Mei, V. C., and Emerson, C. J., 1985, "New Approach for Analysis of Ground-Coil Design for Applied Heat Pump Systems," *ASHRAE Transactions*, Vol. 91, Part 2B, pp. 1216-1224.

Mulholland, G. P., and Cobble, M. N., 1972, "Diffusion Through Composite Media," *Int. J. Heat Mass Transfer*, Vol. 15, pp. 147-160.

Muraya, K. N., 1994, "Numerical Modeling of the Transient Thermal Interference of Vertical U-Tube Heat Exchangers," Ph.D. Dissertation, Texas A&M University, College Station.

Özisik, M. K., 1980, *Heat Conduction*, John Wiley & Sons, New York, pp. 295-329.

Özisik, M. K., 1968, *Boundary Value Problems of Heat Conduction*, International Textbook Co., Scranton, Pennsylvania, pp. 273-299.

Remund, C. P., and Lund, J. T., 1993, "Thermal Enhancement of Bentonite Grouts for Vertical GSHP Systems," *Heat Pump and Refrigeration Systems Design, Analysis, and Applications*, ASME, AES-Vol. 29, pp. 95-106.

Svec, O. J., Goodrich, L. E., and Palmer, J. H. L., 1983, "Heat Transfer Characteristics of In-Ground Heat Exchanger," *Int. J. of Energy Research*, Vol. 7, pp. 265-278.

Tittle, C. W., 1965, "Boundary Value Problems in Composite Media: Quasi-Orthogonal Functions," *J. Appl. Phys.*, Vol. 36, pp. 1486-1488.

Tittle, C. W., and Robinson, V. L., 1965, "Analytical Solution of Conduction Problems in Composite Media," ASME paper No. 65-WA-HT-52.

Vodicka, V., 1955, "Eindimensionale Wärmeleitung in Geschichteten Körpern," *Mathematische Nachrichten*, Vol. 14, pp. 47-55.

Vodicka, V., 1950, "Wärmeleitung in Geschichteten Kugel und Zylinderkörpern," *Schweizer Archiv*, Vol. 10, pp. 297-304.

Winders, J. J., Jr., 1973, "Computer Program Analyzes Heat Flow From Cables Buried in Regions of Discontinuous Thermal Resistivity," presented at the IEEE PES Summer Meeting & EHV/UHV Conference, Vancouver, B.C., Canada, July 15-20.

Yang, S. M., 1980, *Heat Transfer*, 2nd ed., Advanced Education Press, Beijing, China, p. 336.

**APPENDIX A****INPUT DATA USED IN PARAMETRIC STUDIES****WATER PROPERTIES**

Thermal Conductivity	0.63	W/ m-K
Density	994	kg / m <sup>3</sup>
Specific Heat	4.17	kJ / kg-K
Kinematic Viscosity	0.732 x 10 <sup>-6</sup>	m <sup>2</sup> / s
Prandtl Number	5.2	-
Gravitational Acceleration	9.8	m / s <sup>2</sup>
Thermal Expansion Coefficient	3.54 x 10 <sup>-4</sup>	K <sup>-1</sup>
Inlet Water Temperature During On-Cycle	35	°C

**U-TUBE PROPERTIES**

Thermal Conductivity	0.46	W/ m-K
Inner Radius	1.1	cm
Outer Radius	1.34	cm
Leg Spacing	2.68 - 26.8	cm
Depth	134	m
Volumetric Flow Rate	11.36	l / min

**SOIL AND BACKFILL PROPERTIES**

Soil:

Thermal Conductivity	1.732	W/ m-K
Thermal Diffusivity	$0.96 \times 10^{-6}$	$\text{m}^2/\text{s}$
Radius of Far-Field Boundary	12	m
Far-Field Temperature	22	$^{\circ}\text{C}$
Backfill:		
Thermal Conductivity	0.346 - 8.66	W/ m-K
Thermal Diffusivity	$(0.192 - 4.8) \times 10^{-6}$	$\text{m}^2/\text{s}$
Radius of Backfill Region	6.7 - 53.6	cm

## APPENDIX B

### EXPERIMENTAL UNCERTAINTY

The experimental uncertainty included various uncertainties in measurement of the water temperature and mass flowrate, thermal properties of the soil and backfills, as well as the effective heat transfer length of the U-tube, etc. In general, on the side of the U-tube heat exchanger, various errors in measurement led to the uncertainty in calculation of the heat transfer rate of the U-tube; on the side of the heat transfer medium around the U-tube heat exchanger, errors in measurement of various thermal properties resulted in the uncertainty in evaluation of the thermal diffusivity of the soil and backfill. The analyses of these two uncertainties are discussed below. The uncertainty of variables in this appendix is denoted by adding a prefix "δ" to a variable.

The calculation of the uncertainty is based on the following formulation. If a calculated quantity,  $N$ , is a function of  $n$  measured variables  $v_1, v_2, v_3, \dots, v_n$  such that

$$N = f(v_1, v_2, v_3, \dots, v_n) \quad (\text{B.1})$$

and if the uncertainty in each variable of  $v_1, v_2, v_3, \dots, v_n$  is denoted as  $\pm\delta v_1, \pm\delta v_2, \pm\delta v_3, \dots, \pm\delta v_n$ , respectively, then the uncertainty for  $N$  is given as

$$\frac{\delta N}{N} = \pm \sqrt{\sum_{j=1}^n \left( \delta v_j \frac{\partial f}{\partial v_j} \right)^2} \quad (\text{B.2})$$

Equation (B.2) was used to calculate the uncertainties.

#### I. Average Heat Transfer Rate Along the U-Tube Heat Exchanger for On-Cycles

The heat transfer rate along the U-tube heat exchanger during the on-cycles was determined by the relationship

$$Q' = \dot{m}c_p(IWT - OWT) / L \quad (B.3)$$

Neglecting the influence of  $c_p$ , the uncertainty in calculation of the heat transfer rate can be evaluated in terms of the uncertainties of the water flow rate ( $\dot{m}$ ), the inlet and outlet water temperatures (IWT and OWT) and the effective heat transfer length ( $L$ )

$$\frac{\delta Q'}{Q'} = \pm \left[ \left( \frac{\delta \dot{m}}{\dot{m}} \right)^2 + \left( \frac{\delta IWT}{IWT} \right)^2 + \left( \frac{\delta OWT}{OWT} \right)^2 + \left( \frac{\delta L}{L} \right)^2 \right]^{\frac{1}{2}} \quad (B.4)$$

The individual uncertainties of the variables at the right-hand side of equation (B.2) were determined as follows:

⇒ thermocouple readings  $\delta IWT / IWT = \delta OWT / OWT = \pm 0.6\%$ ,

⇒ flowmeter readings  $\delta \dot{m} / \dot{m} = \pm 2.0\%$ ,

⇒ effective heat transfer length  $\delta L / L = \pm 1.0\%$ .

Substituting these values into equation (B.2) gives the uncertainty

$$\delta Q' / Q' = \pm 2.4\%$$

## 2. Average Thermal Diffusivity of the Soil and Backfill

The thermal diffusivity was determined as

$$\alpha = k / \rho c \quad (B.5)$$

Therefore, the uncertainty of the thermal diffusivity is given as

$$\frac{\delta \alpha}{\alpha} = \pm \left[ \left( \frac{\delta k}{k} \right)^2 + \left( \frac{\delta \rho}{\rho} \right)^2 + \left( \frac{\delta c}{c} \right)^2 \right]^{\frac{1}{2}} \quad (B.6)$$

The uncertainty of the thermal conductivity and specific heat were  $\pm 12\%$  as provided by the Heat Transfer Laboratory at TAMU and that of the density was  $\pm 5\%$ . Upon



substituting the relevant values, the uncertainty is

$$\delta \alpha / \alpha = \pm 17.7\%$$

### VITA

Yian Gu was born on February 17, 1960 in Shanghai, China to Yasheng Gu and Puying Zhang. Yian Gu attended Jiaotong University in Xian, China in 1978 and received a B.S. in mechanical engineering in 1982. After graduation, he worked as an assistant mechanical engineer in a textile manufacturer for nearly two years. He entered the Graduate School at Xian Jiaotong University in 1983 and earned his M.S. in mechanical engineering in 1986. He wed Ying Zhou on February 4, 1986, and two children (twin sons) were born to them the next year. Yian Gu worked in the Power Machinery Department at Xian Jiaotong University for five years and was a lecturer before joining the Ph.D. program at Texas A&M University in 1991. His permanent mailing address is North 2-1-3, Northwestern Polytechnic University, Xian (710072), P. R. China.